Numerical Simulation of Density Stratified Flows by Lattice Vortex Method

Zhang, Xiaofeng

(Degree)
博士（工学）

(Date of Degree)
1999-03-31

(Date of Publication)
2014-02-24

(Resource Type)
doctoral thesis

(Report Number)
甲1933

(JaLCDOI)
https://doi.org/10.11501/3156334

(URL)
https://hdl.handle.net/20.500.14094/D1001933

Doctoral Dissertation

Numerical Simulation of Density Stratified Flows by Lattice Vortex Method

格子渦法による密度成層流の数値シミュレーション

by

Xiaofeng Zhang

張　暁峰

January, 1999

Graduate School of Science and Technology

Kobe University

Doctoral Dissertation

Numerical Simulation of Density Stratified Flows by Lattice Vortex Method

by

Xiaofeng Zhang

January, 1999

Graduate School of Science and Technology

Kobe University

Contents

Acknowledgements

I would like to express my gratitude to Professor Michihisa Tsutahara for his support and encouragement during my academic years at Kobe University (1994~1999). I am very grateful to him not only for his academic advice on scientific matters but also for his thoughtfulness. Without his guidance and encouragement, I would not have been able to complete this study.

I am also very grateful to the members of my dissertation committee: Professor Tsuyoshi Nakajima and Professor Akihiko Nakayama for their helpful comments and suggestions.

I would like to thank Professor Teruhiko Kida of University of Osaka Prefecture for his valuable advice and for providing me with the opportunity to study at Kobe University.

I also wish to thank Associate Professor Kazuhiko Ogawa for his priceless suggestions and enthusiastic discussions.

I owe much to all the past and present fellow students at Kobe University fluid energy morphology laboratory. In particular, I would like to thank the members of the lattice vortex method study group, Mr. Yasuhiro Hosokawa, Mr. Hajime Kakuda, and Mr. Toshiyuki Mizuno, not only for valuable suggestions but also for their friendship.

This study was made possible largely through the Kobe Sugahara scholarship of Kobe International Association, and I would like to acknowledge

here the financial support given to me during my years in the doctoral degree program.

I also wish to give my thanks to Dr. Zhong-hua Sun and Mr. Shi-de Feng. Without their help, I would not have been able to solve my terrible "family war".

I would like to give my special thanks to Mr. Takeshi Kataoka, not only for his helpful suggestions in academic research but also for his kindness in enjoying the Boling and Karaoke.

I would like to dedicate this dissertation to my parents, who taught me patience, possibility, and hope in my life with their full love and spirit. Finally, I would like to say "SORRY" to my son Mo-Ruo Zhang, because I have not given enough love to him after his birth.

Nomenclature

A	Area for integration
c	Propagation speed of internal wave
CFL	Courant-Friedrichs and Lewy number
D	Depth of the stream
F_r	Froude number
g	Acceleration due to gravity
H	Channel depth
h	Vertical height of obstacle
K	Density stratification degree
k	Wave number
L	Calculation range
L_1	Upstream calculation range
m	Strength of line sink
N	*Brunt – Väisälä* frequency
p	Pressure
p'	Perturbation pressure
Q	Discharge of line sink
R_i	Richardson number
t	Time

t^*	Dimensionless time
Δt	Time step
$U(z)$	Velocity profile at far upstream
U_0	Reference velocity
u_n	Normal velocity
W	Channel width
u, v, w	Velocity components in the x-, y- and z-directions
Γ	Circulation of vortex
ξ	Vorticity
ρ	Density
ρ_0	Reference density
λ	Wavelength

Chapter 1

Introduction

1.1 Background of the research on vortex method

In the research on fluid mechanics, much of the modern work has been made possible by the remarkable advances in experimental techniques and the development of powerful computers, coupled with progress in numerical method. With the rapid development of the computer technology, as a new branch of fluid mechanics, computational fluid dynamics was established and widely used in solving many practical problems. For improving calculation speed and accuracy, many numerical simulation methods are proposed.

In the computational fluid dynamics, vortex method is widely used in the simulation of unsteady separated flow with high Reynolds number. Vortex method was proposed in 1932 for investigating the Helmholtz instability [1]. Because its algorithm is simple, it is used in many practical applications. Vortex methods offer a number of advantages over the more traditional Eulerian schemes

(for example, finite difference method). Four advantages and their side effects are cited below: 1. Because computational points are required only in the rotational parts of the flow, vortex methods use a minimal description of the flow field which is pleasing theoretically and requires only a relatively small number of storage locations. On the other hand, the number of operations per time step is roughly proportional to the square of the number of vortex elements or coordinates in the discretization, rapidly leading to excessive computation times as the number of elements is increased. 2. The Lagrangian treatment eliminates the need to explicitly treat convetive derivatives. Because of this, small-scale features can often be convected accurately with a relatively large time step and certain singular distributions in vorticity may be treated exactly by vortex method. 3. In turbulent fluid flows and in many high Reynolds number laminar flows, fine-scale structures may develop in an intermittent manner throughout the flow field. Vortex methods can automatically allow such regions to develop by a local concentration of computational points. 4. Boundary conditions at infinity may be treated exactly, and accurate outflow boundary conditions are available and easy to implement. Various vortex method schemes have been devised to improve its computational efficiency and keep its advantages. J. C.Wu and J. F. Thompson [2] gave a hybrid method which combining the vortex method and finite difference method, so in Wu's method there also has the limitation of CFL. The discrete vortex method is a pure Lagrangian method, in which there is no CFL limitation, but the growth of the cost of computations with the square of the number of vortex elements is the greatest disadvantage. To overcome this disadvantage, cutoff schemes and rediscretization methods are used in discrete vortex method. Leonard [3] and Sarpakaya [4] made a review on discrete vortex method in detail. In rediscretization methods, the vortex in cell method (VIC) is one effective kind of vortex method. As a branch of the vortex method, it is widely used. However, untill now, the application of this method is limited in the simulation of

incompressible homogenous fluid flow.

1.2 Purposes of the research

In this paper, we simplified VIC method and proposed a lattice vortex method (LVM) for improving the calculation speed, and extended this method to simulate a three dimensional nonhomogenous fluid flow.

In vortex method, the most part of calculation time is due to the calculation of velocity induced by vortex, which number increases with the number of calculation step. In VIC, the vortex distribution method is only used to calculate velocity field, so the number of vortex will increase with the increase of calculation time. In LVM, the vorticities are defined in mesh points and vorticity distribution scheme are used, so that the number of vortex is same with that of mesh points in the simulation. Because the regular cubic mesh is used, the look-up-table is made from the regularity of the distance between vortex and calculation point, and it is used to save CPU time.

1.3 Contents of the dissertation

For example, the selective withdrawal by a line sink, the flow past an obstacle and the generation of internal wave in an inviscid incompressible density stratified fluid flow are researched.

This dissertation consists of seven chapters.

Chapter 2 Principles of lattice vortex method

Chapter 3 Numerical procedure of lattice vortex method in stratified flows

Chapter 4 Line sink flows of density stratified flows

Chapter 5 Density stratified flows past an obstacle in a channel with finite depth

Chapter 6 Numerical simulation of 3D stratified flows by lattice vortex method

Chapter 7 Conclusion, the results obtained in this study are Summarized and dissertation is concluded by suggesting the direction of future research.

Chapter 2

Principles of Lattice Vortex Method

2.1 Introductory remarks

In the past three decades, the study of vortices and vortex motions has received continuing impetus from problems arising in physics, engineering and mathematics. The vortex method originated in Helmholtz's great paper of 1858, "Uber Integrale der hydrodynamischen Gleichungen welche den Wirbel-bewegungen entsprechen", and continued in the brilliant work of Lord Kelvin and others in the nineteenth century, and Prandtl and his *Göttingen* school in the first half of this century. As aptly remarked by *Küchemann* [1965], vortices are the "sinews and muscles of fluid motions". Aerodynamic problems of stability, control, delta wing aerodynamics, high lift devices, the jumbo jet wake hazard phenomenon, among other concerns, have led to a myriad of studies. Much of modern work has been made possible by the remarkable advances in experimental techniques and the development of powerful computers, coupled with progress in numerical methods.

Helmholtz (1858) was the first to show, in what is now regarded as one of the most important contributions in fluid mechanics, that in an inviscid fluid vortex lines remain continually composed of the same fluid elements and flows with

vorticity can be modeled with vortices of appropriate circulation and "infinitely small cross section" ----quantum vortex lines. It is this realization that led to the discretization of the compact regions of vorticity into an assembly of vortices (with finite or infinite vorticity) embedded in a potential flow. By the theorems of Helmholtz and Kelvin we know that the inviscid motion of the vorticity in these regions is given by the local fluid velocity which in turn is determined kinematically from the vorticity field. Thus, it is mathematically correct and often very convenient to consider inviscid fluid dynamics in terms of parcels of vorticity which induce motion on each other as an alternative to pressure-velocity considerations. Vortex methods simulate flows by discretizing the vorticity-containing regions and tracking this discretization in a Lagrangian reference frame. The Langrangian or the Langrangian-Eulerian description of the evolution of the discretized vorticity field constitutes the essence of the computational methods with vortices. The required local velocities are computed as the solution to the Poisson equation for the velocity field, often in terms of a Green's function or Biot-Savart integration. With few notable exceptions, applications have been limited to incompressible flow cases for which the Biot-Savart law or Green's function method applies. Typically, the Lagrangian coordinates of this discretization satisfy a nonlinear system of ordinary differential equations giving the time evolution of the coordinates.

Isolated line vortices, vorticity blobs, vortex balls or vortons, or toroidal vortices are introduced into the flow field and tracked numerically by a Langrangian or a mixed Langrangian-Eulerian scheme. In this process, the representation of the body, with the imposed boundary conditions, often becomes an integral part of the computation of the flow field. When geometrically simple solid boundaries are present, suitable image vortices are introduced to satisfy the zero normal velocity condition. For complex geometries, boundary integral or panel methods are used and the free vortex filaments, vortex rings, vortex sheets, or blobs are included in the potential flow model.

Vorticity moves with the local velocity in the inviscid motion of a fluid. If the

fluid is incompressible, knowledge of the vorticity distribution is sufficient to determine the velocity field. Vortex methods essentially represent a direct translation of these facts to a numerical algorithm for flow simulation. The Lagrangian treatment eliminates the need to explicitly treat convective derivatives. Because of this, the severe restriction of CFL condition for the stability in Eulerian treatment can be released, which implies the allowable large time step length in numerical calculation.

Various schemes have been devised to reduce the computer time and to delay, limit, circumvent, or bound the instabilities or chaotic behavior which may result either from the singular behavior of the computational elements or from the ill-posed nature of the problem solved. Vortex-in-cell (VIC) methods is one of the methods widely used to improve dramatically the computational efficiency when a large number of vortex elements are required. With the increase of the number of vortex, the use of the Biot-Savart law to calculate the induced velocities of large number of vortices (as many as 100,000) will stretch the capacity of even the fastest computers of the day and requires methods to reduce the CPU time. Based on VIC method, we proposed a new version, lattice vortex method (LVM), to limit the number of vortex in numerical simulation, and extended its application from homogeneous incompressible flows to non-homogeneous flow fields.

The lattice vortex method has combined the best features of both the Lagrangian and Eulerian approaches. The Lagrangian particles representing the elements of fluid move through a fixed Eulerian mesh which, in turn, is used to characterize the field variables. In the LVM, all parameters are defined on mesh points, the fixed Eulerian mesh is not only used to determine velocity field, but also applied to redistribute vorticity distribution. A vorticity allotment scheme allocates vorticity to the surrounding mesh points (i.e., from the location of the vortices to the nearest node points of the mesh). The Lagrangian part of the hybrid scheme enables the vortical structures to "float" over the fixed Eulerian mesh of the velocity field. The mesh cells are only used to redistribute vorticities,

so that there is also no limitation of the CFL condition in the LVM. All above means that in the LVM the vortex can move beyond one mesh cell in one time step, and we can choose larger time step to increase calculation efficiency.

In section 2.2, we explained the principle of lattice vortex method in two-dimensional flows. The technique used to improve the calculation speed in induced velocity calculation is introduced, and the accuracy of distribution method is also discussed in this section. The principle of the lattice vortex method in three-dimensional flows is explained in section 2.3.

2.2 Lattice vortex method for two-dimensional flows

2.2.1 Principle of 2D lattice vortex method

In this section, we shall introduce the principle of lattice vortex method in two-dimensional flows. In the lattice vortex method, the calculation region is divided by regular mesh. The parameters of the flow field (vorticity , velocity , pressure, and density) are defined on mesh points (Fig.2.1). The vorticity on a mesh point represents the vorticity distributed in the area around the mesh point (i.e. the shadow cell in Fig.2.1). In vortex method, the vortices will move according to Lagrangian method. Because the vorticity is defined at mesh points in LVM, we must renew the vorticity distribution after each calculation time step. The mesh is applied to redistribute the vorticity. Therefore, the numbers of vortex are limited to equal of the numbers of mesh points in each calculation time step, so that the calculation speed is improved. We shall explain the vorticity redistrbution method in two-dimensional flow field.

For example, a vorticity Γ_n at mesh point P moved to position Q at the velocity at mesh point P after time step Δt, and the position Q is inside the ABCD mesh cell (Fig.2.2). The vorticity Γ_n at a new position Q will be allocated to the four surrounding mesh points A, B, C and D.

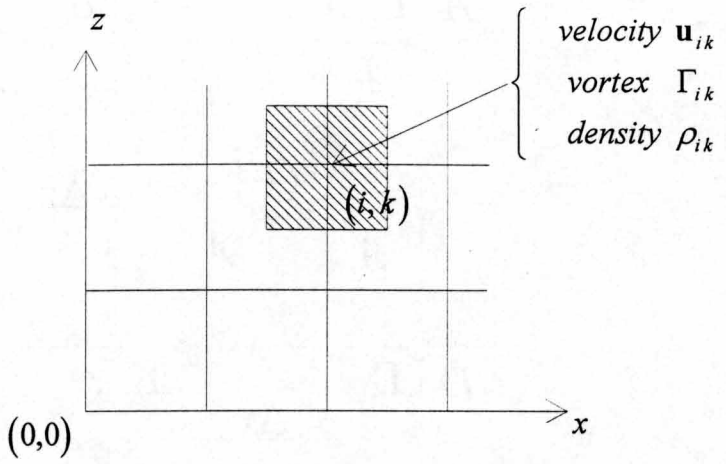

Fig.2.1 Definition of parameters in 2D lattice vortex method

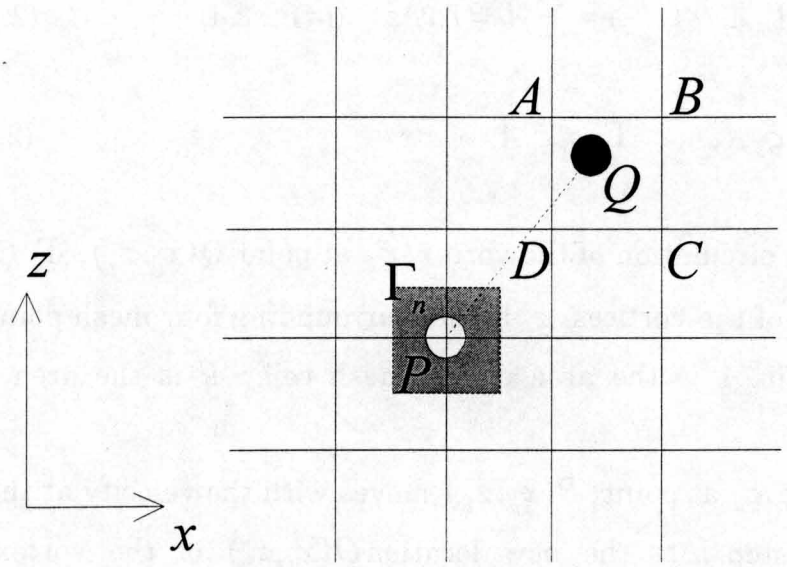

Fig.2.2 Vorticity moves by Lagrangian manner

In the distribution of first order accuracy, the vorticity at position Q will be distributed to mesh point A,B,C and D by the area weighting scheme (Fig.2.3). The vorticity at mesh point A,B,C and D is determined by Eq.2.1 and Eq.2.2.

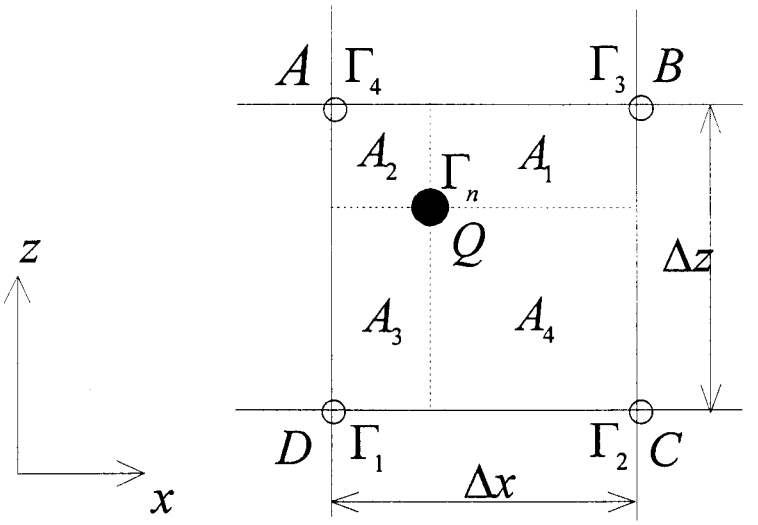

Fig. 2.3 Area weighting scheme for the distribution of vorticity

$$\Gamma_i = \Gamma_n A_i / A \quad A = \sum A_i = \Delta x \Delta z \quad \text{(i=1,2,3,4)} \tag{2.1}$$

$$\Gamma_n = \xi_n A, \qquad \Gamma_i = \xi_i A \tag{2.2}$$

where Γ_n is the circulation of the vortex ξ_n at point $Q(x_q, z_q)$. Γ_i (i=1,2,3,4) are the circulations of the vortices ξ_i at the surrounding four mesh points (A,B,C,D), respectively, and A is the area of the mesh cell. A_i is the area displayed in Fig.2.3.

The vortex ξ_n at point $P(x_p, z_p)$ moves with the velocity at the mesh point P. After time step Δt, the new location $Q(x_q, z_q)$ of the vortex ξ_n can be determined by Eq.2.3 and Eq.2.4.

$$x_q(t+\Delta t) = x_p(t) + u_p(t) * \Delta t \tag{2.3}$$

$$z_q(t+\Delta t) = z_p(t) + w_p(t) * \Delta t \tag{2.4}$$

where (u_p, w_p) is the velocity at point $P(x_p, z_p)$.

The coordinates of mesh point A,B,C and D are determined by Eq.2.5~Eq.2.8, respectively (here, we assume $\Delta x = \Delta z = 1$).

$$\begin{cases} x_a = \text{int}(x_q) \\ z_a = \text{int}(z_q) + 1 \end{cases} \tag{2.5}$$

$$\begin{cases} x_b = \text{int}(x_q) + 1 \\ z_b = \text{int}(z_q) + 1 \end{cases} \tag{2.6}$$

$$\begin{cases} x_c = \text{int}(x_q) + 1 \\ z_c = \text{int}(z_q) \end{cases} \tag{2.7}$$

$$\begin{cases} x_d = \text{int}(x_q) \\ z_d = \text{int}(z_q) \end{cases} \tag{2.8}$$

To determine Γ_i, A_i is calculated by Eq.2.9~Eq.2.12.

$$A_1 = [\Delta x - (x_q - x_d)] * [\Delta z - (z_q - z_d)] \tag{2.9}$$

$$A_2 = (x_q - x_d) * [\Delta z - (z_q - z_d)] \tag{2.10}$$

$$A_3 = (x_q - x_d) * (z_q - z_d) \tag{2.11}$$

$$A_4 = [\Delta x - (x_q - x_d)] * (z_q - z_d) \tag{2.12}$$

where (x_d, z_d) is location of mesh point D.

Therefore, Eq.2.1 and Eq.2.2 can be written as Eq.2.13~Eq.2.12.

$$\xi_1 = \frac{\{\Delta x - [(x_p + u_p \Delta t) - x_d]\}\{\Delta z - [(z_p + w_p \Delta t) - z_d]\}}{\Delta x \Delta z} \xi_n \tag{2.13}$$

$$\xi_2 = \frac{[(x_p + u_p\Delta t) - x_d]\{\Delta z - [(z_p + w_p\Delta t) - z_d]\}}{\Delta x \Delta z}\xi_n \tag{2.14}$$

$$\xi_3 = \frac{[(x_p + u_p\Delta t) - x_d][(z_p + w_p\Delta t) - z_d]}{\Delta x \Delta z}\xi_n \tag{2.15}$$

$$\xi_4 = \frac{\{\Delta x - [(x_p + u_p\Delta t) - x_d]\}[(z_p + w_p\Delta t) - z_d]}{\Delta x \Delta z}\xi_n \tag{2.16}$$

According to above method, each vortex is distributed to surrounding mesh points after each time step with first order accuracy.

In the second-order accurate distribution, the vorticity at new position Q will be distributed to mesh points A,B,C and D by volume weighting scheme (Fig.2.4). The vorticity at mesh point A,B,C and D is determined by Eq.2.17 and Eq.2.14.

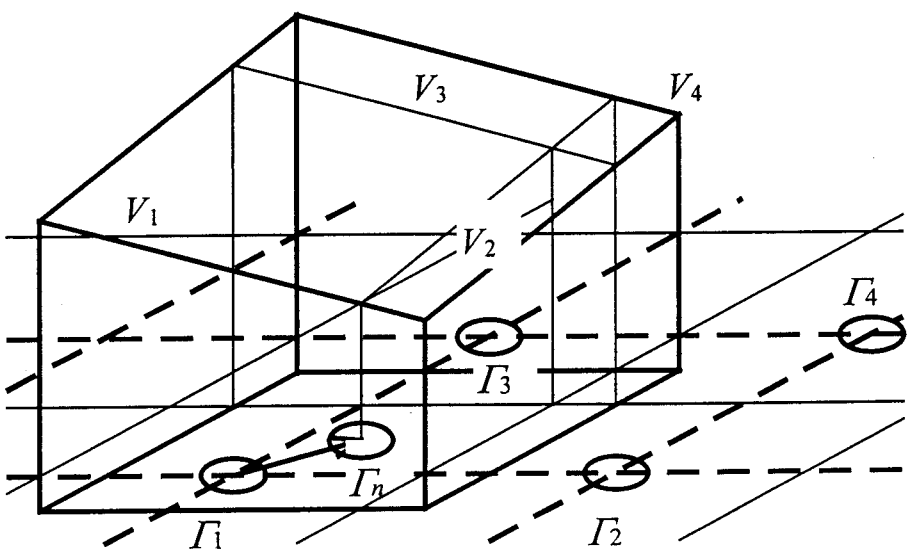

Fig.2.4 Volume weighting scheme for the distribution of vorticity

$$\Gamma_i = \frac{V_i}{V}\Gamma_n \qquad (i=1,2,3,4) \tag{2.17}$$

$$V = V_1 + V_2 + V_3 + V_4 = \Delta x \Delta z \Gamma_n \tag{2.18}$$

where V_i is the volume displayed in Fig.2.4.

The calculation of volume V_i is implemented as follows. We consider the distribution of vorticity $\Gamma_{i,k}$ at time t, which represents the distribution on the area centered by point (i,k). Instead of the uniform vorticity distribution method, The slope distribution is used (Fig.2.5). The slope plane of vorticity distribution at the cell around vorticty $\Gamma_{i,k}$ is determined by the gradients of vorticy at x direction and that at z direction between the nearest two points.

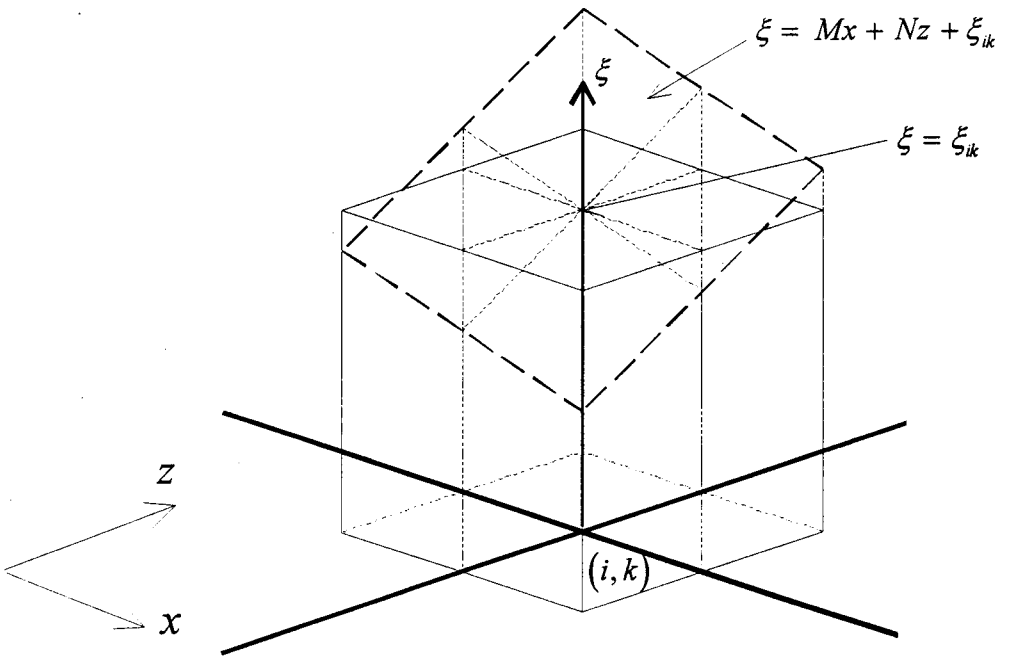

Fig.2.5 Slope distribution of vorticity

The vorticity distribution in the cell is described by Eq.2.19 (for simplicity, here we take $\Delta x = 1$ and $\Delta z = 1$).

$$\xi = Mx + Nz + \xi_{i,k} \quad (i - \frac{1}{2} \le x \le i + \frac{1}{2}, k - \frac{1}{2} \le z \le k + \frac{1}{2}) \tag{2.19}$$

where coefficients $M = \frac{\xi_{i+1,k} - \xi_{i-1,k}}{2}$ and $N = \frac{\xi_{i,k+1} - \xi_{i,k-1}}{2}$,respectively.

Therefore, there is the relation Eq.2.20 for vorticicty $\Gamma_{i,k}$.

$$\Gamma_{i,k} = \int_{k-\frac{1}{2}}^{k+\frac{1}{2}} \int_{i-\frac{1}{2}}^{i+\frac{1}{2}} \xi \, dx \, dz = \int_{k-\frac{1}{2}}^{k+\frac{1}{2}} \int_{i-\frac{1}{2}}^{i+\frac{1}{2}} (Mx + Nz + \xi_{i,k}) \, dx \, dz = \xi_{i,k} \Delta x \Delta z \tag{2.20}$$

When vorticity $\Gamma_{i,k}$ moves with the velocity $(u_{i,k}, w_{i,k})$ at point (i,k), we consider that it is equal to move the cubic volume with slope top plane displayed in Fig.2.5 at the velocity $(u_{i,k}, w_{i,k})$. After time step Δt, The vorticity volume will move by distance $u_{i,k}\Delta t$ at x direction and distance $w_{i,k}\Delta t$ at z direction, respectively. The center of the vorticity volume will move to $(i + u_{i,k}\Delta t, k + w_{i,k}\Delta t)$ from (i,k). Therefore, The vorticity volume is located on the shaded region in Fig.2.6 after time step Δt (for simple, we think $u_{i,k}\Delta t < 1$ and $w_{i,k}\Delta t < 1$). The equation describing slope top plane of vorticity volume is changed to Eq.2.21.

$$\xi' = M(x - u_{i,k}\Delta t) + N(z - w_{i,k}\Delta t) + \xi_{i,k} \tag{2.21}$$

$$\left(i - \frac{1}{2} + u_{i,k}\Delta t \le x \le i + \frac{1}{2} + u_{i,k}\Delta t, \; k - \frac{1}{2} + w_{i,k}\Delta t \le z \le k + \frac{1}{2} + w_{i,k}\Delta t \right)$$

where coefficients $M = \frac{\xi_{i+1,k} - \xi_{i-1,k}}{2}$ and $N = \frac{\xi_{i,k+1} - \xi_{i,k-1}}{2}$,respectively.

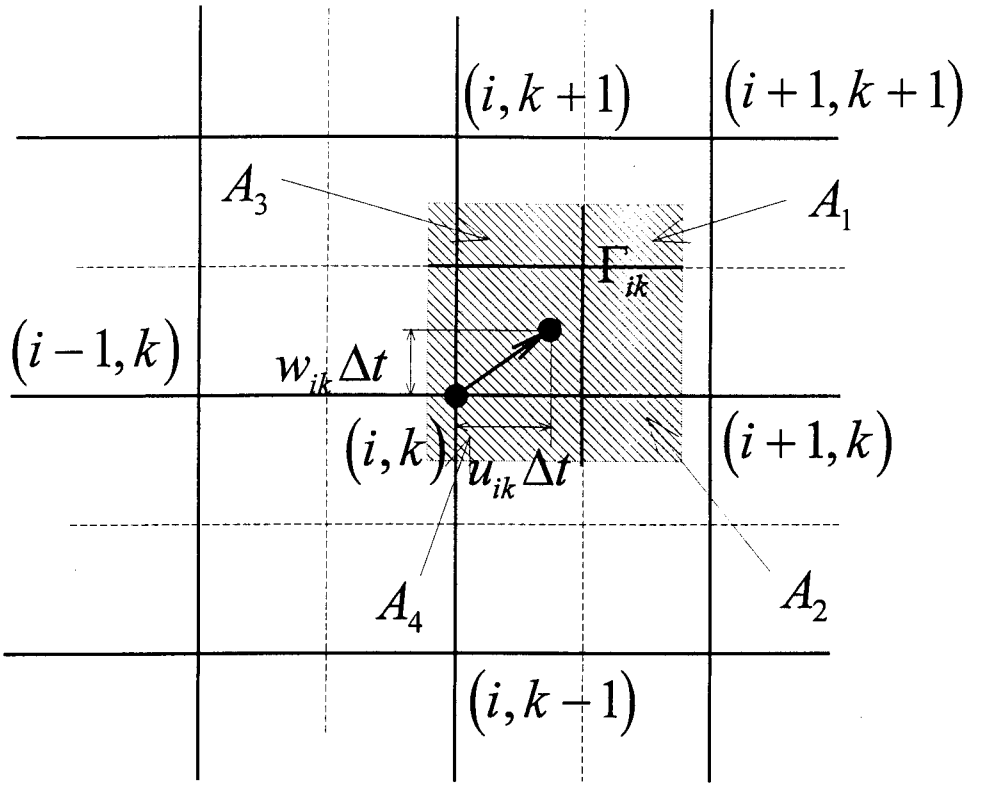

Fig.2.6 New location of vorticity volume after time step Δt

After moving, the vorticity $\Gamma_{i,k}$ will be distributed to surrounding four point $(i,k),(i+1,k),(i,k+1)$ and $(i+1,k+1)$ by Eq.2.22 ~Eq.2.31

$$\Gamma'_{i,k} = \int_{k-\frac{1}{2}+w_{ik}\Delta t}^{k+\frac{1}{2}} \int_{i-\frac{1}{2}+u_{ik}\Delta t}^{i+\frac{1}{2}} \xi' dxdz = \left(\xi_{i,k} - \frac{u_{ik}\Delta t}{2} M - \frac{w_{ik}\Delta t}{2} N \right) A_1 \qquad (2.22)$$

$$\Gamma'_{i+1,k} = \int_{k-\frac{1}{2}+w_{ik}\Delta t}^{k+\frac{1}{2}} \int_{i+\frac{1}{2}}^{i+\frac{1}{2}+u_{ik}\Delta t} \xi' dxdz = \left(\xi_{i,k} + \frac{1-u_{i,k}\Delta t}{2} M - \frac{w_{i,k}\Delta t}{2} N \right) A_2 \qquad (2.23)$$

$$\Gamma'_{i,k+1} = \int_{k+\frac{1}{2}}^{k+\frac{1}{2}+w_{ik}\Delta t} \int_{i-\frac{1}{2}+u_{ik}\Delta t}^{i+\frac{1}{2}} \xi' dxdz = \left(\xi_{i,k} - \frac{u_{i,k}\Delta t}{2} M + \frac{1-w_{i,k}\Delta t}{2} N \right) A_3 \qquad (2.24)$$

$$\Gamma'_{i+1,k+1} = \int_{k+\frac{1}{2}}^{k+\frac{1}{2}+w_{ik}\Delta t} \int_{i+\frac{1}{2}}^{i+\frac{1}{2}+u_{ik}\Delta t} \xi' dxdz = \left(\xi_{i,k} + \frac{1-u_{i,k}\Delta t}{2} M + \frac{1-w_{i,k}\Delta t}{2} N \right) A_4 \quad (2.25)$$

$$\Gamma_{i,k} = \Gamma'_{i,k} + \Gamma'_{i+1,k} + \Gamma'_{i,k+1} + \Gamma'_{i+1,k+1} \quad (2.26)$$

$$A_1 = (1-u_{i,k}\Delta t)(1-w_{i,k}\Delta t)A \quad (2.27)$$

$$A_2 = u_{i,k}\Delta t(1-w_{i,k}\Delta t)A \quad (2.28)$$

$$A_3 = (1-u_{i,k}\Delta t)w_{i,k}\Delta tA \quad (2.29)$$

$$A_4 = u_{i,k}\Delta t w_{i,k}\Delta tA \quad (2.30)$$

$$A = \sum A_i \quad (i = 1,2,3,4) \quad (2.31)$$

From above, we know that the volume weighing scheme becomes area weighing scheme when $M = N = 0$, which means vorticity distribution is uniform in the cell centered by mesh point.

2.2.2 Distribution of density in 2D lattice vortex method

Because we shall extend the application of LVM to stratified fluid flows, we discuss the distribution of density here. In the lattice vortex method, we also consider that the density at a mesh point represents the density distributed in the cell around this mesh point (the shadow cell in Fig.2.1). The density at a mesh point also moves according to Largragian method. After moving, the density is also redistributed by area weighting scheme or volume weighting scheme, same as that used in redistribution of vorticity.

We can obtain the equations of density distribution in the same way as the discussion for vorticity redistribution, replacing vorticity Γ with density ρ in the equations of vorticity distribution.

In the distribution of first-order accurate area scheme, the density is redistributed according to Eq.2.32

$$\rho_i = \rho_n A_i / A, \quad A = \sum A_i = \Delta x \Delta z \quad \text{(i=1,2,3,4)} \tag{2.32}$$

where ρ_n is the density at point $Q(x_q, z_q)$. ρ_i (i=1,2,3,4) are the density at the surrounding four mesh points (A,B,C,D), respectively. A is the area of the mesh cell (see Fig.2.3). A_i (i=1,2,3,4) is also calculated by Eq.2.9~Eq.2.12.

In the distribution of second-order accurate volume scheme, the density is redistributed according to Eq.2.33~Eq.2.36 as

$$\rho'_{i,k} = \left(\rho_{i,k} - \frac{u_{i,k}\Delta t}{2} M - \frac{w_{i,k}\Delta t}{2} N \right) A_1 \tag{2.33}$$

$$\rho'_{i+1,k} = \left(\rho_{i,k} + \frac{1-u_{i,k}\Delta t}{2} M - \frac{w_{i,k}\Delta t}{2} N \right) A_2 \tag{2.34}$$

$$\rho'_{i,k+1} = \left(\rho_{i,k} - \frac{u_{i,k}\Delta t}{2} M + \frac{1-w_{i,k}\Delta t}{2} N \right) A_3 \tag{2.35}$$

$$\rho'_{i+1,k+1} = \left(\rho_{i,k} + \frac{1-u_{i,k}\Delta t}{2} M + \frac{1-w_{i,k}\Delta t}{2} N \right) A_4 \tag{2.36}$$

where coefficients $M = \frac{\rho_{i+1,k} - \rho_{i-1,k}}{2}$, $N = \frac{\rho_{i,k+1} - \rho_{i,k-1}}{2}$, and A_i (i=1,2,3,4) are also calculated by Eq.2.27~Eq.2.30.

2.2.3 Velocity calculation in 2D lattice vortex method

The velocity field induced by vortices is determined by Bio-Savart law. The induced velocity at a mesh point is inverse proportion to the distance between this point and vortex, and direct proportion to the strength of the vortex (Eq.2.37)

$$|\mathbf{u}| = \frac{1}{2\pi}\frac{\Gamma}{r} \tag{2.37}$$

where Γ is the strength of vortex, r is the distance between a mesh point and the vortex, and u is the velocity induced by vortex (Fig.2.7).

In calculation, the velocity field is determined by Eq.2.38

$$\begin{cases} u_i = -\dfrac{1}{2\pi}\displaystyle\sum_{j=1}^{M}\frac{\Gamma_j(z_i - z_j)}{(x_i - x_j)^2 + (z_i - z_j)^2} \\ w_i = \dfrac{1}{2\pi}\displaystyle\sum_{j=1}^{M}\frac{\Gamma_j(x_i - x_j)}{(x_i - x_j)^2 + (z_i - z_j)^2} \end{cases} \tag{2.38}$$

where u_i, w_i are the velocity components in x and z direction at point(x_i, z_i), respectively. Γ_j is the circulation of the vortex at point(x_j, z_j), M is the total number of vortices.

In lattice vortex method, the vorticity and velocity are defined at the mesh points, which limited the number of vortex in all calculation and overcame the problem that the number of vortex increases with calculation time step development in discrete vortex method. The position relation between vortices and velocity calculation points is determined by the fix mesh. In our calculation, the regular Eulerian mesh (1×1) is used. It is easy to make a look-up-table memorizing the distance between vortex and velocity calculation point. We can use this look-up-table to improve the calculation speed. The look-up-table is explained as follow.

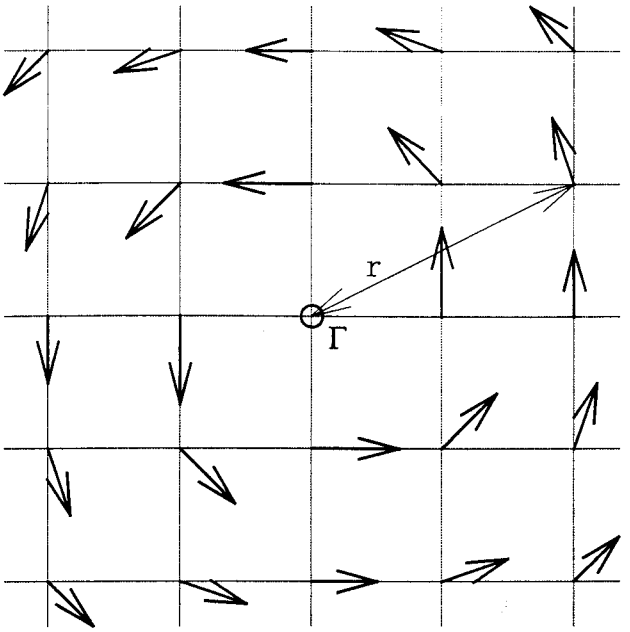

Fig.2.7 Velocity induced by vortex

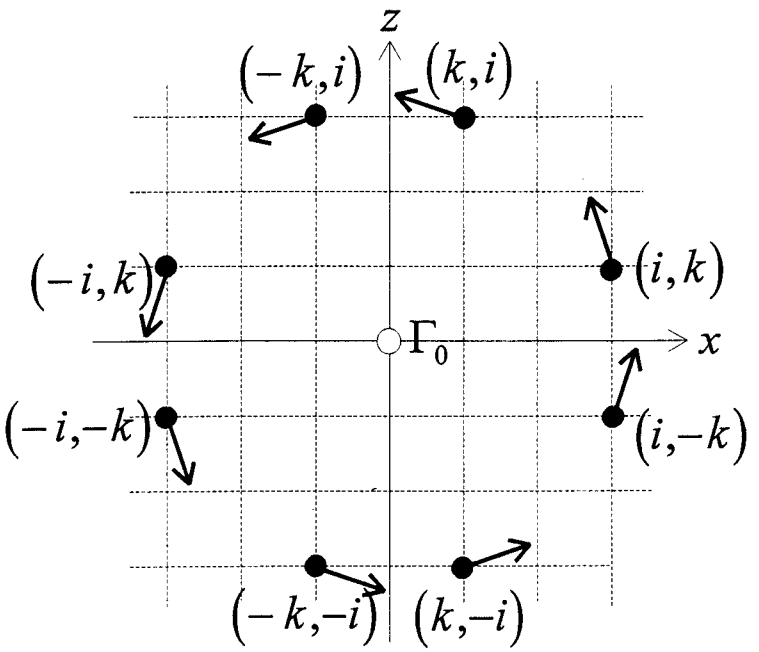

Fig.2.8 Definition of look-up-table

For example, if there is a vortex Γ_0 at point $(0,0)$ (Fig.2.8), the velocity at mesh point $(i,k),(-i,k),(i,-k),(-i,-k),(k,i),(-k,i),(k,-i)$ and $(-k,-i)$ can be calculated by Eq.2.39 and Eq.2.40.

$$\begin{aligned} u_{(i,k)} &= u_{(-i,k)} = -u_{(i,-k)} = -u_{(-i,-k)} \\ &= -w_{(k,i)} = w_{(-k,i)} = -w_{(k,-i)} = w_{(-k,-i)} \\ &= \left(-\frac{1}{2\pi} \underline{\underline{\frac{k}{i^2+k^2}}} \right) \Gamma_0 \end{aligned} \tag{2.39}$$

$$\begin{aligned} w_{(i,k)} &= -w_{(-i,k)} = w_{(i,-k)} = -w_{(-i,-k)} \\ &= -u_{(k,i)} = -u_{(-k,i)} = u_{(k,-i)} = u_{(-k,-i)} \\ &= \left(\frac{1}{2\pi} \underline{\underline{\frac{i}{i^2+k^2}}} \right) \Gamma_0 \end{aligned} \tag{2.40}$$

The value of the part with double line in the bracket of Eq.2.39 and Eq.2.40 will be stored in look-up-table. In calculating the velocity, we can simply read the look-up-table according to the position relation between the vortex and velocity calculation point to get the value in the bracket of Eq.2.39 and Eq.2.40, which avoid the calculation of necessary distance in velocity calculation. Multiplying the strength of the vorticity we can get the velocity induced by the vortex at any mesh points. Using the symmetry of the regular mesh, we can get the velocity at eight points in one time calculation. Therefore, we can save much CPU time in calculation by using the look-up-table and the symmetry of regular mesh.

2.3 Lattice vortex method in three-dimensional flows

2.3.1 Principle of 3D lattice vortex method

In 3D lattice vortex method, the calculation region is divided by regular cubic mesh. For simplicity, the regular cubic mesh $(1\times1\times1)$ is used in our calculation. Density and velocity is defined at the mesh points, and vortex circulation is defined on cube surfaces. The definition of density and vortex circulation will be explained in detail as follow.

2.3.1.1 Definition of density in 3D lattice vortex method

In 3D lattice vortex method, density is defined at the mesh points. The density at a mesh point represents the density uniformly distributed in the cubic cell centered by this mesh point (shadowed volume in Fig.2.9). When the density at a mesh point moves, we think that it is equal to the density distributed in the shadow cell moves.

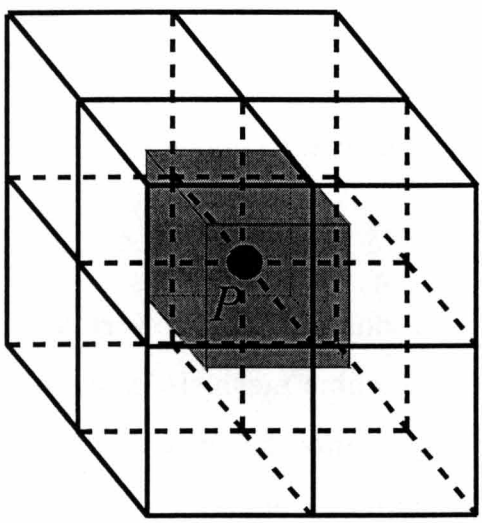

Fig.2.9 Definition of density on grid

2.3.1.2 Definition of vortex circulation in 3D lattice vortex method

In 3D lattice vortex method, for improving the calculation speed and limiting the numbers of vortex ring, vortex ring is only defined on each surface of cubic mesh. Therefore, there are three kinds of vortex rings, which are the vortex ring in x direction, the vortex ring in y direction and the vortex ring in z direction, respectively (Fig.2.10).

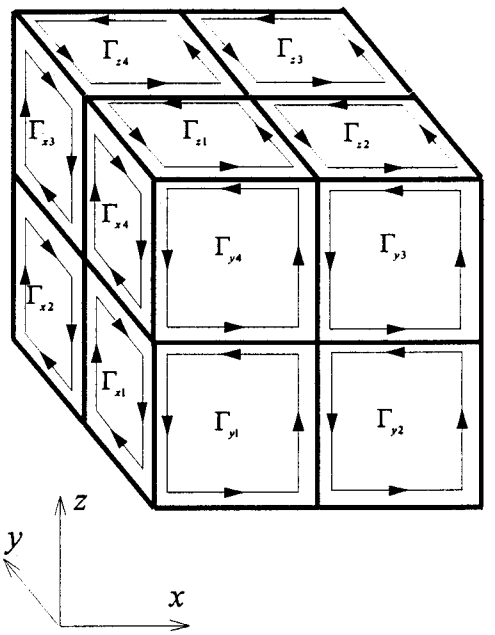

Fig.2.10 Definition of vortex ring on the surfaces of cubic mesh

For simplification, we consider that the vortex ring is formed by four vortex sticks located on the sides of cubic mesh. In calculation, the direction of vortex ring shown in Fig.2.11(a) represents the positive direction of each vortex ring. The relation between vortex ring and vortex stick is displayed in Fig.2.11(b)(c)(d).

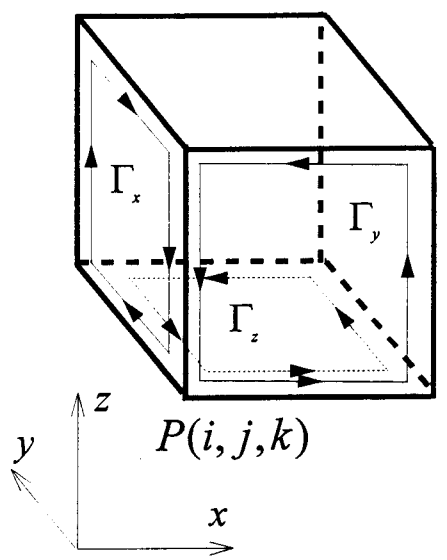

(a) Positive direction of vortex ring

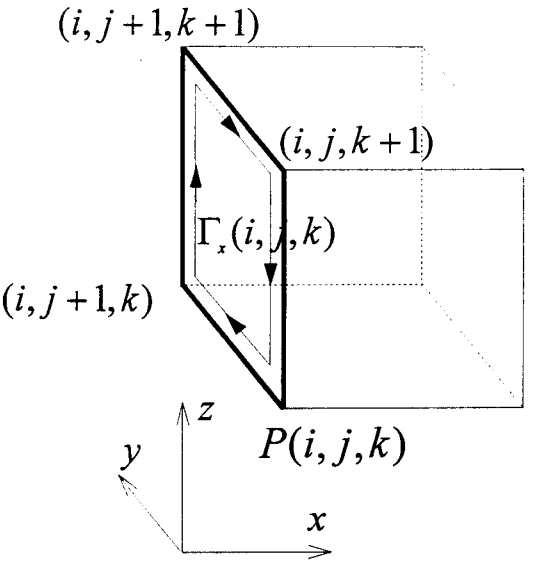

(b) Vortex ring in x direction

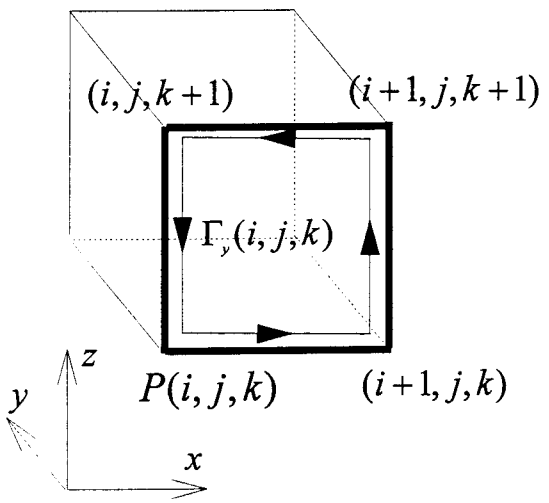

(c) Vortex ring in y direction

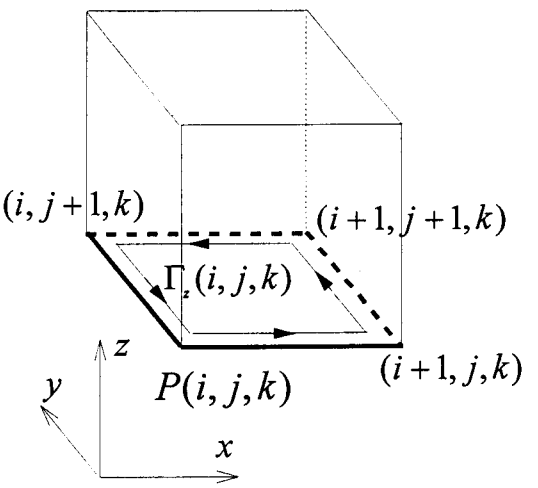

(d) Vortex ring in z direction

Fig.2.11 Definition of the coordinate of vortex rings

According to the definition of vortex ring, there are three kinds of vortex stick at one mesh point, which is the vortex stick in x direction, the vortex stick in y direction and the vortex stick in z direction, respectively (Fig.2.12). The strength of vortex stick at an edge of cubic mesh is considered as a set of four vortex sticks distributed by the vortex ring around this edge (Fig.2.13). The vortex stick at an edge of the cubic mesh represented by its direction and the coordinate of its beginning point.

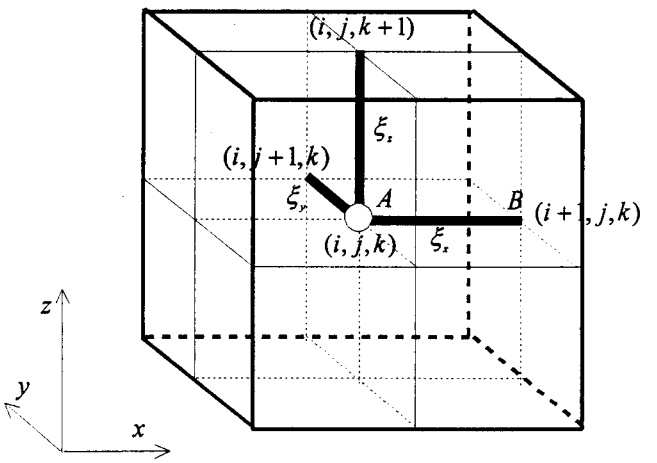

Fig.2.12 Definition of vortex stick

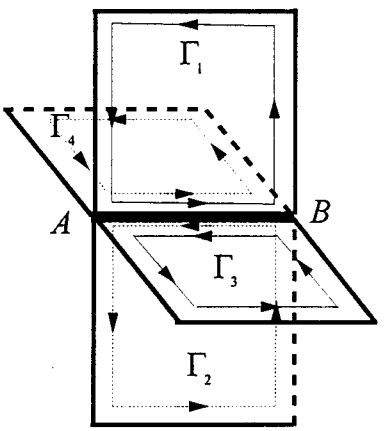

Fig.2.13 Definition of vortex stick on an edge of cubic mesh

2.3.2 Distribution of density and vorticity in 3D lattice vortex method

In 3D lattice vortex method, the density and vorticity moves according to Largrangian method, and they are defined at cubic mesh points. Therefore, after their movement, density and vorticity must be distributed to cubic mesh points. The distribution method is explained as follow.

2.3.2.1 Distribution of density in 3D lattice vortex method

According to Lagrangian method, the density defined at a cubic mesh point moves at the velocity on this mesh point. Because the density at a cubic mesh point represents the mass density distributed in a cube centered by this cubic mesh point, we can use volume distribution method to distribute this density to the surrounding eight points.

For example, we consider that the density ρ_0 at a mesh point $P(x_p, y_p, z_p)$ moves at the velocity $(u_p(t), v_p(t), w_p(t))$. After a time step Δt, ρ_0 moved to new position $Q(x_q, y_q, z_q)$ (Fig.2.14).

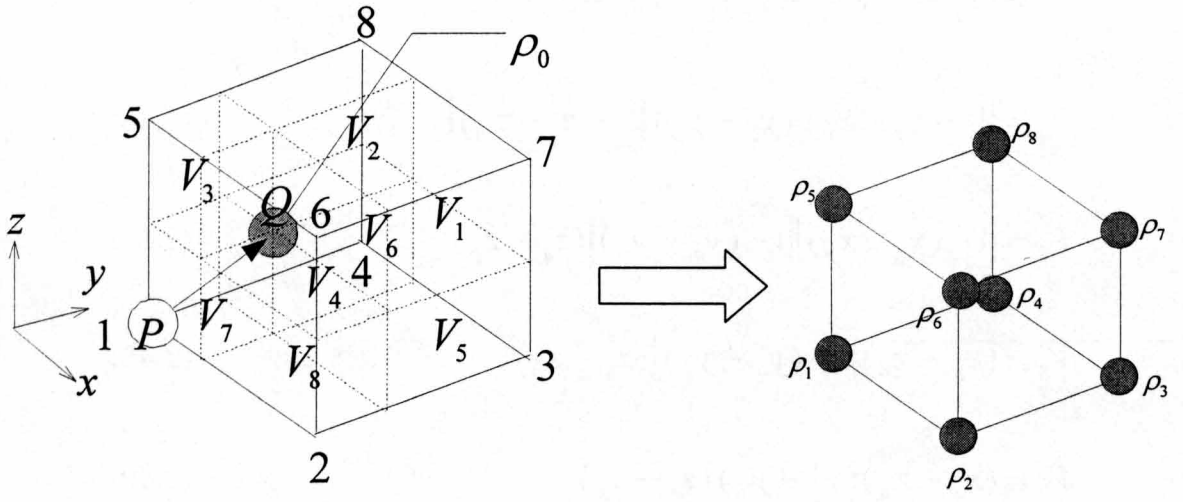

Fig.2.14 Distribution of density in 3D lattice vortex method

The new position of the density ρ_0 is determined by Eq.2.41

$$\begin{cases} x_q = x_p + u_p(t)\Delta t \\ y_q = y_p + v_p(t)\Delta t \\ z_q = z_p + w_p(t)\Delta t \end{cases} \tag{2.41}$$

where $(u_p(t), v_p(t), w_p(t))$ is the velocity at mesh point $P(x_p, y_p, z_p)$ at time t.

Then the density moved to position $Q(x_q, y_q, z_q)$ is distributed to the surrounding eight mesh points by volume scheme. The densities distributed to eight mesh points are calculated by Eq.2.42~Eq.2.50

$$\rho_i = \rho_0 \frac{V_i}{V} \tag{2.42}$$

$$\rho_0 = \sum \rho_i \qquad V = \sum V_i \qquad (i = 1 \sim 8)$$

$$V_1 = [1-(x_q - x_p)][1-(y_q - y_p)][1-(z_q - z_p)] \tag{2.43}$$

$$V_2 = (x_q - x_p)[1-(y_q - y_p)][1-(z_q - z_p)] \tag{2.44}$$

$$V_3 = (x_q - x_p)(y_q - y_p)[1-(z_q - z_p)] \tag{2.45}$$

$$V_4 = [1-(x_q - x_p)](y_q - y_p)[1-(z_q - z_p)] \tag{2.46}$$

$$V_5 = [1-(x_q - x_p)][1-(y_q - y_p)](z_q - z_p) \tag{2.47}$$

$$V_6 = (x_q - x_p)[1-(y_q - y_p)](z_q - z_p) \tag{2.48}$$

$$V_7 = (x_q - x_p)(y_q - y_p)(z_q - z_p) \tag{2.49}$$

$$V_8 = [1-(x_q - x_p)](y_q - y_p)(z_q - z_p) \tag{2.50}$$

2.3.2.2 Distribution of vortex ring in 3D lattice vortex method

In 3D lattice vortex method, the vortex ring is defined on each surface of cubic mesh, and we assume that the vortex ring is formed by four vortex sticks. Therefore, the movement of a vortex ring can be described by the movement of the four vortex sticks.

For example, we consider the movement of vortex ring Γ_a on the cubic mesh surface $(A-B-C-D)$, which is in the x_1x_2 plane (Fig.2.15(a)). The movement of vortex ring Γ_a can be replace by the movement of vortex stick AB, vortex stick BC, vortex stick CD and vortex stick DA. Here we focus our discussion on the movement of vortex stick BC. If the velocity at cubic mesh point B and point C is $(u_B(t),v_B(t),w_B(t))$ and $(u_C(t),v_C(t),w_C(t))$, respectively. The vortex stick BC will move at the velocity $\left(\frac{u_B(t)+u_C(t)}{2},\frac{v_B(t)+v_C(t)}{2},\frac{w_B(t)+w_C(t)}{2}\right)$.

Firstly, we discuss the case of $\left(\frac{u_B(t)+u_C(t)}{2}=0\right)$, which is displayed in Fig.2.15(b).

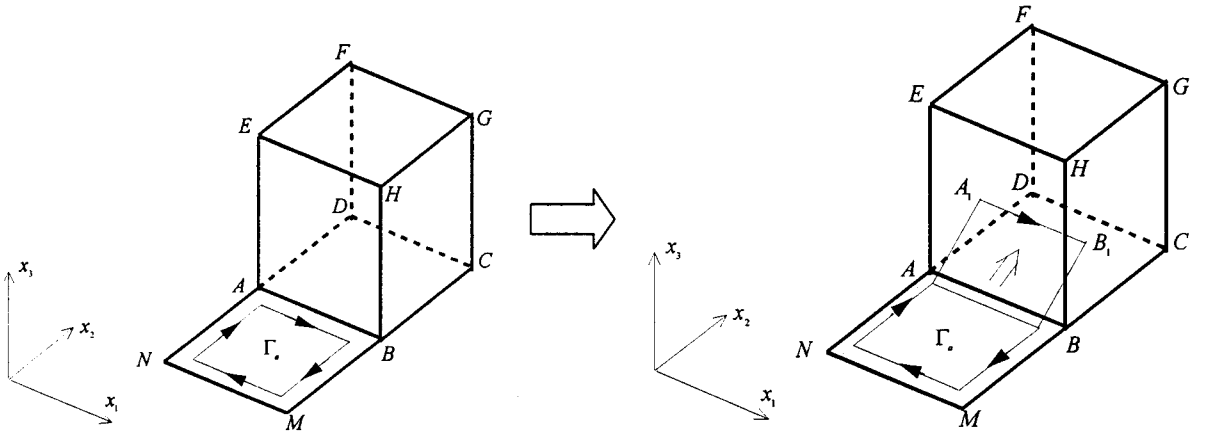

(a) (b)

Fig.2.15 Movement of vortex ring

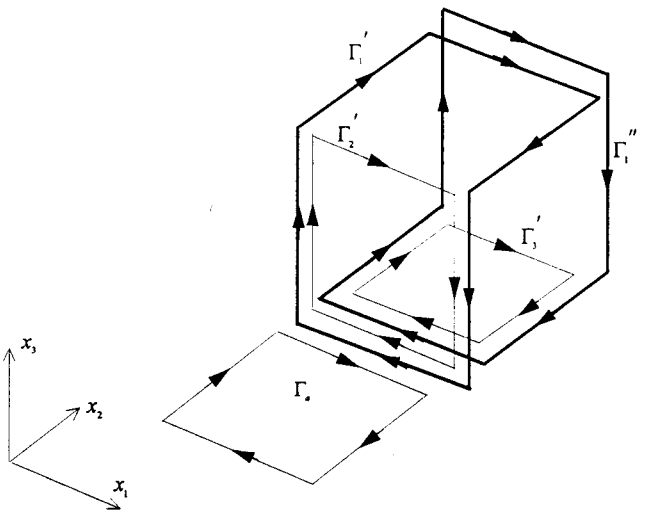

Fig.2.16 Distribution of vortex ring

When vortex ring moves like displayed in Fig.2.15(b), The extending part $(A-B-B_1-A_1)$ of vortex ring Γ_a will be distributed on surrounding cubic mesh surface $(B-G-H-I-J-C-B),(B-E-H-I-J-C-B),(B-G-J-C-B)$ and $(B-E-F-C-B)$ with vortex ring $\Gamma_1',\Gamma_1'',\Gamma_2'$ and Γ_3' (Fig.2.16).

In following, we discuss the calculation method of vortex ring $\Gamma_1',\Gamma_1'',\Gamma_2'$ and Γ_3'. When vortex stick moved from AB to A_1B_1 according to Lagrangian method (Fig.2.17), the vortex stick A_1B_1 will be distributed to surrounding cubic mesh edge AB,CD,GF and HE using vortex volume distribution scheme (Fig.2.18).

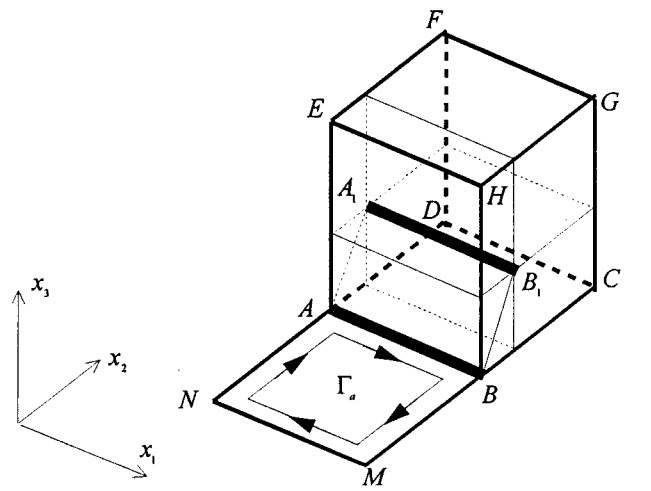

Fig.2.17 Movement of vortex stick

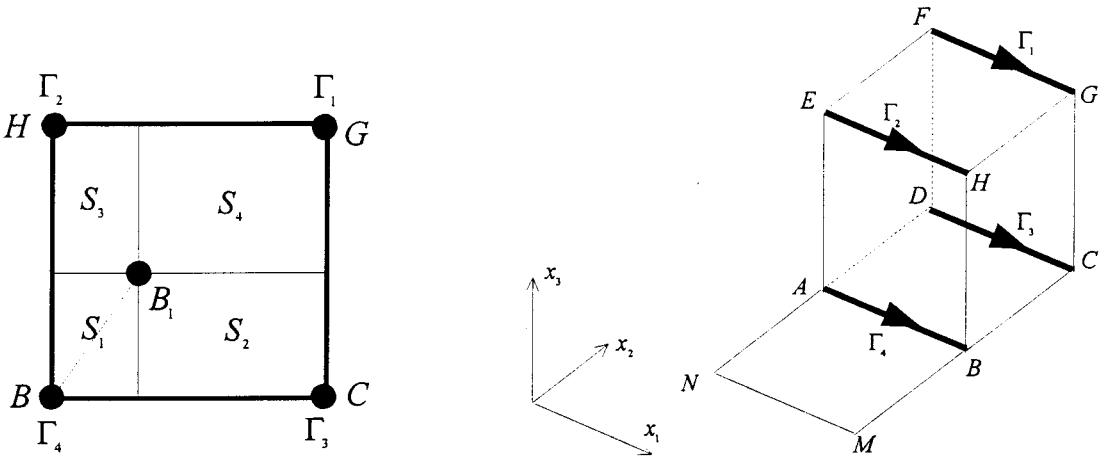

Fig.2.18 Distribution of vortex stick

Therefore, the strength of vortex stick at cubic mesh edge AB, CD, GF and HE is calculated by Eq.2.51~Eq.2.55

$$\Gamma_i = \Gamma_a \frac{S_i}{S} \qquad \Gamma_a = \sum \Gamma_i \qquad S = \sum S_i = 1 \qquad (i = 1 \sim 4) \tag{2.51}$$

$$S_1 = \left(\frac{u_B + u_C}{2} \Delta t \right) \left(\frac{v_B + v_C}{2} \Delta t \right) \tag{2.52}$$

$$S_2 = \left(1 - \frac{u_B + u_C}{2} \Delta t \right) \left(\frac{v_B + v_C}{2} \Delta t \right) \tag{2.53}$$

$$S_3 = \left(\frac{u_B + u_C}{2} \Delta t \right) \left(1 - \frac{v_B + v_C}{2} \Delta t \right) \tag{2.54}$$

$$S_4 = \left(1 - \frac{u_B + u_C}{2} \Delta t \right) \left(1 - \frac{v_B + v_C}{2} \Delta t \right) \tag{2.55}$$

where (u_B, v_B, w_B) and (u_C, v_C, w_C) is the velocity at mesh point B and C, respectively, Δt is the time increment, and we assume $w_B = w_C = 0$ here.

According to the distrbution method displayed in Fig.2.16, there are the following equations.

$$\begin{cases} \Gamma_1 = \Gamma_1' + \Gamma_1'' \\ \Gamma_2 = \Gamma_2' \\ \Gamma_3 = \Gamma_3' \\ \Gamma_4 = \Gamma_a - \Gamma_1' - \Gamma_1'' - \Gamma_2' - \Gamma_3' \end{cases} \tag{2.56}$$

For determining Γ_1' and Γ_1'', we assume that there is the relation Eq.2.57 and Eq.2.58

$$\Gamma_1' = \frac{\Gamma_2}{\Gamma_2 + \Gamma_3}\Gamma_1 \tag{2.57}$$

$$\Gamma_1'' = \frac{\Gamma_3}{\Gamma_2 + \Gamma_3}\Gamma_1 \tag{2.58}$$

Therefore, the strength of vortex stick on each edge of cubic mesh can be determined by Eq.2.51~Eq.2.58. After the move of vortex ring Γ_a, vortex stick on each edge of cubic mesh is displayed in Fig.2.19.

In generally, we discuss the case of $\left(\frac{u_B(t) + u_C(t)}{2} \neq 0\right)$, which is displayed in Fig.2.20. In this case, after Lagrangian movement, the new position A_1B_1 of vortex stick AB will be inside two cubic meshes. If $|A_1Q| = k$, $|QB_1| = l$, and $|A_1B_1| = k + l$, there are $\Gamma_{A_1Q} = \frac{k}{k+l}\Gamma_a$ and $\Gamma_{QB_1} = \frac{l}{k+l}\Gamma_a$, where $l = \left(\frac{u_B(t) + u_C(t)}{2}\right)\Delta t$, $k + l = 1$.

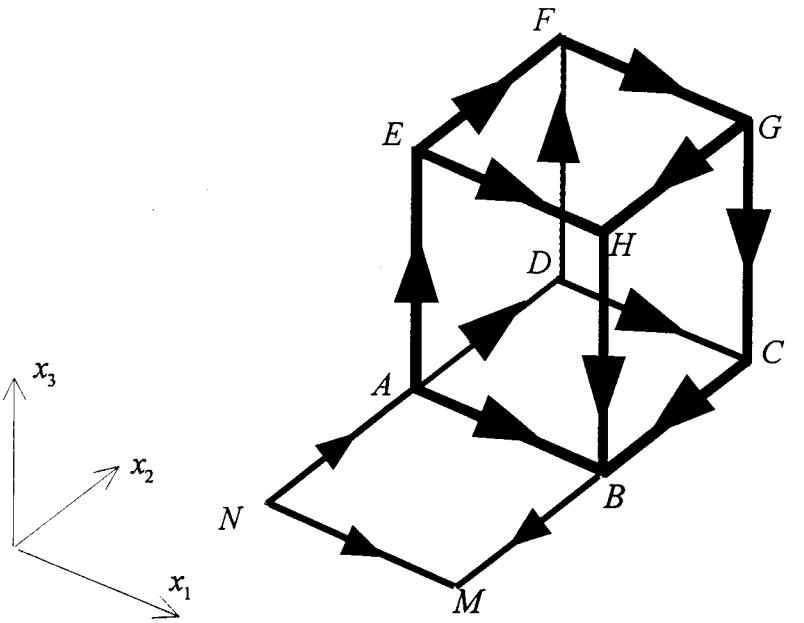

Fig.2.19 Vortex stick on each edge of a cubic mesh after distribution

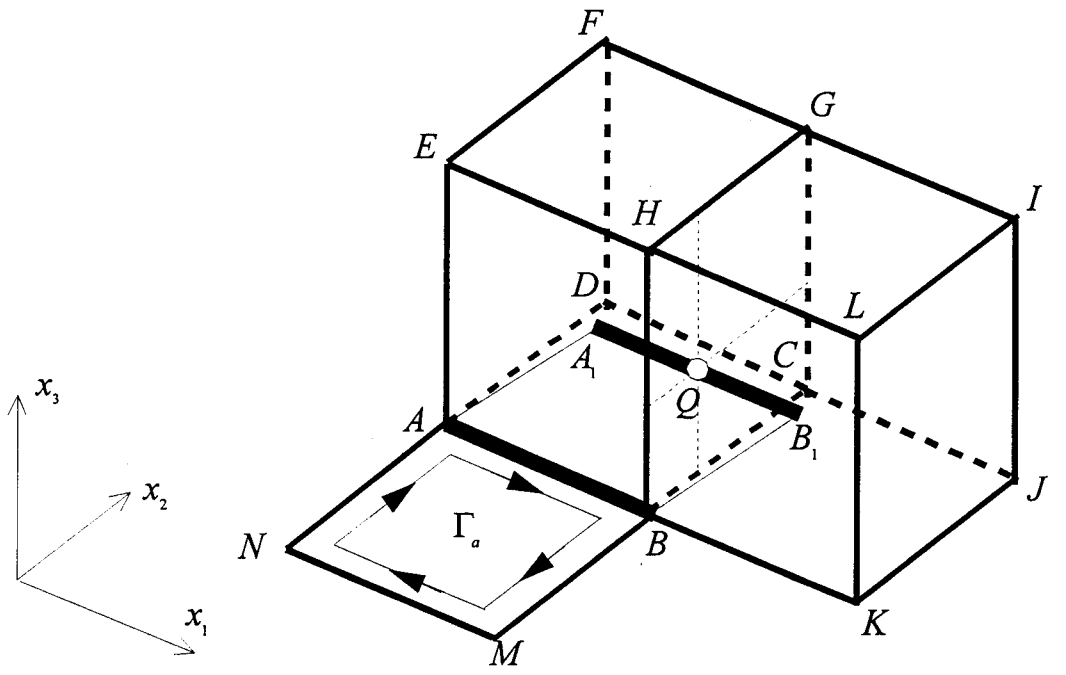

Fig.2.20 Vortex ring moves between two cubic mesh

Then, using the distribution method displayed above, we can distribute Γ_{A_1Q} in cubic mesh $(A-B-C-D-E-F-G-H)$ and Γ_{QB_1} in cubic mesh $(B-K-J-C-H-L-I-G)$, respectively.

2.3.3 Velocity calculation in 3D lattice vortex method

In 3D lattice vortex method, the calculation region is divided by regular cubic mesh. Vortex ring is defined on each surface of cubic mesh, and we assumed that each vortex ring is formed by four vortex sticks which located on each edge of cubic mesh. Therefore, the velocity field can be decided through calculating the velocity induced by all vortex sticks using Biot-Savart law.

In the following, we will show the calculation method of velocity field induced by vortex sticks. Firstly, we consider the calculation of velocity induced by a finite length vortex stick AB (Fig.2.21). P is velocity calculation point, which has the distance h from vortex stick AB. The strength of vortex stick AB is Γ.

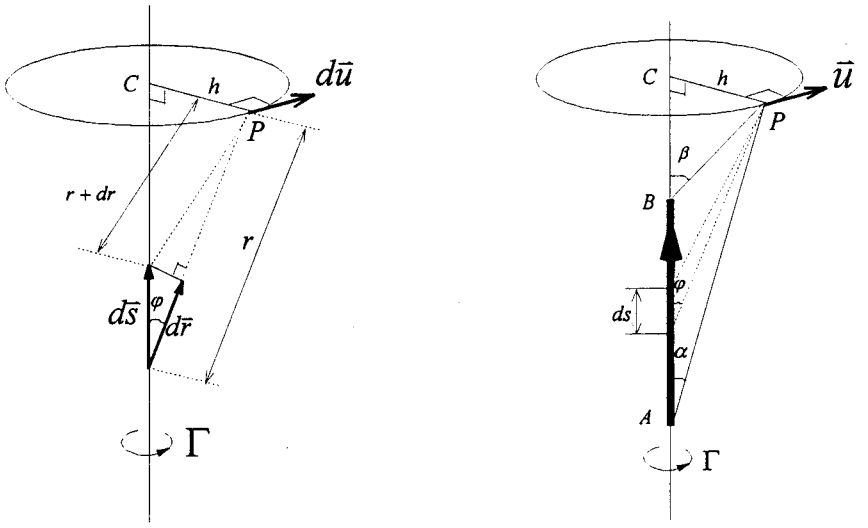

(a) (b)

Fig.2.21 Velocity induced by a vortex stick with finite length

From Biot-Savart law, we have Eq.2.59.

$$d\vec{u} = \frac{\Gamma}{4\pi}\frac{d\vec{S} \times \vec{r}}{r^3} \tag{2.59}$$

Because $d\vec{S} \times \vec{r} = ds \bullet r\sin\varphi$, we obtain

$$du = \frac{\Gamma}{4\pi}\frac{\sin\varphi}{r^2}ds \tag{2.60}$$

From Fig.2.21(b), we have

$$r = \frac{h}{\sin\varphi}\ ,\ ds = -\frac{dr}{\cos\varphi}. \tag{2.61}$$

$$dr = -\frac{h\cos\varphi}{\sin^2\varphi}d\varphi,\ ds = -\frac{h}{\sin^2\varphi}d\varphi \tag{2.62}$$

So that, Eq.2.60 can be written as

$$du = \frac{\Gamma}{4\pi}\frac{\sin\varphi}{h}d\varphi \tag{2.63}$$

Therefore, the velocity at point P induced by a finite length vortex stick AB can be calculated as follows.

$$u = \frac{\Gamma}{4\pi h}\int_{AB}\sin\varphi d\varphi = \frac{\Gamma}{4\pi h}\int_{\alpha}^{\beta}\sin\varphi d\varphi \tag{2.64}$$

$$\left|\vec{u}\right| = \left|\frac{\Gamma}{4\pi h}(\cos\alpha - \cos\beta)\right| \tag{2.65}$$

In 3D lattice vortex method, regular cubic mesh is used, and the vortex stick is defined each edge of cubic mesh. In our calculation, the regular cubic mesh $(1\times1\times1)$ is used. Therefore, the length of all vortex stick is equal to the length of edge of cubic mesh, and the direction of vortex stick is limited in x, y, z direction. According to the relation between cubic mesh points and vortex stick on edges of cubic mesh, we can simplify the calculation of velocity field induced by vortex sticks. To improve the calculation speed, we can make a look-up-table to remember the necessary distances, which must be used in calculating the velocity. In the following, we explain how to make the look-up-table.

In 3D lattice vortex method, vortex sticks are distributed on each edge of cubic mesh. In calculating velocity field, the direction of vortex stick must be considered. In general, we use coordinate x_1, x_2, x_3 to replace coordinate x, y, z. Here we focus our discussion on the calculation of velocity induced by the vortex stick AB, which parallels to coordinate x_1 (Fig.2.22).

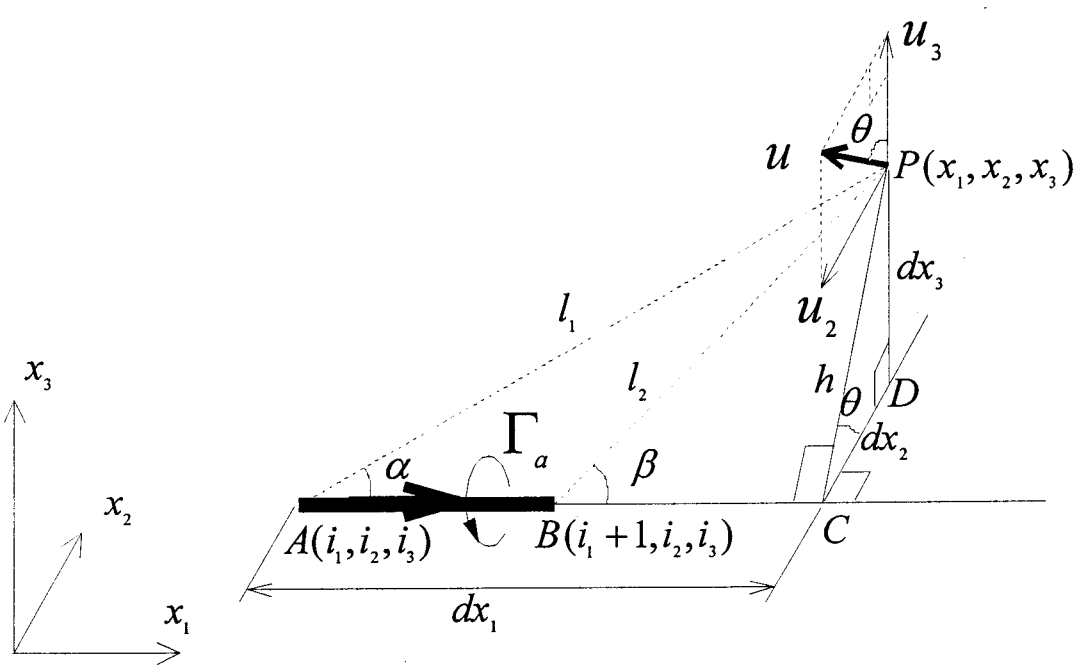

Fig.2.22 Velocity on grid induced by vortex stick

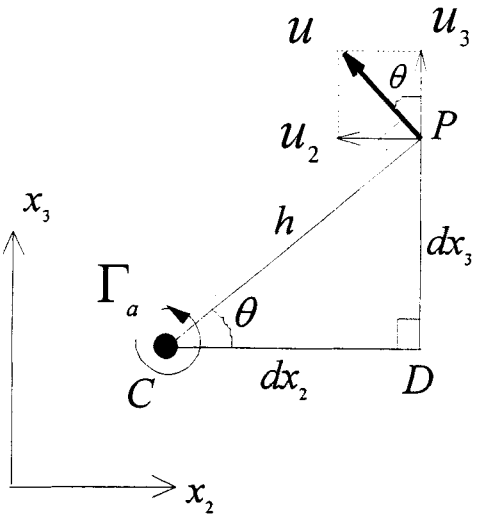

Fig.2.23 Calculation of induced velocity

We use the coordinate of the beginning point $A(i_1,i_2,i_3)$ to represent vortex stick AB, and assume that the strength of vortex stick AB is Γ_a and the length of vortex stick AB is $|AB|=1$. The coordinate of velocity calculation point is $P(x_1,x_2,x_3)$.

Therefore, the velocity induced by vortex stick AB can be calculated by Eq.2.66~Eq.2.71.

$$u_1 = 0 \tag{2.66}$$

$$u_2 = -|\vec{u}|\sin\theta = \left|\frac{(\cos\alpha - \cos\beta)}{4\pi h^2}\right| dx_3\Gamma_a \tag{2.67}$$

$$u_3 = |\vec{u}|\cos\theta = \left|\frac{(\cos\alpha - \cos\beta)}{4\pi h^2}\right| dx_2\Gamma_a \tag{2.68}$$

$$h=\sqrt{dx_2^2+dx_3^2} \tag{2.69}$$

$$\cos\alpha=\frac{dx_1}{\sqrt{dx_1^2+dx_2^2+dx_3^2}} \tag{2.70}$$

$$\cos\beta=\frac{dx_1}{\sqrt{(dx_1-1)^2+dx_2^2+dx_3^2}} \tag{2.71}$$

where $dx_1=x_1-i_1$, $dx_2=x_2-i_2$, $dx_3=x_3-i_3$.

Therefore, we can calculate the velocity induced by vortex stick AB at point P by the following equations.

$$\begin{cases} u_1=0 \\ u_2=-K(dx_1,dx_2,dx_3)dx_3\Gamma_a \\ u_2=K(dx_1,dx_2,dx_3)dx_2\Gamma_a \end{cases} \tag{2.72}$$

where (u_1,u_2,u_3) is the velocity induced by vortex stick AB at point P corresponding to coordinate x_1,x_2,x_3, and

$$K(dx_1,dx_2,dx_3)=\left|\frac{1}{4\pi(dx_2^2+dx_3^2)}\left(\frac{dx_1}{\sqrt{dx_1^2+dx_2^2+dx_3^2}}-\frac{dx_1-1}{\sqrt{(dx_1-1)^2+dx_2^2+dx_3^2}}\right)\right| \tag{2.73}$$

Using the position relation between mesh points and edges of cubic mesh, we can make a look-up-table to remember $K(dx_1,dx_2,dx_3)$ in Eq.2.72. In velocity

calculation we can get the value of $K(dx_1, dx_2, dx_3)$ through reading look-up-table according to (dx_1, dx_2, dx_3), and using Eq.2.72 we can easily calculating velocity induced by vortex Γ_a, which avoided the distance calculation in each time step and greatly improved the calculation speed.

For using the same subroutine in numerical calculation, we discussed the calculation of induced velocity in coordinates (x_1, x_2, x_3) above. In the following, we will discuss the parameter change between coordinate (x_1, x_2, x_3) and coordinate (x, y, z). In coordinates (x_1, x_2, x_3), the distance between velocity calculation point P and the vortex stick is (dx_1, dx_2, dx_3), the induced velocity is (u_1, u_2, u_3). Corresponding to this, in coordinate (x, y, z), the distance between velocity calculation point P and the vortex stick is and (dx, dy, dz), and the induced velocity is (V_x, V_y, V_z). The velocity calculation in coordinate (x, y, z) can be done by Eq.2.74~Eq.2.76.

When vortex stick AB is parallel to x direction, we have

$$\begin{cases} dx_1 = dx, \quad dx_2 = dy, \quad dx_3 = dz \\ V_x = u_1 \\ V_y = u_2 \\ V_z = u_3 \end{cases} \tag{2.74}$$

When vortex stick AB is parallel to y direction, we have

$$\begin{cases} dx_1 = dy, \quad dx_2 = dz, \quad dx_3 = dx \\ V_x = u_3 \\ V_y = u_1 \\ V_z = u_2 \end{cases} \tag{2.75}$$

When vortex stick AB is parallel to z direction, we have

$$\begin{cases} dx_1 = dz, \quad dx_2 = dx, \quad dx_3 = dy \\ V_x = u_2 \\ V_y = u_3 \\ V_z = u_1 \end{cases} \tag{2.76}$$

In Eq.2.74, Eq.2.75 and Eq.2.76, (u_1, u_2, u_3) is calculated by Eq.2.72 corresponding to its (dx_1, dx_2, dx_3).

Chapter 3

Numerical Procedure of Lattice Vortex Method for Stratified Flows

3.1 Introductory remarks

The term "stratified flow" is commonly used to denote the flow of "stratified fluid", or more correctly "density-stratified fluid". In such fluids the density (mass per unit volume) varies with position in the fluid, and this variation is dynamically important. Normally this density variation is stable with lines of constant density oriented nearly horizontally, with lighter fluid above and heavier fluid below. The density variation may be continuous, as occurs in most of the atmosphere and ocean, or be concentrated in discontinuous interfaces, such as at the surface of the ocean. In many situations the variation in density is very small, but such variation may have a dominant effect on the flow if the small buoyancy forces are given sufficient time to act. Due to this effect, the motion of stratified fluid often exhibits many special characteristics different from the motion of homogeneous fluids.

The subject of stratified flows is relevant to meteorology, oceanography and environmental engineering in the broad sense, with specific applications ranging

from flow around hills to flow under ice keels. Many researches have been done on the motion of stratified fluids in recent years. There has been substantial progress in this area. However, the impetus for the recent progress has been driven by atmospheric considerations more than others. This is for two reasons. Firstly, it has become clear that a lack of understanding of the effects of mountain ranges and smaller topographic features on the atmosphere has been a significant impediment to the improvement in weather forecasting. The form drag (as distinct from surface frictional drag) of the topography is known to constitute about 50% of the total drag on the atmosphere (e.g. Palmer *et al.* 1986), and this drag is manifested in stratified effects such as internal gravity waves. The correction of this deficiency requires adequate parametrisation of sub-grid-scale topographic effects in large-scale models for numerical weather prediction. Secondly, and on a smaller scale, increasing concerns about environmental issues such as atmospheric pollution and air quality have instigated a number of mesoscale field and other studies which aim to describe the motion of air in or around mountains, hills and valleys. However, field programmes do not usually provide mechanistic answers by themselves, because of the general sparseness, paucity and ambiguity of most field data sets. Consequently, most of the improved understanding in dynamics has instead come from analytical, numerical and laboratory studies, with the field data supplying confirmation of applicability to the atmosphere.

In this paper, we shall extend the application of vortex method to nonhomogeneous fluid (i.e. density stratified fluid), so we focus our discussion on incompressible and inviscid stratified fluid. The behavior of a density stratified fluid is very complicated, and in a gravitational field often exhibit large departures from the motion of homogenous fluids. There are some special phenomena (blockings and lee waves) in a stratified flow due to the movement of generated vortices.

The theory of stratified flows is described in detail by Yih[5] and Baines[6]. In the following sections, we firstly introduce some approximations and

terminology, which must be used in the numerical simulation. Then the basic equations governing stratified flows are given. Finally, the numerical procedure of lattice vortex method in density stratified flows is explained in detail.

3.2 Boussinesq approximation

The behavior of a density stratified fluid is very complicated, and in a gravitational field often exhibit large departures from the motion of homogeneous fluids. In the research on the motion of stratified fluids, some approximations will provide a useful simplification of the dynamical equations in appropriate circumstances, without significantly affecting the character of the motion being studied. In addition to inviscity and incompressibility, the Boussinesq approximation will often be made. The conditions for its validity are as follows.

In a density stratified fluid, we express density ρ as $\rho = \rho_0 + \rho'(x,y,z,t)$, where ρ_0 is a mean density in the fluid. If all variations of density ρ' are very much smaller than any reference density ρ_0 (i.e. $\rho'/\rho_0 << 1$), the effects of density variations are significant only in the gravity force terms, and are negligible in inertia terms. Therefore, we may replace $\rho_0 + \rho'$ in inertia terms by its mean value ρ_0, and incur an error of relative magnitude ρ'/ρ_0. The density variations are thereby neglected in the inertia term, but retained in the buoyancy-force term where they are multiplied by g. This constitutes the Boussinesq approximation. It is normally a good approximation for all watery fluids in geophysical situations, and the analytic simplification that it provides is valuable. In our research, we will mostly be concerned with the Boussinesq form of the equations.

3.3 Basic equations governing 2D stratified flows

In our research we just only focus our interest on inviscid and incompressible fluid flows, so the equations governing the motion of a two-dimensional stratified fluid are the Euler equations:

$$\rho(\frac{\partial u}{\partial t}+u\frac{\partial u}{\partial x}+w\frac{\partial u}{\partial z})=-\frac{\partial p}{\partial x} \tag{3.1}$$

$$\rho(\frac{\partial w}{\partial t}+u\frac{\partial w}{\partial x}+w\frac{\partial w}{\partial z})=-\frac{\partial p}{\partial z}-\rho g \tag{3.2}$$

where u and w are the fluid velocity components in x and z direction, respectively. p is the pressure. ρ is the density. g is the acceleration due to gravity, and t is the time.

From incompressible condition, we have

$$\frac{\partial \rho}{\partial t}+u\frac{\partial \rho}{\partial x}+w\frac{\partial \rho}{\partial z}=0 \tag{3.3}$$

Considering incompressible condition, the equation of continuity becomes

$$\frac{\partial u}{\partial x}+\frac{\partial w}{\partial z}=0 \tag{3.4}$$

Under most circumstances, it is often appropriate to consider these motions as variations about a basic state, which is in hydrostatic equilibrium. The pressure and density fields may be expressed as

$$p=p_0(z)+p'(x,z,t) \tag{3.5}$$

$$\rho = \rho_0(z) + \rho'(x,z,t) \tag{3.6}$$

where p' is the perturbation pressure, ρ' is the perturbation density, p_0 and ρ_0 represent the values in hydrostatic equilibrium, which are related by

$$\frac{dp_0}{dz} = -\rho_0 g \tag{3.7}$$

The inviscid equations of motion for the perturbations may then be written

$$(\rho_0 + \rho')(\frac{\partial u}{\partial t} + u\frac{\partial u}{\partial x} + w\frac{\partial u}{\partial z}) = -\frac{\partial p'}{\partial x} \tag{3.8}$$

$$(\rho_0 + \rho')(\frac{\partial w}{\partial t} + u\frac{\partial w}{\partial x} + w\frac{\partial w}{\partial z}) = -\frac{\partial p'}{\partial z} - \rho' g \tag{3.9}$$

Considering the Boussinesq approximation, we have

$$\frac{\partial u}{\partial t} + u\frac{\partial u}{\partial x} + w\frac{\partial u}{\partial z} = -\frac{1}{\rho_0}\frac{\partial p'}{\partial x} \tag{3.10}$$

$$\frac{\partial w}{\partial t} + u\frac{\partial w}{\partial x} + w\frac{\partial w}{\partial z} = -\frac{1}{\rho_0}\frac{\partial p'}{\partial z} - \frac{\rho'}{\rho_0}g \tag{3.11}$$

From Eq.3.8 and Eq.3.9, and considering the equation of continuity Eq.3.4, we have

$$\Delta p' = -\rho_0\left[\left(\frac{\partial u}{\partial x}\right)^2 + 2\frac{\partial u}{\partial z}\frac{\partial w}{\partial x} + \left(\frac{\partial w}{\partial z}\right)^2\right] - g\frac{\partial \rho'}{\partial z} \tag{3.12}$$

Assuming

$$S_0 = -\rho_0\left[\left(\frac{\partial u}{\partial x}\right)^2 + 2\frac{\partial u}{\partial z}\frac{\partial w}{\partial x} + \left(\frac{\partial w}{\partial z}\right)^2\right] - g\frac{\partial \rho'}{\partial z}, \tag{3.13}$$

we have

$$\Delta p' = S_0 \tag{3.14}$$

If we know the velocity field and density distribution, the value of S_0 in the right hand of Eq.3.14 can be calculated. Solving Poisson equation Eq.3.14 by SOR method, we can determine the perturbation pressure field.

For applying vortex method to simulate stratified flows, we shall transform Eq.3.10 and Eq.3.11 to vorticity equations.

We define the vorticity ξ by

$$\xi = \frac{\partial u}{\partial z} - \frac{\partial w}{\partial x}, \tag{3.15}$$

taking cross differentiation of Eq.3.10 and Eq.3.11 to eliminate the pressure term in equations, and considering the equation of continuity Eq.3.4, we can obtain the vorticity equation

$$\frac{\partial \xi}{\partial t} + u\frac{\partial \xi}{\partial x} + w\frac{\partial \xi}{\partial z} = \frac{g}{\rho_0}\frac{\partial \rho'}{\partial x} \tag{3.16}$$

According to the Lagrangian description, from Eq.3.3 and Eq.3.16 we can calculate the vorticity evolution and density field by

$$\rho(x + u\Delta t, z + w\Delta t, t + \Delta t) = 0 \tag{3.16}$$

$$\xi(x+u\Delta t, z+w\Delta t, t+\Delta t) = \xi(x,z,t) + \frac{g}{\rho_0}\frac{\partial \rho}{\partial x}\Delta t \qquad (3.17)$$

Therefore, for two-dimensional inviscid and incompressible stratified flows, the basic equations used in the lattice vortex method are Eq.3.14, Eq.3.16 and Eq.3.17.

3.4 Basic equations governing 3D stratified flows

In general, we also assume that the fluid is inviscid and incompressible. Therefore, the equations governing the motion of three-dimensional stratified flows are the Euler equations

$$\rho\left(\frac{\partial u_i}{\partial t} + u_\alpha \frac{\partial u_i}{\partial x_\alpha}\right) = -\frac{\partial p}{\partial x_i} + \rho X_i \qquad \text{(i=1,2,3)} \qquad (3.18)$$

in which t is the time, ρ is the density of the fluid, p is the pressure, X_i is the ith component of the body force per unit mass, u_i is the velocity component in the direction of x_i, with $i=1$, 2, and 3, and x_1, x_2 and x_3 are Cartesian coordinates. In Eq.3.18, repeated indices in one term indicate summation. Thus,

$$u_\alpha \frac{\partial u_i}{\partial x_\alpha} = u_1 \frac{\partial u_i}{\partial x_1} + u_2 \frac{\partial u_i}{\partial x_2} + u_3 \frac{\partial u_i}{\partial x_3}. \qquad (3.19)$$

Except in trivial or a few very special cases, vorticity is created in a nonhomogeneous fluid in motion. The simplest way to show this is by cross differentiation of Eq.3.18, after division by ρ, and setting i equal to 1 and 2 in turn, if the difference of the results of the cross differentiation is taken, and ξ_3 is used to denote the vorticity component

$$\xi_3 = \frac{\partial u_2}{\partial x_1} - \frac{\partial u_1}{\partial x_2}, \tag{3.20}$$

we have, after some simplification,

$$\frac{D\xi_3}{Dt} + \xi_3 \frac{\partial u_\alpha}{\partial x_\alpha} = \xi_\alpha \frac{\partial u_3}{\partial x_\alpha} - \left(\frac{\partial \rho^{-1}}{\partial x_1} \frac{\partial p}{\partial x_2} - \frac{\partial \rho^{-1}}{\partial x_2} \frac{\partial p}{\partial x_1} \right) \tag{3.21}$$

Considering the the equation of continuity of incompressible fluid

$$\frac{\partial u_\alpha}{\partial x_\alpha} = 0, \tag{3.22}$$

Eq.3.21 can be written as

$$\frac{D\xi_3}{Dt} = \xi_\alpha \frac{\partial u_3}{\partial x_\alpha} - \frac{1}{\rho^2} \left(\frac{\partial \rho}{\partial x_1} \frac{\partial p}{\partial x_2} - \frac{\partial \rho}{\partial x_2} \frac{\partial p}{\partial x_1} \right) \tag{3.23}$$

By symmetry the vorticity eqations can be written in the vector form

$$\frac{D}{Dt}\xi = (\xi \cdot \nabla)u + \frac{1}{\rho^2}(\nabla\rho \times \nabla p) \tag{3.24}$$

where $\xi = (\xi_1, \xi_2, \xi_3)$ is vorticity vector. $u = (u_1, u_2, u_3)$ is velocity vector. D/Dt denotes the Lagrangian derivative with respect to time t.

The left-hand side of Eq.3.24 represents the rate of change of vorticity. The first term on the right-hand side represents the rate of change of ξ due to stretching and turning of the vortex lines. Thus the last term in Eq.3.24 represents the creation of vorticity by density variation. Significant is the fact

that vorticity is created only if the gradient of ρ and that of p are not in the same direction. If ρ is constant, of course the term responsible for the creation of vorticity vanishes, and persistence of irrotationality follows from the Helmholtz-Kelvin theorem of the preservation of circulation along any material circuit and from the well-known kinematic relationship between circulation and vorticity.

The creation of vorticity entails the creation of circulation. Let an elemental length along a material circuit C be ds, with components dx_1, dx_2 and dx_3, and let the differnce of the velocity component u_i at the ends of ds be du_i. Then

$$du_i = \frac{\partial u_i}{\partial x_\alpha} dx_\alpha = \frac{D}{Dt} dx_i \tag{3.25}$$

Multiplying Eq.3.18 by dx_i/ρ, summing over i, and integrating over C, we have

$$\int_C \frac{Du_i}{Dt} dx_i = \int_C X_i dx_i - \int_C \frac{1}{\rho} \frac{\partial p}{\partial x_i} dx_i \tag{3.26}$$

or, by virtue of Eq.3.25,

$$\frac{D}{Dt} \int_C u_i dx_i = \int_C \left(X_i dx_i + u_i du_i \right) - \int_C \frac{1}{\rho} \frac{\partial p}{\partial x_i} dx_i \tag{3.27}$$

If the body force X_i has a single-valued potential, and u_i is single-valued, from Eq.3.27, we have

$$\frac{D}{Dt} \Gamma = - \int_C \frac{1}{\rho} \frac{\partial p}{\partial x_i} dx_i \tag{3.28}$$

in which

$$\Gamma = \int_C u_i dx_i \tag{3.29}$$

is the circulation. Now , by Stokes' theorem, with S indicating a surface bounded by C,

$$\begin{aligned}\int_C \frac{1}{\rho}\frac{\partial p}{\partial x_i}dx_i &= \iint_S \mathrm{curl}\left(\frac{1}{\rho}\mathrm{grad}\,p\right)\cdot dA \\ &= \iint_S \left(\mathrm{grad}\frac{1}{\rho}\times \mathrm{grad}\,p\right)\cdot dA\end{aligned} \tag{3.30}$$

since $\mathrm{curl}\,\mathrm{grad}\,p = 0$. Thus

$$\frac{D\Gamma}{Dt} = -\iint_S \left(\mathrm{grad}\frac{1}{\rho}\times \mathrm{grad}\,p\right)\cdot dA \tag{3.31}$$

where $\Gamma = (\Gamma_1,\Gamma_2,\Gamma_3)$ is circulation vector, dA is the area for integrating.

In the following, we will discus the distribution of pressure gradient under the Boussinesq approximation.

Considering the Boussinesq approximation, Eq.3.18 can be written as

$$\left(\frac{\partial u_i}{\partial t} + u_\alpha \frac{\partial u_i}{\partial x_\alpha}\right) = -\frac{1}{\rho_0}\frac{\partial p}{\partial x_i} + \frac{\rho}{\rho_0}X_i, \tag{3.32}$$

where ρ_0 is the reference density, and $X_i \equiv (0,0,-g)$.

Taking cross differentiation of Eq.3.32 to eliminate the pressure term in equations, and considering the equation of continuity Eq.3.22, we can obtain the vorticity equation

$$\frac{D\xi_1}{Dt} = \xi_\alpha \frac{\partial u_1}{\partial x_\alpha} - \frac{g}{\rho_0}\frac{\partial \rho}{\partial x_2} \tag{3.33}$$

$$\frac{D\xi_2}{Dt} = \xi_\alpha \frac{\partial u_2}{\partial x_\alpha} - \frac{g}{\rho_0}\frac{\partial \rho}{\partial x_1} \tag{3.34}$$

$$\frac{D\xi_3}{Dt} = \xi_\alpha \frac{\partial u_3}{\partial x_\alpha} \tag{3.35}$$

Comparing Eq.3.33~Eq.3.35 with Eq.3.24, and using (x,y,z) to replace (x_1,x_2,x_3), we have

$$\frac{1}{\rho^2}\left(\frac{\partial \rho}{\partial y}\frac{\partial p}{\partial z} - \frac{\partial \rho}{\partial z}\frac{\partial p}{\partial y}\right) = -\frac{g}{\rho_0}\frac{\partial \rho}{\partial y} \tag{3.36}$$

$$\frac{1}{\rho^2}\left(\frac{\partial \rho}{\partial z}\frac{\partial p}{\partial x} - \frac{\partial \rho}{\partial x}\frac{\partial p}{\partial z}\right) = \frac{g}{\rho_0}\frac{\partial \rho}{\partial x} \tag{3.37}$$

$$\frac{1}{\rho^2}\left(\frac{\partial \rho}{\partial x}\frac{\partial p}{\partial y} - \frac{\partial \rho}{\partial y}\frac{\partial p}{\partial x}\right) = 0 \tag{3.38}$$

Therefore, we can get the distribution of pressure gradient under the Boussinesq approximation as follows

$$\frac{\partial p}{\partial x} = 0, \qquad \frac{\partial p}{\partial y} = 0, \qquad \frac{\partial p}{\partial z} = -\frac{\rho^2}{\rho_0} g. \tag{3.39}$$

If we assume there is an uniform distribution of circulation in the integrated area A (for simple, here $A = 1$), from Eq.3.31, we can get the circulation equations under the Boussinesq approximation.

$$\begin{cases} \dfrac{D\Gamma_1}{Dt} = -\dfrac{g}{\rho_0}\dfrac{\partial \rho}{\partial y} \\ \dfrac{D\Gamma_2}{Dt} = \dfrac{g}{\rho_0}\dfrac{\partial \rho}{\partial x} \\ \dfrac{D\Gamma_3}{Dt} = 0 \end{cases} \tag{3.40}$$

From the incompressible condition of fluid, we have

$$\frac{D\rho}{Dt} = 0 \tag{3.41}$$

According to the Lagrangian description, Eq.3.40 and Eq.3.41 can be written as

$$\Gamma_1(x+u\Delta t, y+v\Delta t, z+w\Delta t, t+\Delta t) = \Gamma_x(x,y,z,t) - \frac{g}{\rho_0}\frac{\partial \rho}{\partial y}\Delta t \tag{3.42}$$

$$\Gamma_2(x+u\Delta t, y+v\Delta t, z+w\Delta t, t+\Delta t) = \Gamma_2(x,y,z,t) + \frac{g}{\rho_0}\frac{\partial \rho}{\partial x}\Delta t \tag{3.43}$$

$$\Gamma_3(x+u\Delta t, y+v\Delta t, z+w\Delta t, t+\Delta t) = \Gamma_3(x,y,z,t) \tag{3.44}$$

$$\rho(x+u\Delta t, y+v\Delta t, z+w\Delta t, t+\Delta t) = \rho(x,y,z,t) \tag{3.45}$$

Therefore, for three-dimensional inviscid and incompressible stratified flows, the basic equations used in the lattice vortex method are Eq.3.42~Eq.3.45.

3.5 Some terminology in stratified flows

Here, we will introduce some important terminology often used in the research of the motion of stratified fluids.

An important quantity that characterises continuously stratified fluid is the buoyancy frequency N (formerly known as the $Brunt-Väisälä$ frequency), which for incompressible fluids is defined by

$$N^2 = -\frac{g}{\rho_0}\frac{d\rho}{dz}. \tag{3.46}$$

where ρ is the density of the fluid, ρ_0 is the reference density.

N is the frequency of local unforced vertical oscillations of small amplitude, and is the highest frequency that local buoyancy-driven fluctuations may have. It therefore gives a characteristic time-scale for these motions.

The most important dimensionless parameter in any study of stratified flows is normally called the Froude number, F_r. This typically has the form $F_r = U/\sqrt{gl}$, where U is the fluid speed and l is a length. For flow past an obstacle, there are several possible choices for l: it may be the horizontal length L or the vertical height h of the obstacle, or it may be the depth of the stream, D. The quantities for continuously stratified fluids that correspond to the above parameters are U/NL, U/Nh and U/ND, and these have all been termed the "Froude number" by someone at sometime. These different choices have different dynamical significance. To say that "the Froude number" is "large", "small", or "equal to one" conveys no information unless one specifies how the Froude number is defined. For a continuously stratified fluid, the parameters U/NL, U/Nh and U/ND are all important for stratified flow over topography. U/NL relates to the wave drag produced by an obstacle. U/ND specifies to what extent long linear gravity waves may propagate against the stream, which represents a fluid speed

divided by the significant wave speed. U/Nh relates to non-linear factors, such as the steepness of the wave field and blocking of low-level fluid.

Sometimes, the term "Froude number" for general will be used to denote the mean fluid speed divided by the relevant internal wave speed (usually the fastest). For unsheared uniformly stratified flow, this would be $U/(ND/\pi)$. The flow may then be said to be subcritical if $F_r < 1$, critical if $F_r = 1$, and supercritical if $F_r > 1$.

In the research of the stability of sheared stratified flow, there is an important dimensionless parameter: Richardson number, R_i, which is defined as

$$R_i = \frac{N^2}{(dU/dz)^2} \tag{3.47}$$

where U is the velocity of the background flow, U=U(z). N is buoyancy frequency, defined by Eq.3.46.

The critical Richardson number is equal to $1/4$. If $R_i > 1/4$ at all depth, the fluid must be stable to all small disturbances (Miles 1960[7], Howard 1961[8]). If $R_i < 1/4$ somewhere, the flow may be stable or unstable, and in many cases it is unstable.

3.6 Numerical procedure of lattice vortex method used in density stratified flows

From the theory of stratified flows given above, we know that there is an additional term describing the baroclinic generation of vorticity in the vorticity equation of stratified flows. The vortex is generated by $\nabla\rho \times \nabla p$, and moves with fluid. Due to motion of these generated vortices, stratified flows have some special behaviors, such as blocking and lee wave phenomena, which can not occur in homogeneous fluid flows. The interaction of vorticity and buoyancy forces is of

major important in the study of a stratified flow. It is convenient and simple using vortex method to investigate stratified flows.

We shall apply the lattice vortex method proposed in chapter 2 to simulate stratified flows. For simple, we limit our calculation on the Bossinesq approximation. Therefore, we can calculate the strength of generated vortices by density gradient. In our calculation, the solid boundaries are treated by panel method , in which the solid boundaries are replaced by boundary vortices.

In general, the simulation of a stratified flow by lattice vortex method is done according to the following algorithm.

1. Deciding the initial velocity field. According the calculation model, the initial velocity field is decided by the velocity profile at far upstream or other sources.
2. Calculating the velocity at control point. The velocity at control points is decided by the velocity profile at far upstream and the velocity induced by inner vortices or other sources in the flow. Because we assume the flow is suddenly started from rest, so that there is no inner vortex in the initial.
3. Determining boundary vorticities. According to panel method, the boundary vorticities must be decided to satisfy the boundary condition on control points, that the normal velocity at control points must be equal to zero ($u_n = 0$). From solving the equations based on $u_n = 0$, we can decide boundary vorticities.
4. Calculating velocity field. The velocity field is decided by the velocity profile at far upstream and the velocity induced by inner vortex and boundary vortex and other sources in the flow..
5. Renewing density field. According to Lagrangian manner, density moves with the velocity field. Because the density is defined on the mesh points, after its move, the density must be distributed by area weighting method or volume weight method explained in chapter 2. Then, the new density

field is gotten.

6. Calculating density gradient. In the renewed density field, the density gradient is calculated by finite difference method.
7. Renewing inner vortex field. The vorticity is generated according to Eq.3.17 (in two-dimensional flows) or Eq.3.42 ~ Eq.3.44 (in three-dimensional flows). The generated vorticity will move with the velocity field. Because vorticity is also defined on the mesh points, after its move, the vorticity also must be distributed by area weighting method or volume weight method explained in chapter 2, and then we can get the new inner vortex field.

Step 2~6 are repeated until a specified time $t = t_f$ is reached. During the calculation, the density, the velocity and the vorticity is saved, and the stream function is calculated and printed out.

In this numerical procedure, most calculation time cost in the calculation of velocity induced by vortices. We use a look-up-table, which is explained in chapter 2, to decrease the time of the calculation of necessary distances, which must be used in the induced velocity calculation by Biot-Savart law. Therefore, the calculation speed is greatly improved.

The flow chart of the simulation of stratified flows by lattice vortex method is displayed in Fig.3.1.

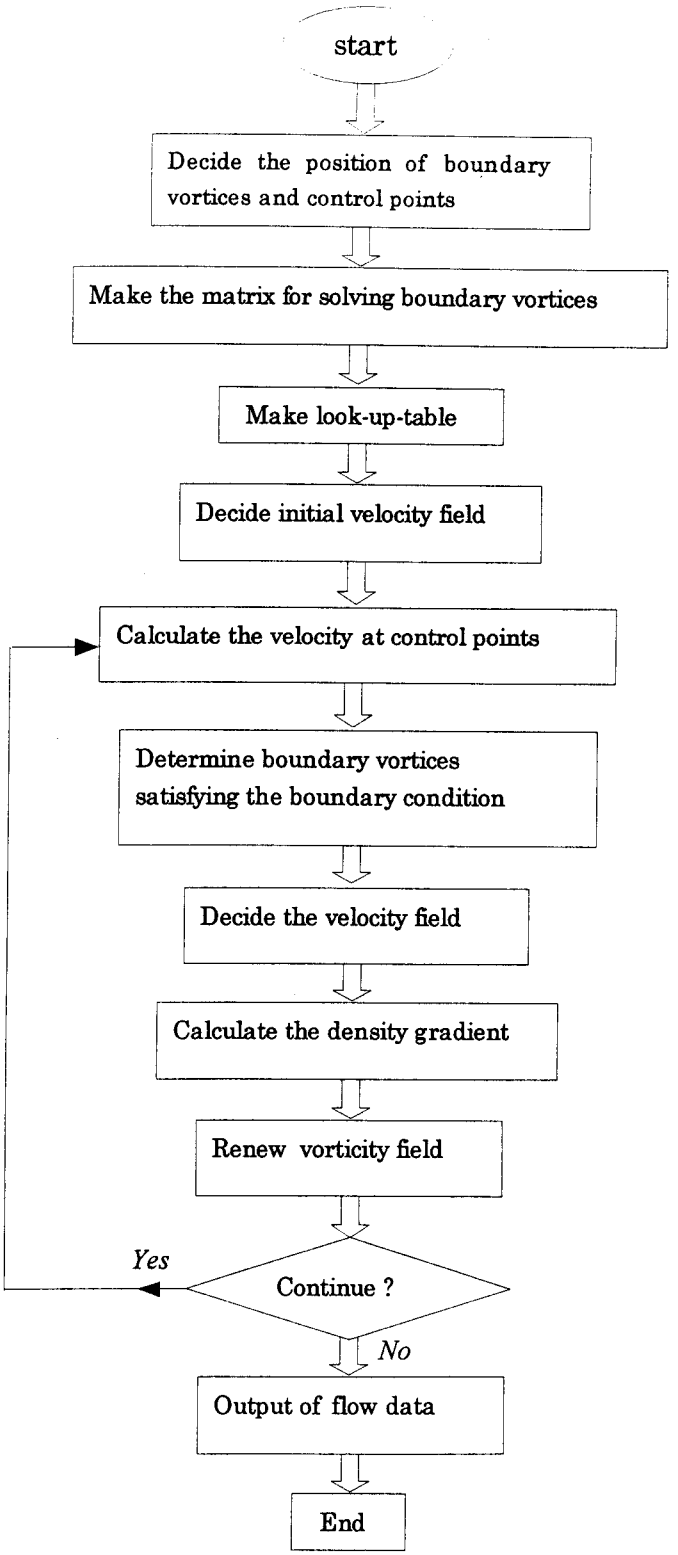

Fig.3.1 Basic flow chart of the simulation of stratified flows by lattice vortex method

Chapter 4

Line Sink Flows of Density Stratified Fluids

4.1 Introductory remarks

The main characteristic that distinguishes a stratified medium in gravitational field from a homogeneous medium is its ability to sustain internal gravity waves and flow concentrations. This has been observed in nature, it has wide spread geophysical implications, and it is of fundamental importance for fluid mechanics. That this is so for water quality management is shown by "selective withdrawal" of water in a reservoir. In deep lakes or reservoirs, seasonal change in solar radiation is the cause of density stratification from spring to late autumn. Solar heating, aided by mixing due to surface winds, penetrates downward, to establish a warm upper layer (the epilimnion), followed by a transition layer (the metalimnion or thermocline), which leads to the lower dense cold region (the hypolimnion). The stable density stratification in lakes or reservoirs is caused primarily by the temperature variation with depth, and

secondarily by a variable concentration of dissolved and suspended solids. When outflow is withdrawn from density stratified reservoirs, the water comes mainly from zones at elevations corresponding approximately, in hydroelectric dams, to the level of the intake openings leading to the turbine penstocks. This is selective withdrawal. The various water quality parameters (such as temperature, dissolved oxygen, foreign mineral contents, etc.) are interrelated with the density and advected by the withdrawal current. Thus, selective withdrawal has a long range effect on the environment, especially on the quality of drinking water and on aquatic life, in both the reservoir and its downstream river. It has been reported that the population of some warm water species declines drastically after a dam begins to release cold water from the lower layers of its reservoir. Furthermore, when a hydroelectric power plant operates as a peaking plant, the quality and quantity of discharge in the downstream river also undergo periodic variation.

The analysis of the flow of a linearly stratified fluid into a horizontal line sink was first made by Yih (1958) [9], who obtained the exact steady state solution, valid for $\pi^{-1} < F_r < \infty$, where F_r is the densimetric Froude number Q/N_0H^2 (Q is the discharge rate per unit width, H is the depth of the channel, the *Väisälä* frequency $N_0 = (\kappa g)^{1/2}$, and $\kappa = -(1/\rho_0)d\bar{\rho}/dz$ is the slope of the density variation far upstream, a constant). Yih assumed the velocity and density to be undisturbed far upstream, so that no solution was obtained for $F_r < \pi^{-1}$. Debler (1959) [10] then showed by experiment that $F_r \approx \pi^{-1}$ is indeed a critical Froude number, above which Yih's solution is valid, and below which the flow separates into a flowing region near the level of the sink, the fluid remaining essentially stagnant elsewhere (i.e. selective withdrawal occurs). Pao&Kao [11] investigated a linearly stratified fluid flow of a line sink in a channel on both aspects of theory and experiment. The dynamics of establishment of selective withdrawal is studied analytically, and some numerical results by the finite difference method are shown

in it. Tsutahara [12] numerically simulated two-dimensional unsteady stratified flows by perturbation method under the linear approximation.

In this chapter, we investigated two-dimensional unsteady stratified flows in terms of the lattice vortex method, and explained the special phenomena (blocking and selective withdrawal in a stratified fluid from a line sink) by the movement of generated vortices.

4.2 Calculation model and boundary conditions

We consider the flow into a line sink situated at the origin of an x, z coordinate system in a channel of depth H (as shown in Fig.4.1). The initial-value problem corresponds to starting the discharge suddenly from an initially stationary state, which is stratified linearly.

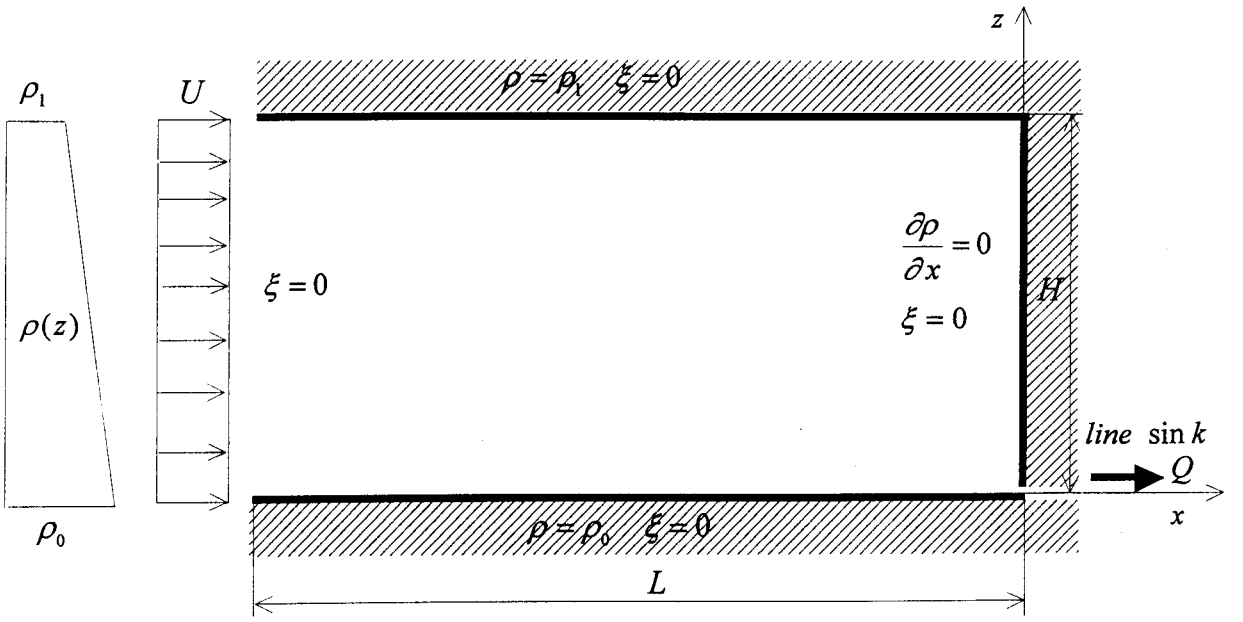

Fig. 4.1 Line sink flow model

If Q is the discharge per unit width of the channel, then, with H taken as the characteristic length, the characteristic velocity is U with $U = Q/H$.

The definitions of the parameters for a line sink flow are as follows:

H: Channel depth

L: Calculation range

Q: Discharge

N: *Brunt – Väisälä* frequency $N^2 = -\frac{g}{\rho_0}\frac{d\overline{\rho}}{dz}$,

here ρ_0 is reference density

K: Density stratification degree $K = \frac{NH}{\pi U}$, here $U = \frac{Q}{H}$

F_r: *Froude* number $F_r = \frac{Q}{NH^2} = \frac{1}{\pi K}$

m : Strength of the point sink with Q discharge $m \approx \frac{4Q}{2\pi}$

t^* : Dimensionless time $t^* = Nt$

The boundary conditions are as follows:

$$\frac{\partial \rho}{\partial z} = -\frac{\rho_1 - \rho_0}{H},\ \vec{u} = (U,0), \xi = 0 \qquad \text{at far upstream}$$

$$\rho = \rho_1,\ u_n = 0, \xi = 0 \qquad \text{on the upper wall}$$

$$\rho = \rho_0,\ u_n = 0, \xi = 0 \qquad \text{on the lower wall}$$

$$\frac{\partial \rho}{\partial x} = 0,\ u_n = 0, \xi = 0 \qquad \text{on the side wall}$$

where the subscript n denotes the normal direction to the boundary and u_n is the velocity component in the n direction, ξ is vorticity, ρ is density, ρ_0 and ρ_1 is a constant, $\vec{u}$ is velocity vector.

In our calculation, the solid boundary is treated by panel method. The positions of boundary vortices and control points are displayed in Fig.4.2.

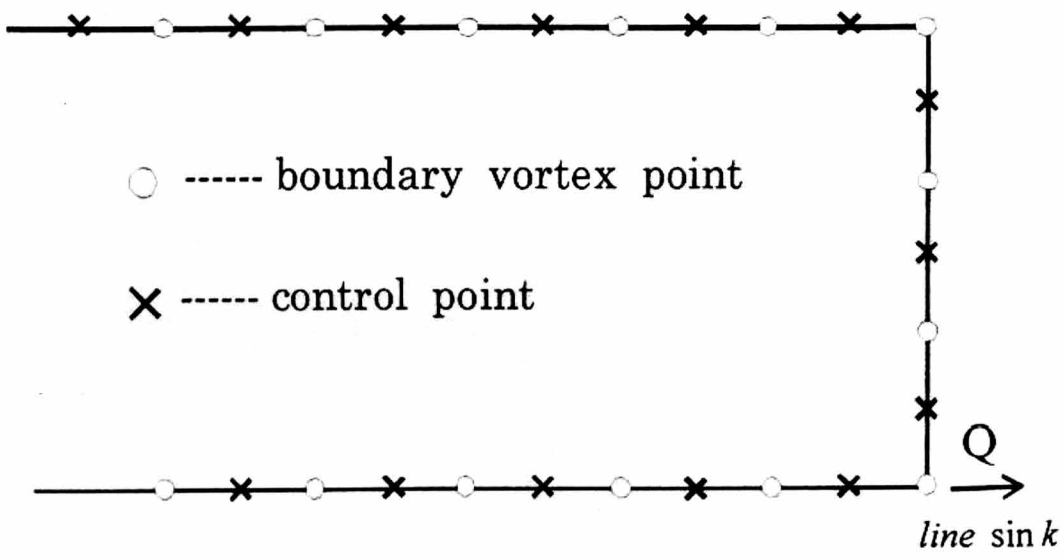

Fig. 4.2 Boundary vortex points and control points in the line sink flow model

In theoretical analysis, the infinite length of channel is assumed to ensure the velocity condition at far upstream. In actual numerical simulation, the calculation range is finite. Therefore, some error will be caused at the inlet. To restain the influence of this error on all flow field, the velocity at inlet is calculated by interpolate its nearest velocity.

The boundary vortices is used to replace the solid boundary in panel method. It is not the real vortex, so the boundary vortices will not move with the velocity field, and not be distributed in the calculation.

4.3 Numerical results and discussions

Figure 4.3 shows the streamlines of a line sink flow at different Froude number when t=20. In this calculation, The calculation range is 100×10 (L×H), where the width of the mesh is unity, and the vorticity is distributed by area weighting method, which has first order accuracy. They coincide with the facts that the selective withdrawal can occur only at small Froude numbers because the eddy regions of cell structures will be propagated upstream fast at small Froude numbers and then a stagnant region is formed. When the internal Froude number is larger than the critical Froude number ($Fr\approx0.32$), only a closed corner eddy appears. These results also have a good agreement with numerical ones by the finite difference method [13].

Figure 4.4 gives the comparisons of the streamline development between the numerical results by LVM and analytical ones [12] of an unsteady line sink flow for $Fr\approx0$. They show a good agreement. It certified that LVM is valid for the simulation of an unsteady stratified flow.

Figure 4.5, Fig.4.6 and Fig.4.7 shows the development of streamlines at Fr=0.32,0.35 and 0.5, respectively. Figure 4.8, Fig.4.9 and Fig.4.10 gives the comparisons between the numerical results by LVM and theoretical ones [5] of steady line sink flows for Fr=0.32, Fr=0.35 and Fr=0.5. They all show good agreements. In Pao&Kao [11], the corner eddy does not appear at Fr=0.32 because they take the viscosity and the diffusion, but in our results the corner eddy appears.

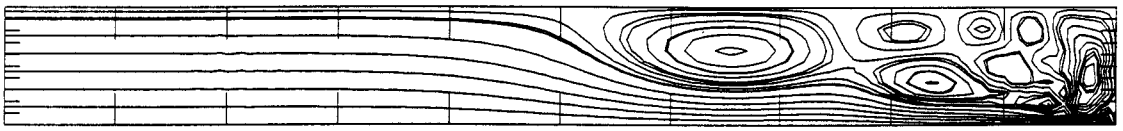

(a) Fr=0.0001, $t^* = 20$

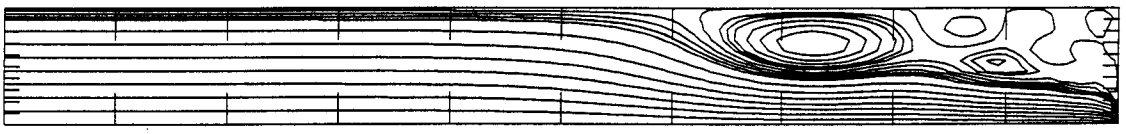

(b) Fr=0.05, $t^* = 20$

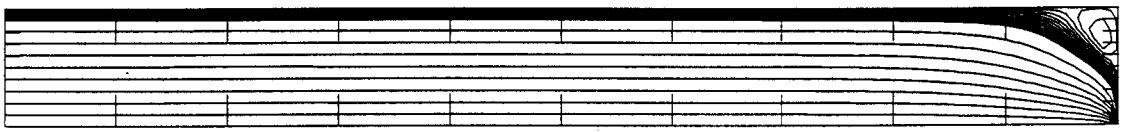

(c) Fr=0.32, $t^* = 20$

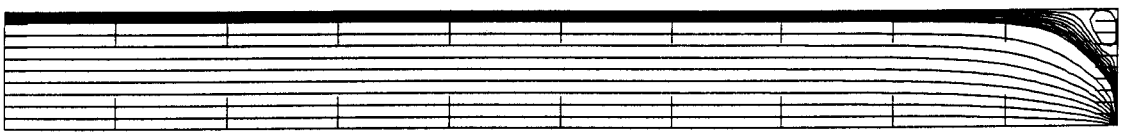

(d) Fr=0.35, $t^* = 20$

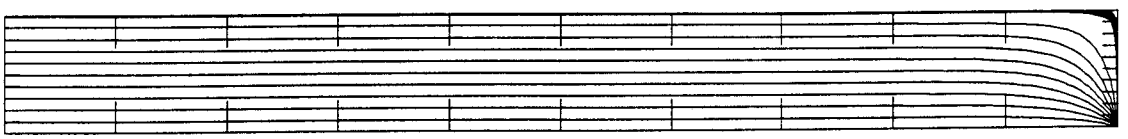

(e) Fr=0.5, $t^* = 20$

Fig.4.3 Streamlines of line sink flows at different Froude numbers

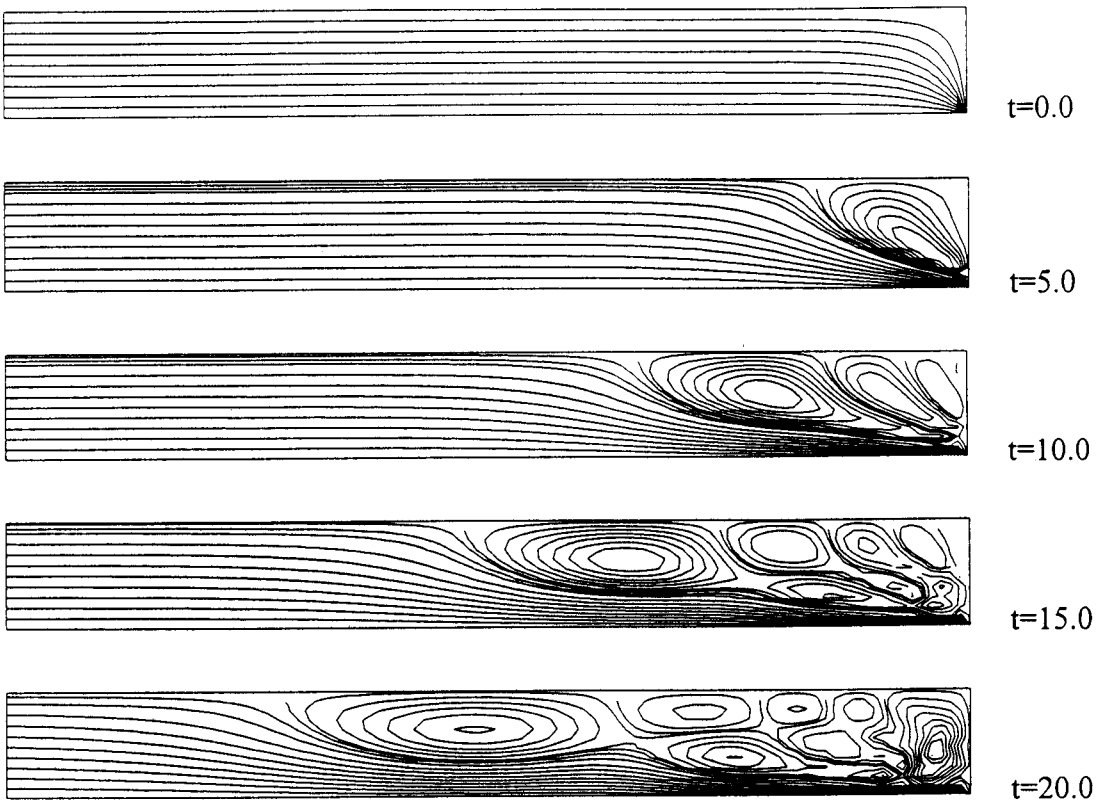

(a) The development of streamlines (numerical results at Fr=0.0001)

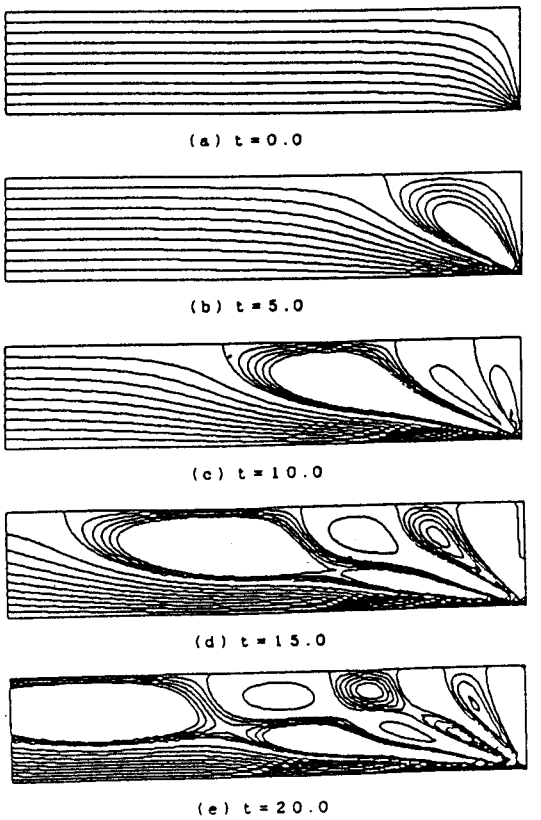

(b) The development of streamlines (theoretical results at Fr=0.0)

Fig.4.4 The comparison between numeric al results and theoretical results of initial stage of point sink flow

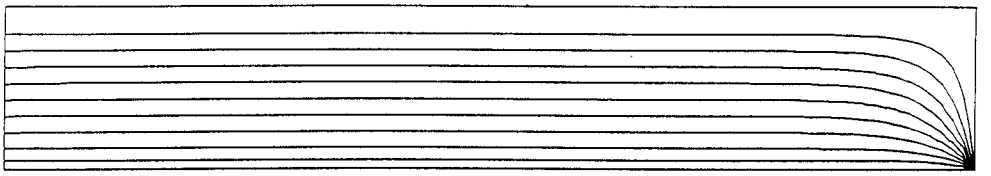

$t^* = 0$

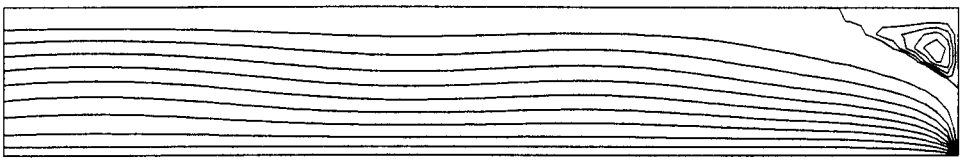

$t^* = 50$

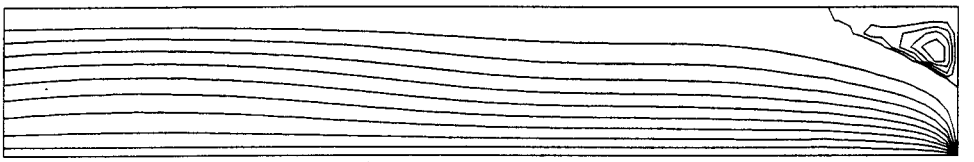

$t^* = 100$

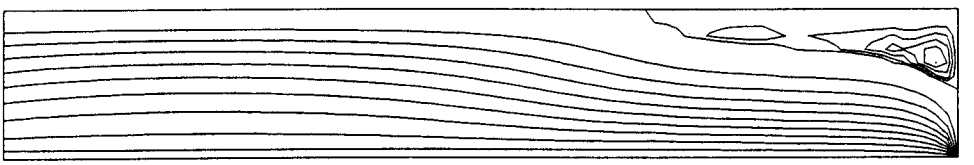

$t^* = 300$

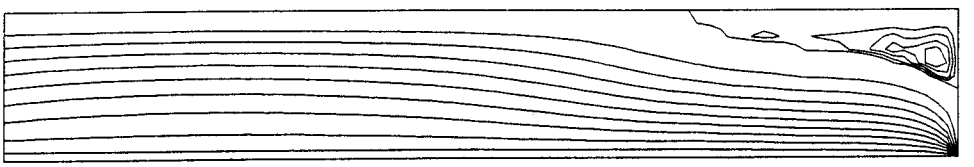

$t^* = 500$

Fig.4.5 Present numerical results of a line sink flow at Fr=0.32

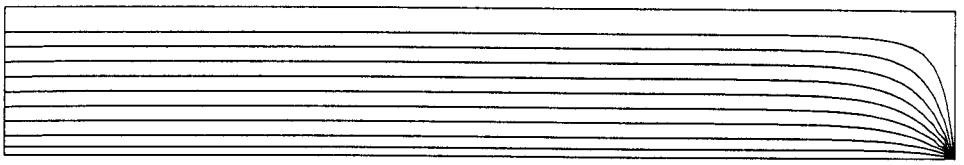

$t^* = 0$

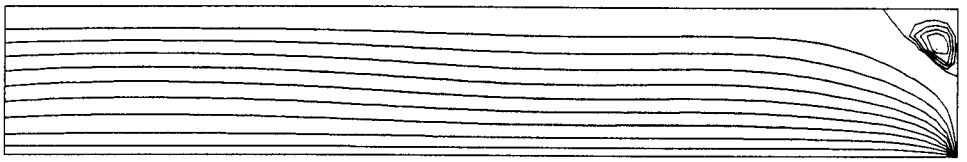

$t^* = 50$

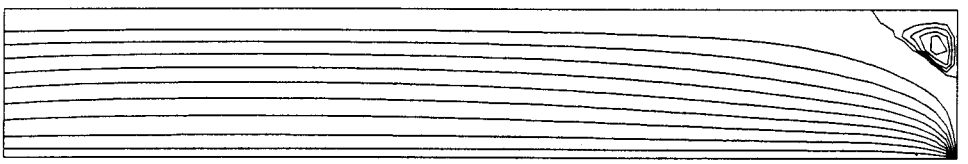

$t^* = 100$

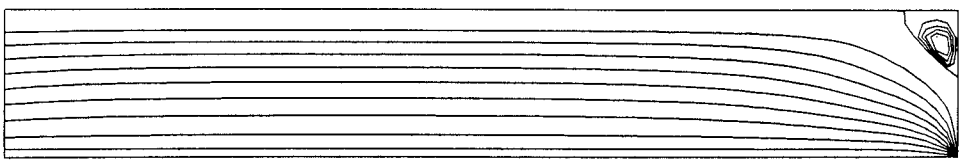

$t^* = 300$

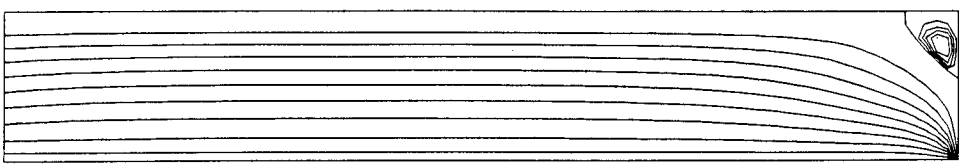

$t^* = 500$

Fig.4.6. Present numerical results of line sink flow at Fr=0.35

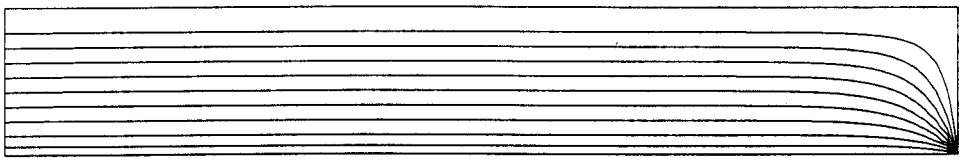

$t^* = 0$

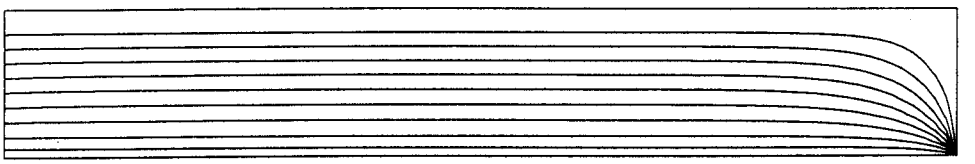

$t^* = 50$

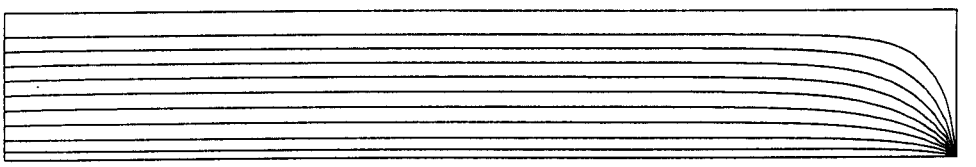

$t^* = 100$

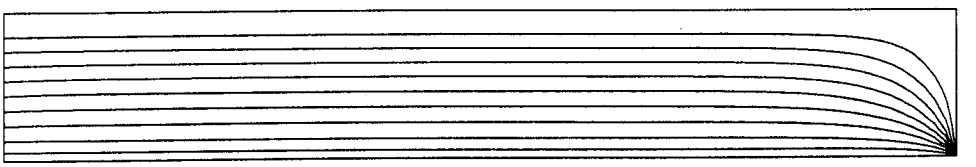

$t^* = 300$

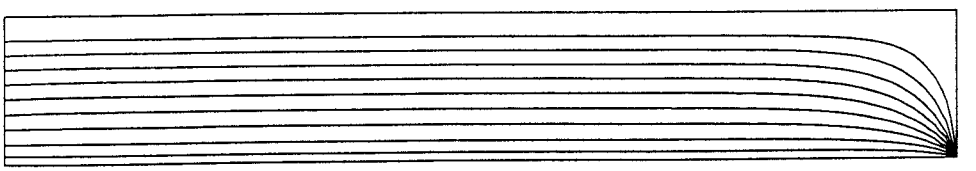

$t^* = 500$

Fig.4.7 Present numerical results of a line sink flow at Fr=0.5

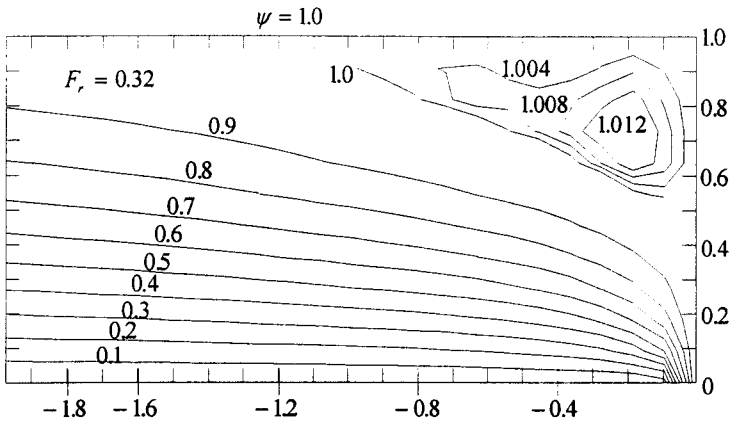

(a) Present numerical result (first order accuracy)

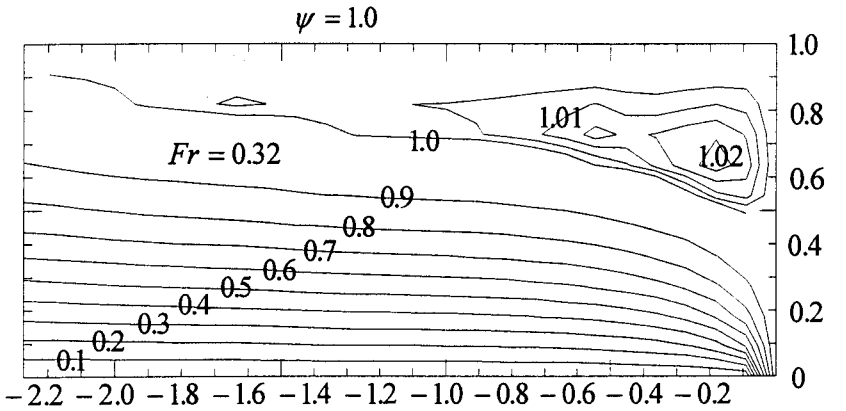

(b) Present numerical result (second order accuracy)

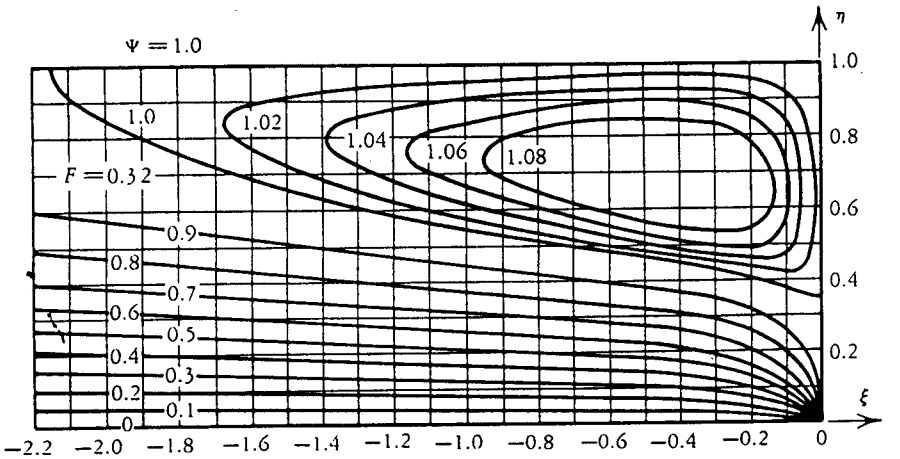

(c) Theoretical result

Fig.4.9 Comparison between present numerical results and theoretical results of steady line sink flows at Fr=0.32

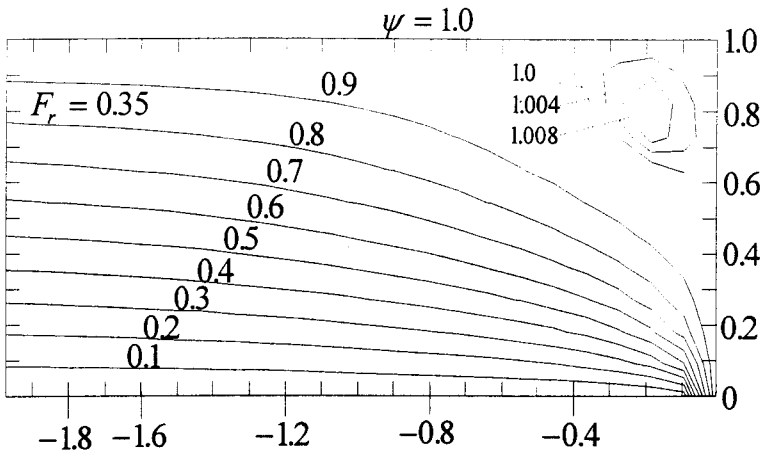

(a) Present numerical result (first order accuracy)

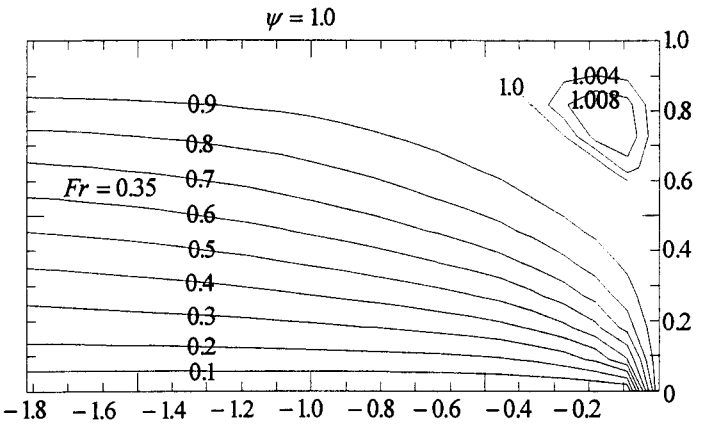

(b) Present numerical result (second order accuracy)

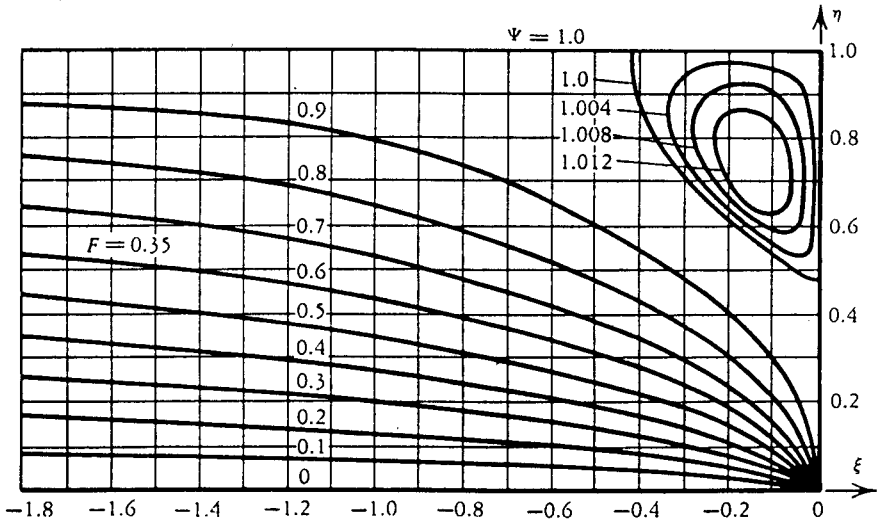

(c) Theoretical result

Fig.4.10 Comparison between present numerical results and theoretical results of steady line sink flows at Fr=0.35

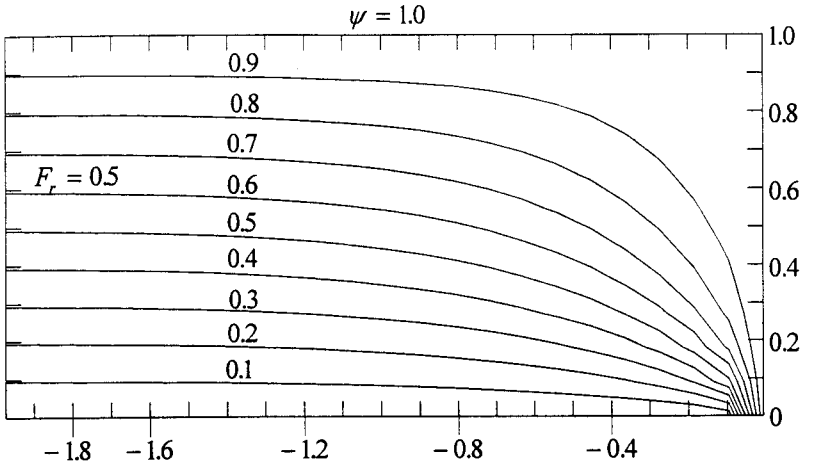

(a) Present numerical result (first order accuracy)

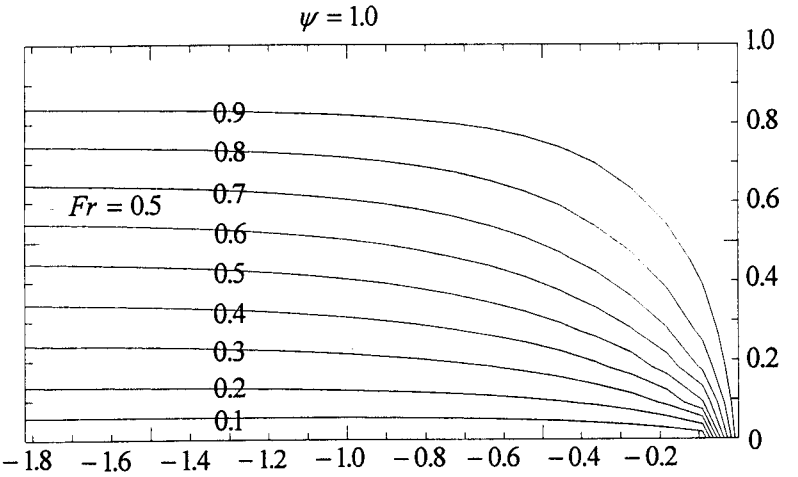

(b) Present numerical result (second order accuracy)

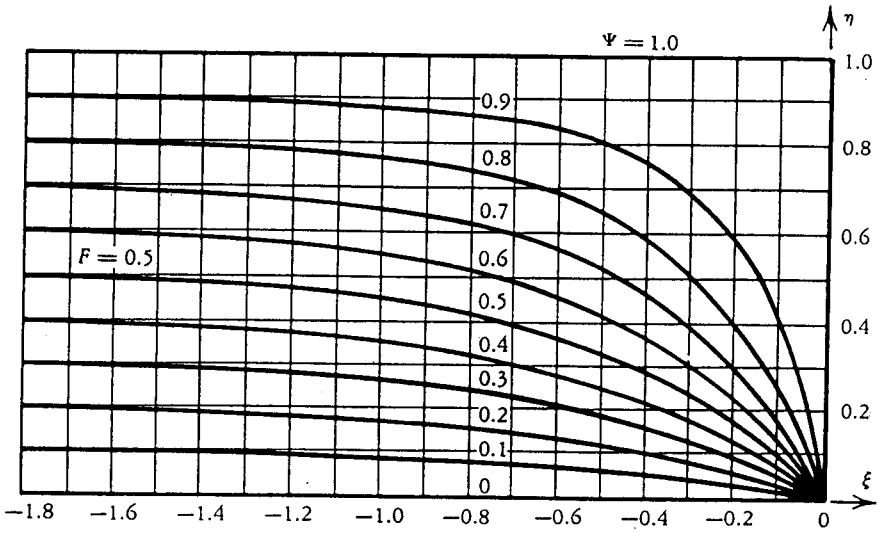

(c) Theoretical result

Fig.4.11 Comparison between present numerical results and theoretical results of steady line sink flows at Fr=0.5

4.4 Concluding remarks

We calculated unsteady density stratified flows of a point sink by lattice vortex method. The characteristic phenomena in stratified flows selective withdrawal is well simulated. There is a good agreement between present results and the analytical ones. It shows that the lattice vortex method is valid for the simulation of unsteady density stratified flows. In lattice vortex method, there is no limitation of CFL condition, so we can simulate a flow with larger time step. With the vortex method, the establishment of selective withdrawal in a stratified flow can be explained clearly and easily.

Chapter 5

Density Stratified Flows past an Obstacle in a Channel with Finite Depth

5.1 Introductory remarks

It is well-known that internal waves propagating in a stratified flow is markedly affected at a "critical level". Miles [7] and Howard [8] provided the basis for the mathematical analysis (linear theory) to demonstrated that a small amplitude internal wave would be completely absorbed at a critical level when its local gradient Richardson number is larger than 0.25, and incident waves are "over-reflected" when the local gradient Richardson number at the critical level is less than 0.25. These linear theoretical results are not liable to remain valid as the wave-induced flow in the vicinity of critical level develops and nonlinear processes become increasingly important. We know that the interaction of vorticity and buoyancy forces is major importance in density stratified fluid flows, which is main source to cause the special phenomena (blocking and lee waves) in a

stratified fluid. In a variable density flow, the vorticity equation Eq.3.24 has an additional term describing the baroclinic generation of vorticity. The character of this baroclinic term is therefore the key to understanding the effects of buoyancy in general. Our motivation for the calculations to be described in this chapter is to investigate the behaviour of vorticity in a density stratified fluid with a shear velocity profile when Richardson number is larger or less than 0.25. We want to explain the dependence of a density stratified fluid flow on Richardson number by means of lattice vortex method.

5.2 Calculation model and boundary conditions

To investigate the special phenomena blocking and lee wave in stratified flow, we consider steady stratified flows past an obstacle in a channel of finite depth. It is similar to the flow past a mountain in the nature. In our calculation, two kinds of obstacle: a vertical plate and a ridge of semi-circular cross section are used. Under the condition of uniform velocity profile at far upstream, we have Model A (Fig.5.1) and Model B (Fig.5.2). To investigate the relation between lee wave and vortex, we calculate the stratified flows with a shear velocity profile at far upstream. In Model C (Fig.5.3), the shear is strong in all flow field. In Model D (Fig.5.4), The strong shear located only on the area near the critical layer. We assume that the initial density field is stratified linearly, which decrease with the height increase, and the variation of the density in vertical direction is very small to ensure the valid of Boussinesiq approximation. The initial velocity field is constructed by the velocity field with the velocity profile at far upstream and the velocity field of the potential flow.

The solid boundary is treated by panel method in the calculation. The

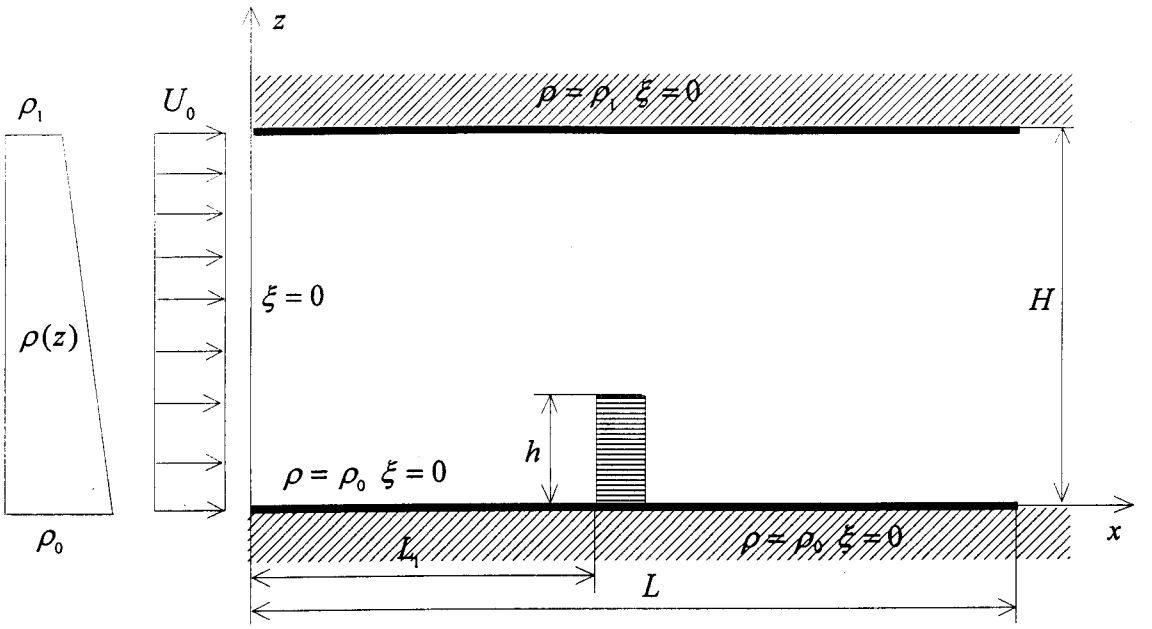

Fig.5.1 Model A: Stratified flows past a plate in a channel of finite depth with an uniform velocity profile at far upstream

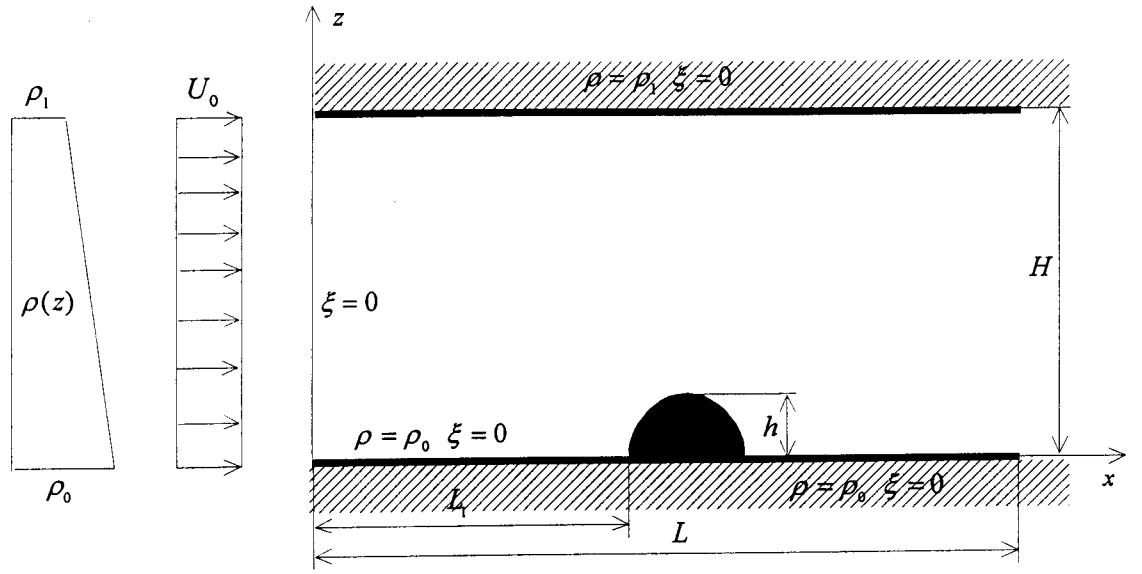

Fig.5.2 Model B: Stratified flows past a ridge of semi-circular cross section in a channel of finite depth with an uniform velocity profile at far upstream

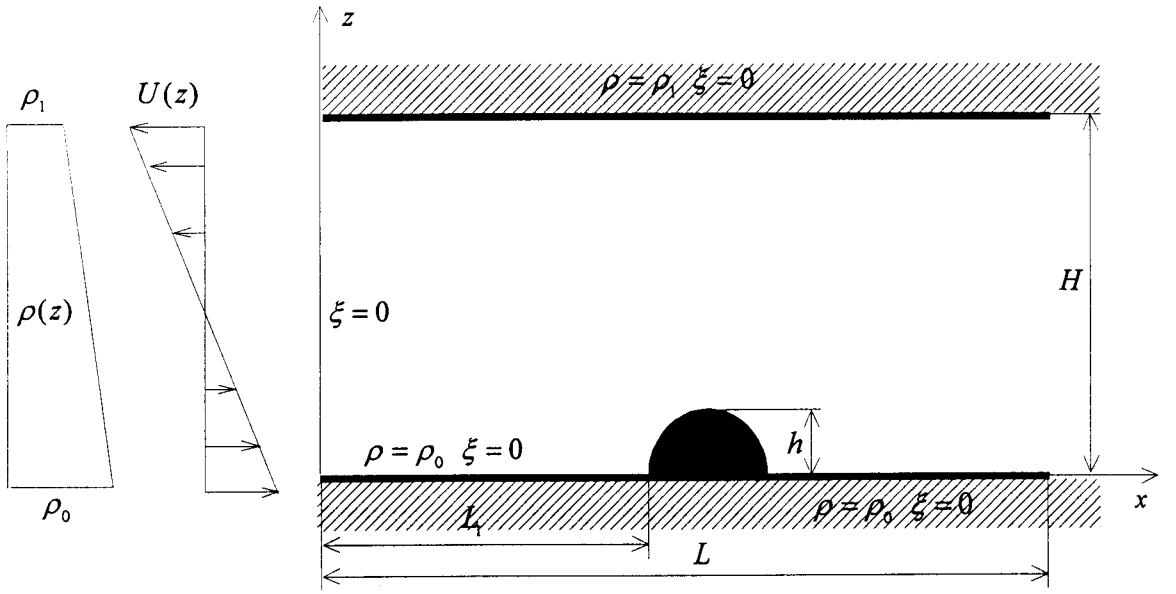

Fig.5.3 Model C: Stratified flows past a ridge of semi-circular cross section in a channel of finite depth with a strong shear velocity profile at far upstream

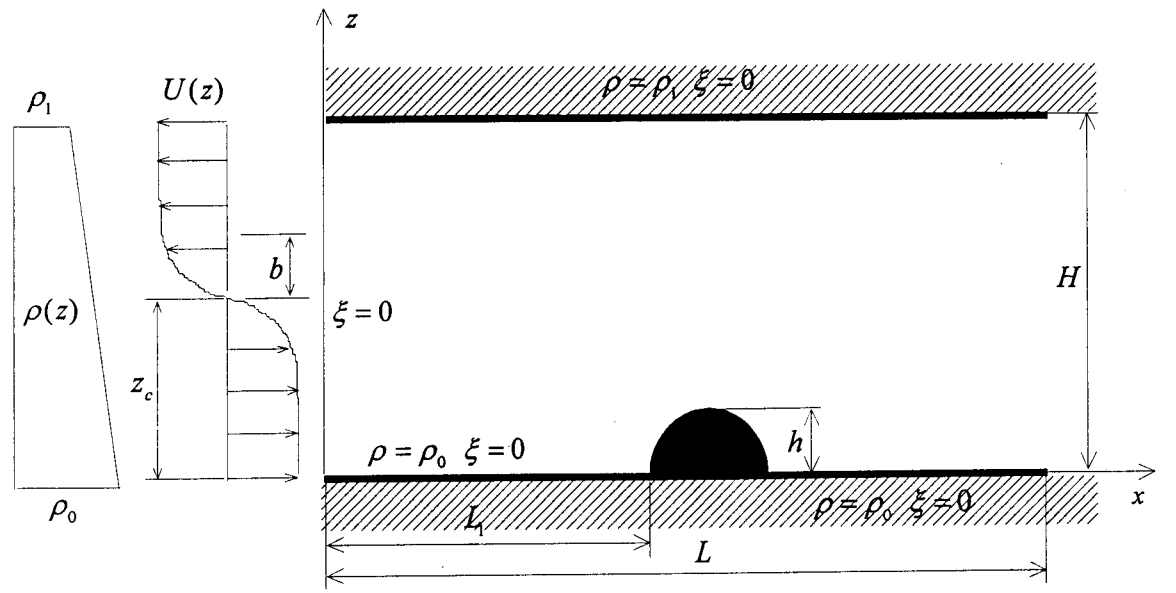

Fig.5.4 Model D: Stratified flows past a ridge of semi-circular cross section in a channel of finite depth with a shear velocity profile at far upstream

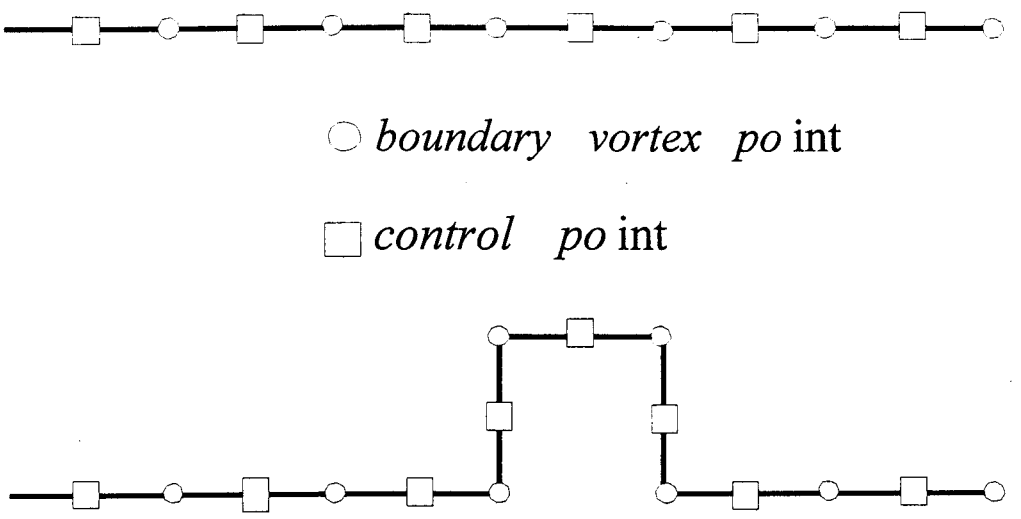

Fig.5.5 Boundary vortexes and control points of flow past an obstacle in a channel of finite depth.

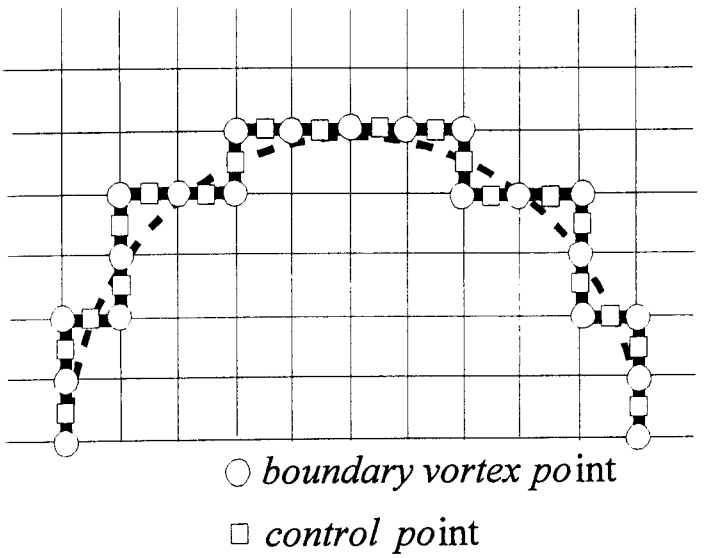

Fig.5.6 Boundary vortexes and control points for a ridge of semi-circular cross section

position of boundary vortices and control points for the vertical plate obstacle model is displayed in Fig.5.5. The ridge of semi-circular cross section is simplified by a zigzag shape body (i.e. the circular ship represented by squares, which grid pitch is equal to mesh length). The position of boundary vortices and control points for a ridge of semi-circular cross section is displayed in Fig.5.6. In our calculation, the radius of the semi circle is 5, so this ridge of semi-circular cross section represented by 10 meshes in horizontal direction and 5 meshes in vertical direction (Fig.5.6).

In theoretical analysis, the infinite length of channel is assumed to ensure the velocity condition at far upstream. In actual numerical simulation, the calculation range is finite. Therefore, some error will be caused at the inlet. To restain the influence of this error on all flow field, the velocity at inlet is calculated by interpolate its nearest velocity.

The boundary vortices is used to replace the solid boundary in panel method. It is not the real vortex, so the boundary vortices will not move with the velocity field, and not be distributed in the calculation.

The definitions of the parameters for a flow past an obstacle in a channel of finite depth are as follows:

H: Channel depth

h: Height of the obstacle

L: All calculation range

L_1: Upstream calculation range

$U(z)$: Velocity profile at far upstream

U_0: Reference velocity (the largest velocity at far upstream)

ρ_0: Reference density

N: *Brunt – Väisälä* frequency $N^2 = -\frac{g}{\rho_0}\frac{d\overline{\rho}}{dz}$

K: Density stratification degree $K = \frac{NH}{\pi U_0}$

F_r: *Froude* number $Fr = \frac{U_0}{Nh} = \frac{H/h}{\pi K}$

R_i: Richardson number $R_i = \frac{N_0^{\,2}}{(\frac{dU(z)}{dz})^2}$

t^*: Dimensionless time $t^* = Nt$

The boundary conditions for a flow past an obstacle in a channel of finite depth are as follows.

$$\frac{\partial \rho}{\partial z} = -\frac{\rho_1 - \rho_0}{H},\ \vec{u} = (U(z),0),\ \xi = 0 \qquad \text{at far upstream}$$

$$\rho = \rho_1,\ u_n = 0, \xi = 0,\ \frac{\partial p'}{\partial z} = 0 \qquad \text{on the upper wall}$$

$$\rho = \rho_0,\ u_n = 0, \xi = 0,\ \frac{\partial p'}{\partial z} = 0 \qquad \text{on the lower wall}$$

$$\frac{\partial \rho}{\partial x} = 0,\ u_n = 0, \xi = 0 \qquad \text{on the obstacle surfaces}$$

where the subscript n denotes the normal direction to the boundary and u_n is the velocity component in the n direction, $\vec{u}$ is velocity vector, $U(z)$ is the velocity

profile at far upstream, ξ is vorticity, p' is the perturbation pressure, ρ is density, ρ_0 and ρ_1 is a constant.

In Model A and Model B, the velocity profile at far upstream $U(z)$ is assumed as

$$U(z) = U_0 \qquad (5.1)$$

so there is no critical layers in the flows, and Richardson number $R_i = 0$.

To ensure the existence of critical layer in the flow field, in Model C, the velocity profile at far upstream $U(z)$ is given by Eq.5.2

$$U(z) = (1 - \frac{2z}{H})U_0 \qquad (5.2)$$

and in Model D, the velocity profile at far upstream $U(z)$ is given by a hyperbolic tangent function

$$U(z) = U_0 \tanh[\frac{z_c - z}{b}] \qquad (5.3)$$

where U_0 is the largest velocity at far upsteam, a constant, Z_c is the position of critical layer and b is the range having stronger shear velocity.

According to the definition of Richardson number, the Richardson number in Model C is

$$R_i = \frac{N^2}{(2U_0/H)^2}. \qquad (5.4)$$

In Model D, from Eq.5.3, we know that the largest velocity gradient occurs in the place $z = Z_c$,

$$(\frac{dU(z)}{dz})^2 |_{max} = \frac{U_0^2}{b^2} \tag{5.5}$$

so that the minimum gradient Richardson number in the flows is

$$R_i |_{min} = b^2 \left(\frac{N}{U_0} \right)^2 . \tag{5.6}$$

We can change *Froude* number F_r by choosing reference velocity U_0, and decide Richardson number according to U_0 and b.

If $R_i|_{min} > 0.25$, then the Richardson number in all flow field is larger than 0.25, so that the flow is stable. If $R_i|_{min} < 0.25$, somewhere, the flow is unstable.

5.3 Numerical results and discussions

Figure 5.7, Fig.5.8 and Fig.5.9 gives the development of streamlines of flows past a plate in a channel (with an uniform velocity profile at far upstream) at Fr=0.01,0.25 and 0.5, respectively (corresponding to Model A). In this calculation, the height of the plate obstacle is 10, mesh number is $250 \times 80 (L \times H)$, and the position of obstacle is $L_1 = 160$. The upstream columnar disturbance and lee wave is observed. At smaller Froude number Fr=0.01, the eddy region of cell

structure is propagated upstream and downsteam fast. With the time increase, the blocking area in front of the plate and lee waves behind it is formed. At Froude number Fr=0.25, the eddy region of cell structure is also observed, but its propagating speed is very slow. When Froude number Fr=0.5, no eddy region of cell structure is observed, the flow seems to be a steady flow. These results are quantitatively in agreement with the results given by Baines [6], that is, when the Froude number is smaller there are upstream waves in front of the obstacle and lee waves behind it.

Figure 5.10, Fig.5.11 and Fig.5.12 gives the development of perturbation streamlines responding to Figure 5.7, Fig.5.8 and Fig.5.9. We can see that the perturbation speeds become larger with the decrease of the Froude number, so that the blockings and lee waves can be formed rapidly at smaller Froude number, which qualitatively in agreement with the results given by Hanazaki [14].

Figure 5.13 shows the streamlines of the flow past a ridge of semi-circular cross section in a channel of finite depth with an uniform velocity profile at far upstream (Model B) by LVM, where mesh number is $100\times50(L\times H)$ and the radius of semicircle is 5. We can see that the lee waves propagate downstream and upward, which is similar to that given by Miles& Huppert [15] (Fig.5.14).

Figure5.15(a)(b)(c)(d) show the simulation results of the flow past a ridge of semi-circular cross section in a channel of finite depth with a shear velocity profile at far upstream (Model C). In this calculation model, mesh number is $150\times 30(L\times H)$, the radius of semicircle obstacle is 5 , and $U_0=3.0$. From the development of streamlines (Figure5.15(a)), we can see that the critical layer (at the level of zero horizontal velocity) absorbs lee waves, and lee waves can not propagate upward through this layer. The development of density contours (Figure5.15(c)) shows that there is the adverse flow area under the critical layer, in which the fluid with heavy density will run over the fluid with light density. In this area, the flow is unstable. From the development of perturbation streamlines

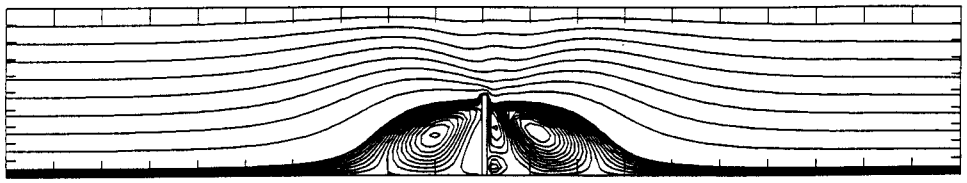

$t^* = 5$

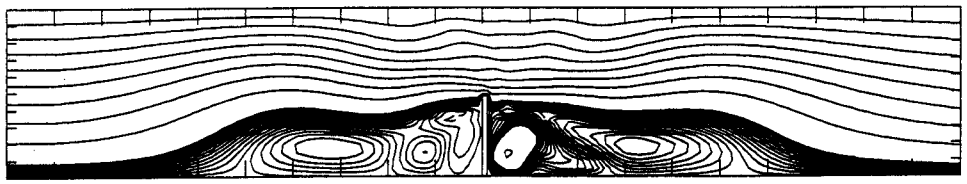

$t^* = 10$

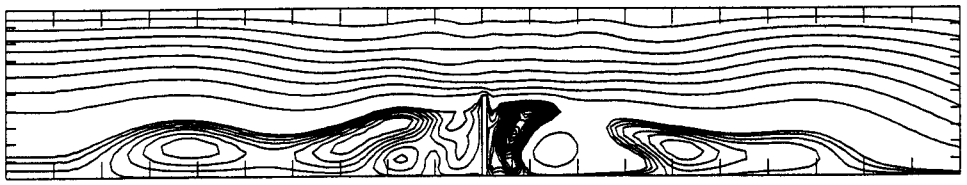

$t^* = 15$

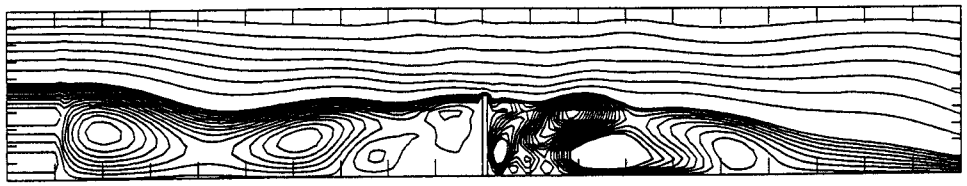

$t^* = 20$

Fig.5.7 Development of streamlines of flows over a plate in a channel with an uniform velocity profile at far upstream at Fr=0.01

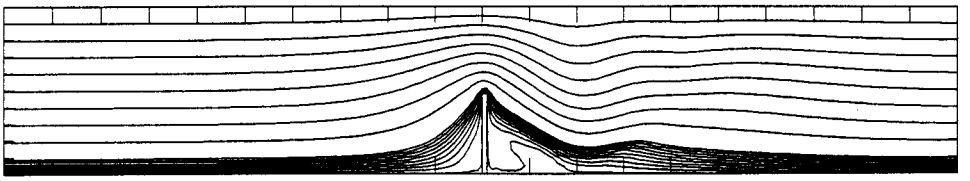

$t^* = 5$

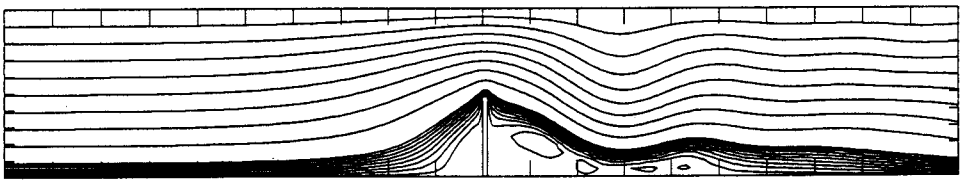

$t^* = 10$

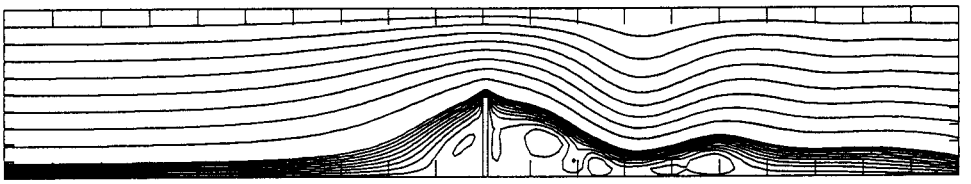

$t^* = 15$

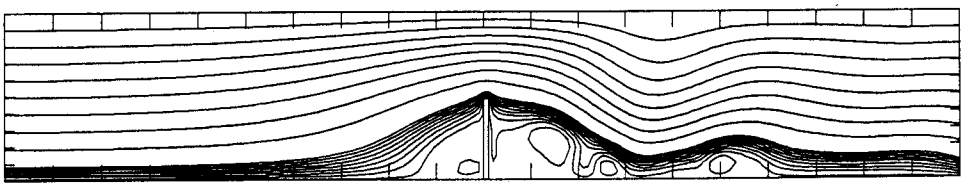

$t^* = 20$

Fig.5.8 Development of streamlines of flows over a plate in a channel with an uniform velocity profile at far upstream at Fr=0.25

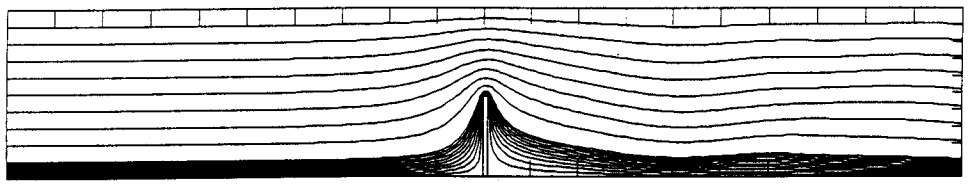

$t^* = 5$

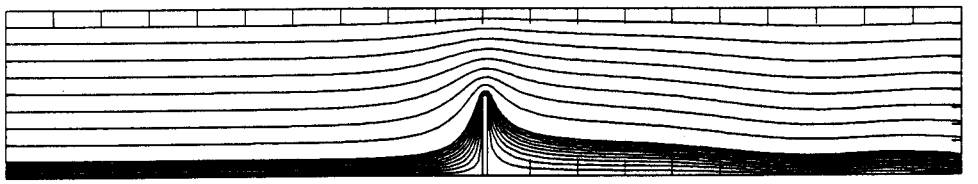

$t^* = 10$

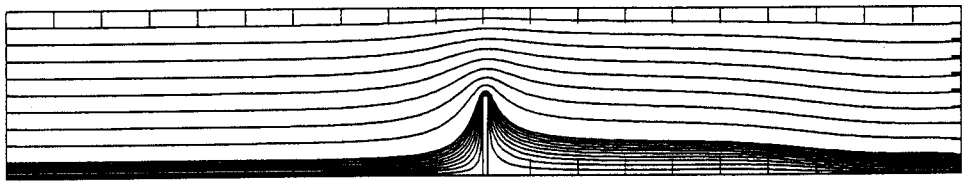

$t^* = 15$

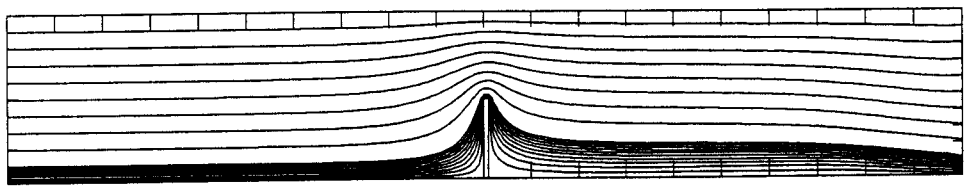

$t^* = 20$

Fig.5.9 Development of streamlines of flows over a plate in a channel with an uniform velocity profile at far upstream at Fr=0.5

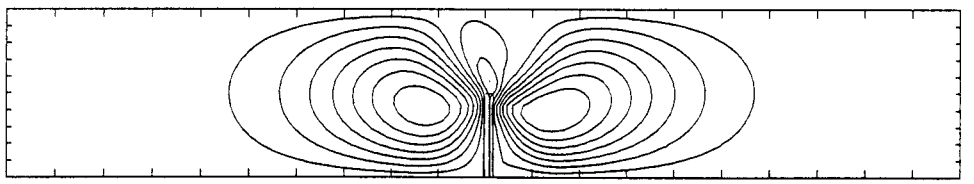

$t^* = 5$

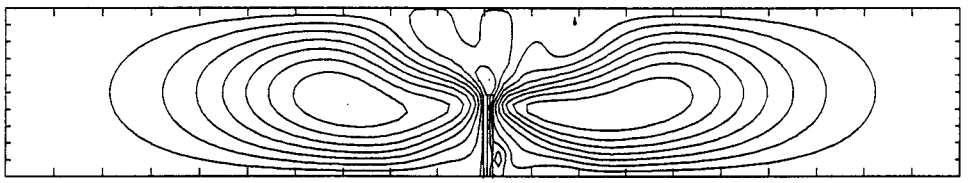

$t^* = 10$

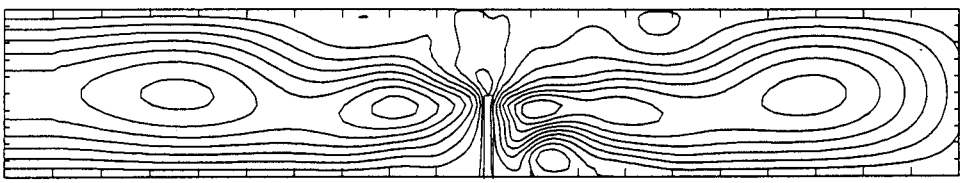

$t^* = 15$

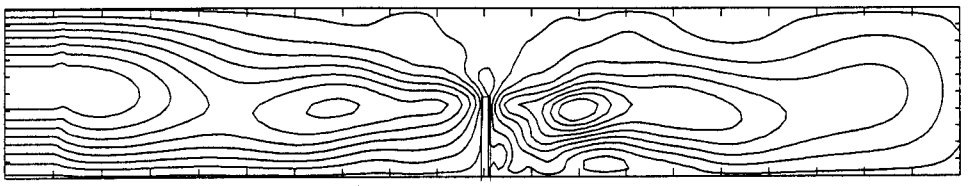

$t^* = 20$

Fig.5.10 Development of perturbation streamlines of flows over a plate in a channel with an uniform velocity profile at far upstream at Fr=0.01

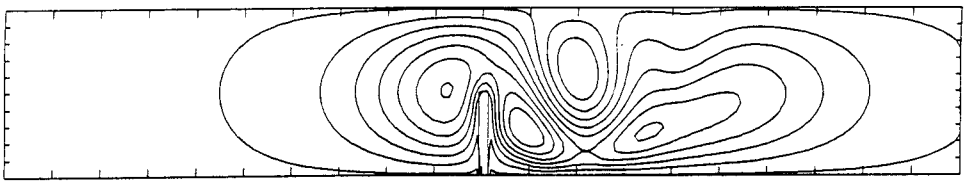

$t^* = 5$

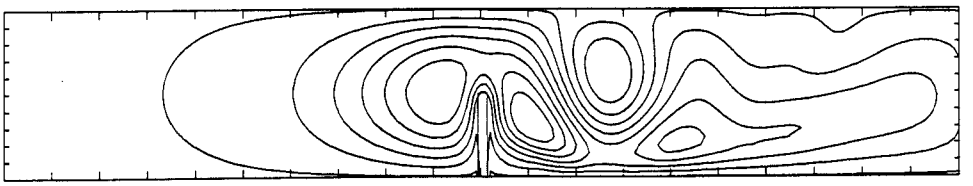

$t^* = 10$

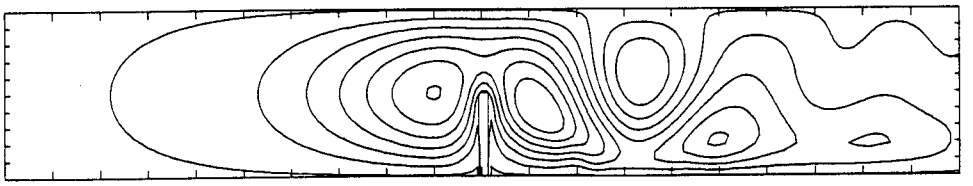

$t^* = 15$

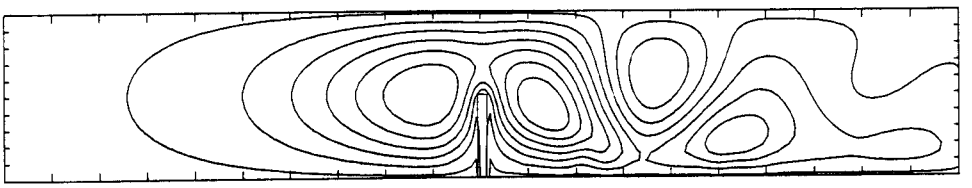

$t^* = 20$

Fig.5.11 Development of perturbation streamlines of flows over a plate in a channel with an uniform velocity profile at far upstream at Fr=0.25

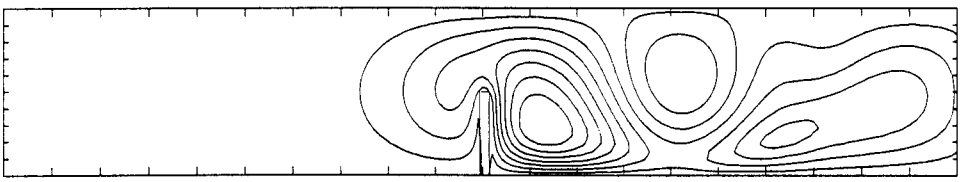

$t^* = 5$

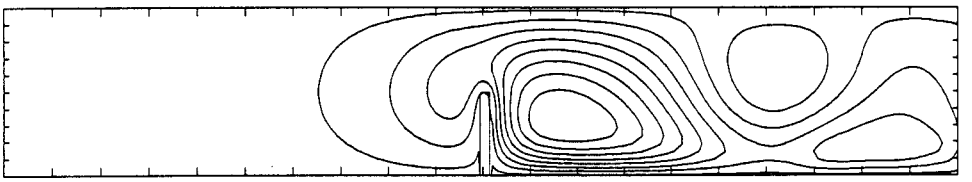

$t^* = 10$

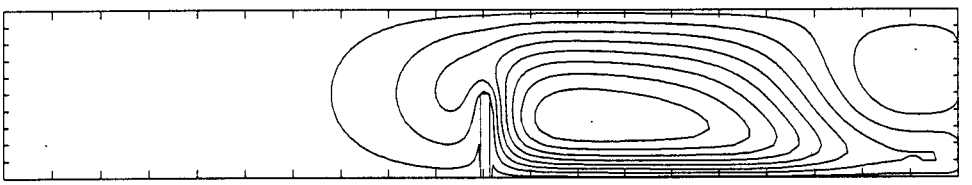

$t^* = 15$

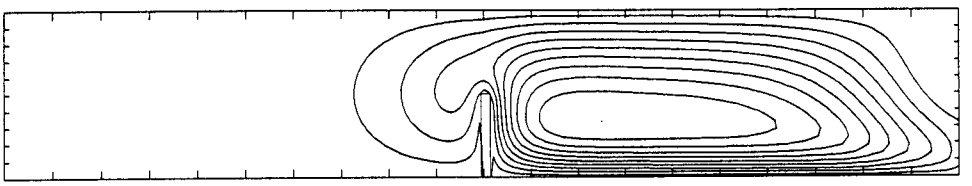

$t^* = 20$

Fig.5.12 Development of perturbation streamlines of flows over a plate in a channel with an uniform velocity profile at far upstream at Fr=0.5

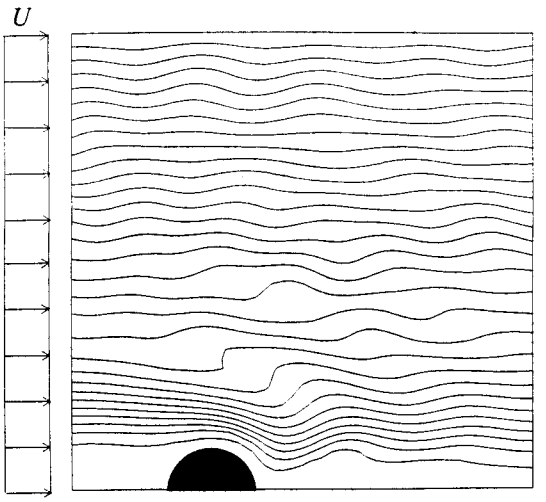

Fig.5.13 Flow over a ridge of semicircular cross section in a channel of finite depth with an uniform velocity profile at far upstream for ($K \approx 4$)
(present numerical result)

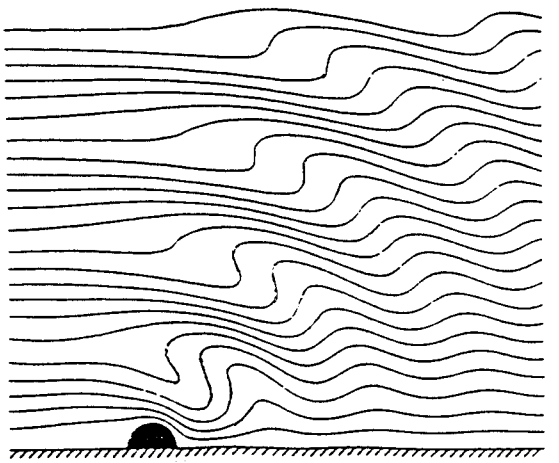

Fig.5.14 Flow over a ridge of semicircular cross section in a channel of finite depth with an uniform velocity profile at far upstream
(numerical result given by Miles & Huppert [14] 1969)

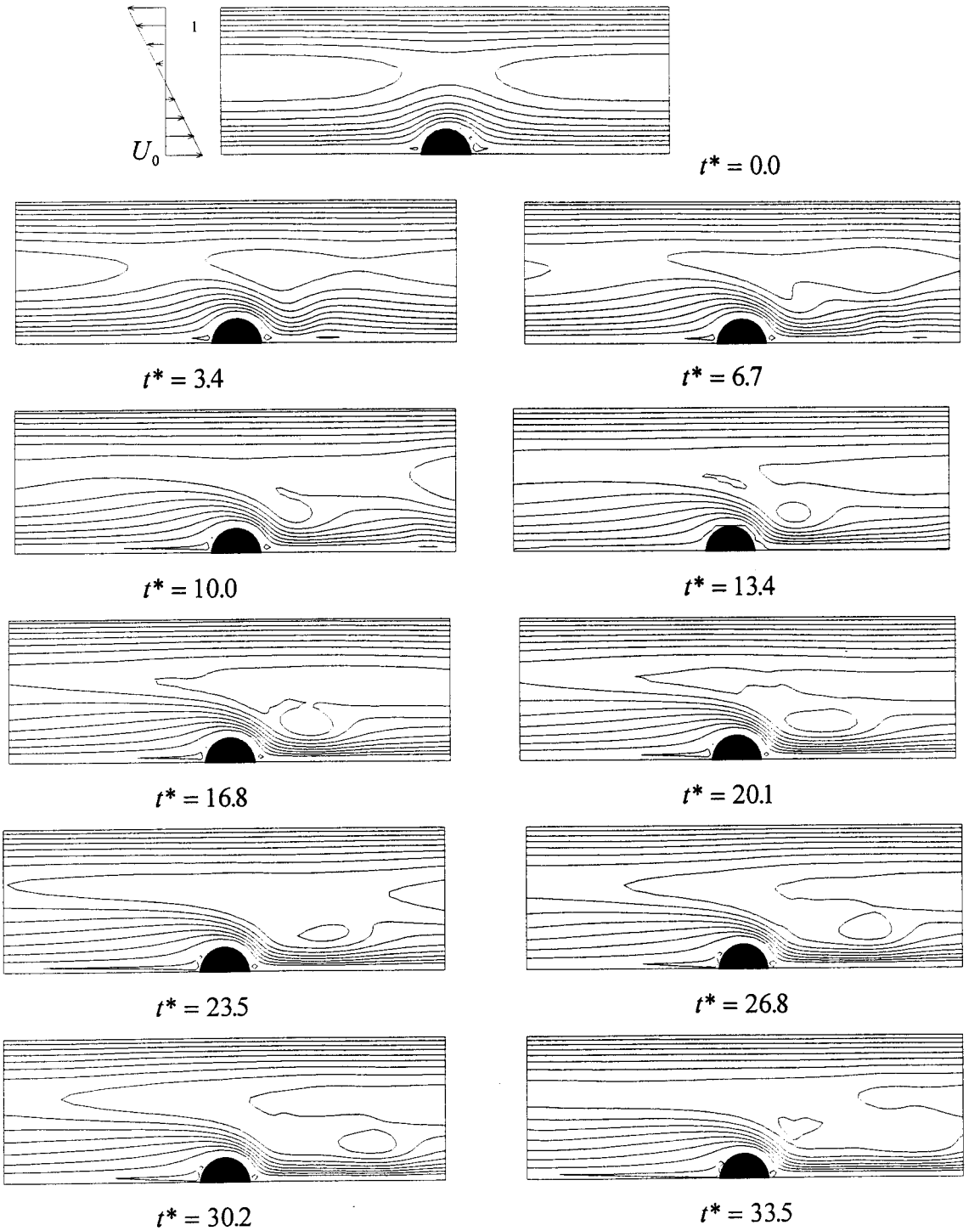

Fig.5.15(a) Streamlines of flows over a ridge of semicircular cross section in a channel of finite depth with a shear velocity profile at far upstream ($K \approx 1.5$)

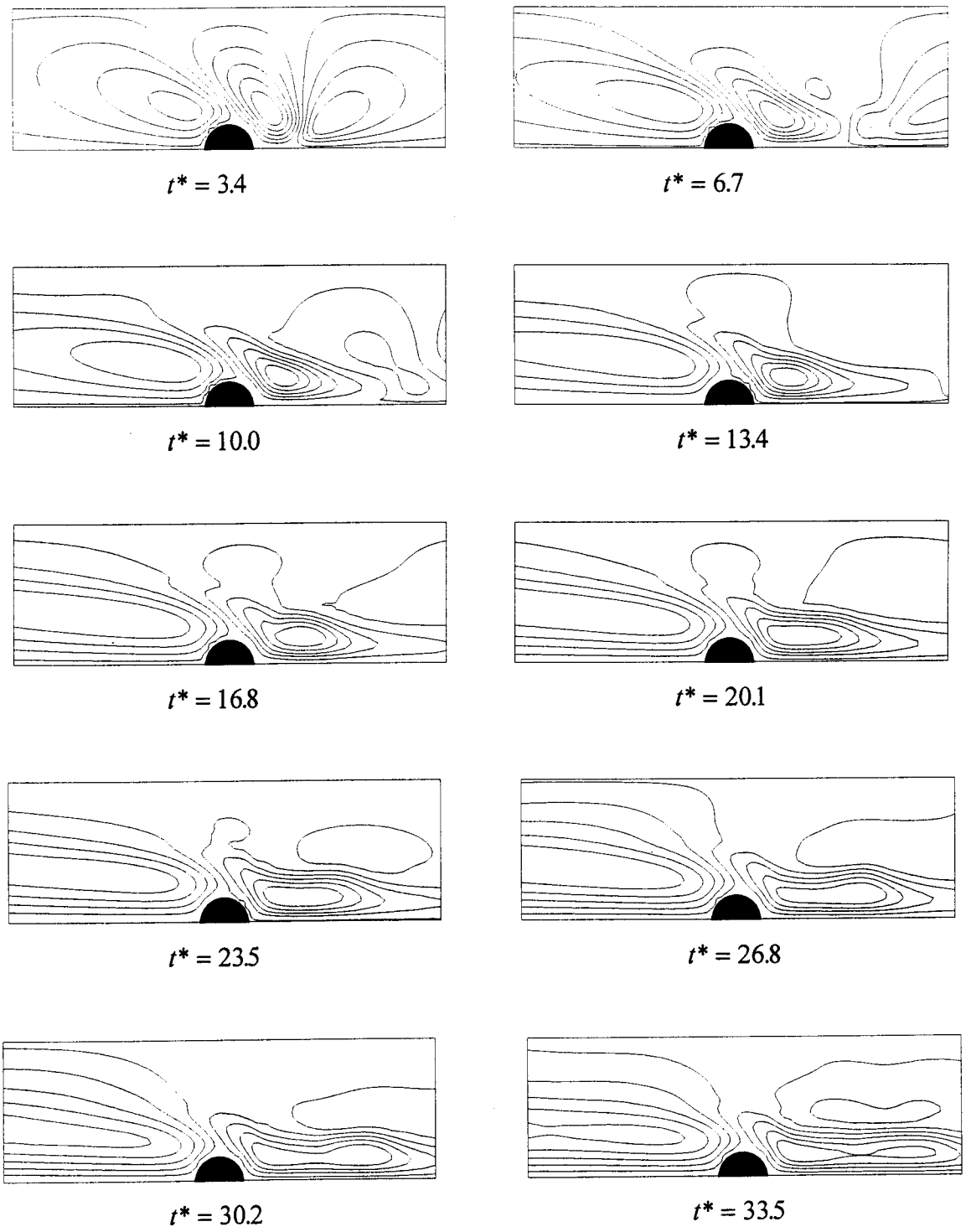

Fig.5.15(b) Perturbation streamlines of flows over a ridge of semicircular cross section in a channel of finite depth with a shear velocity profile at far upstream ($K \approx 1.5$)

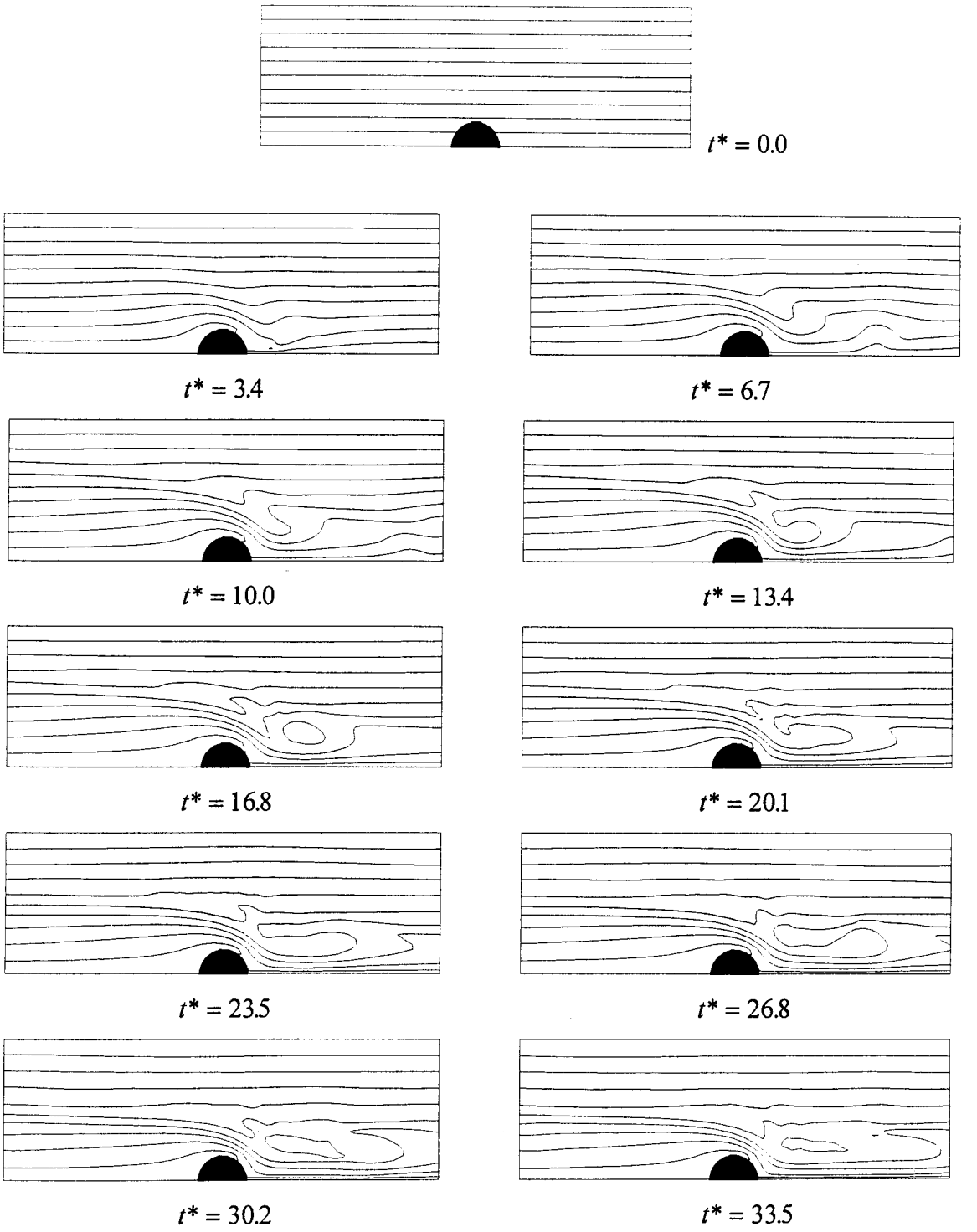

Fig.5.15(c) Density contours of flows over a ridge of semicircular cross section in a channel of finite depth with a shear velocity profile at far upstream ($K \approx 1.5$)

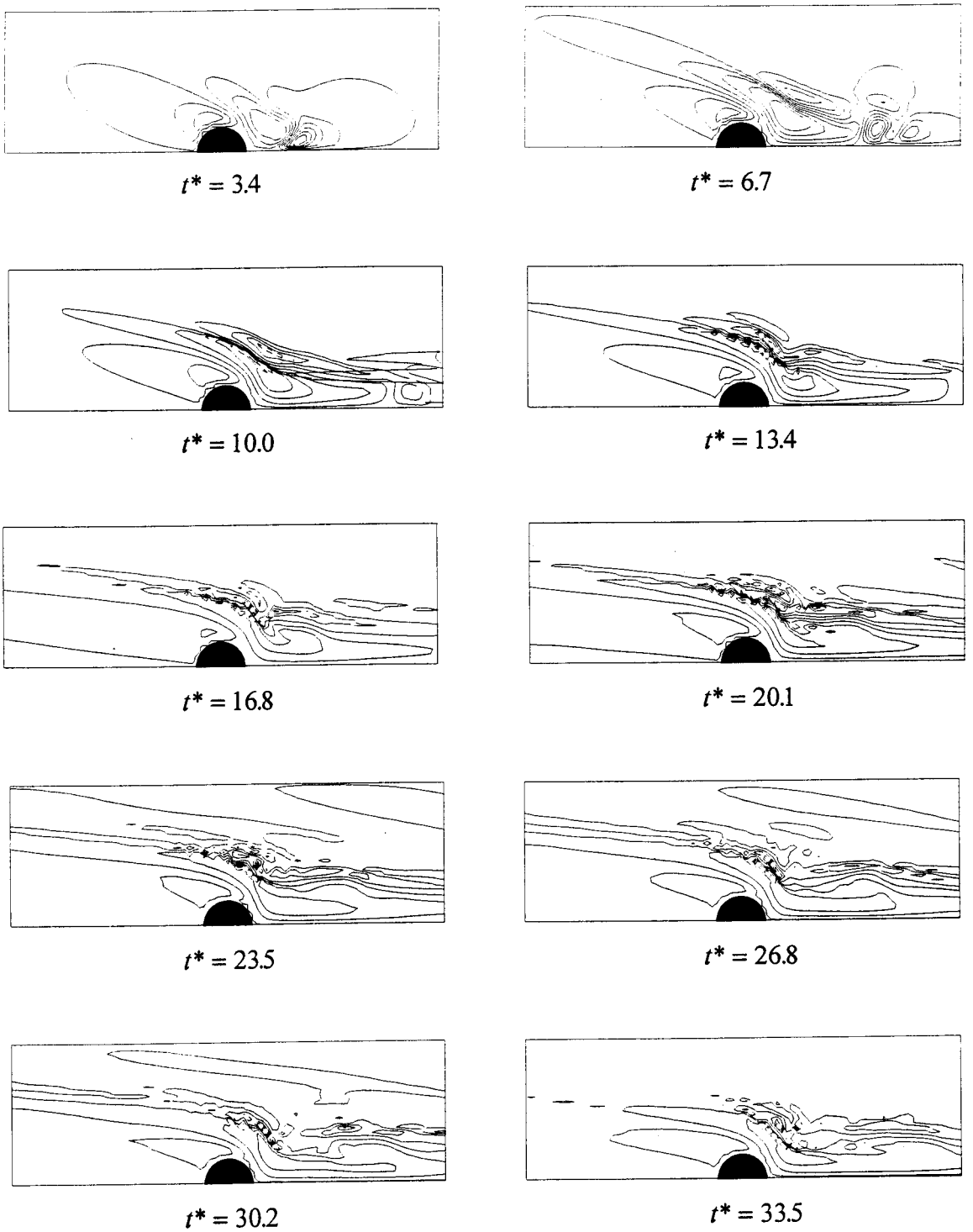

Fig.5.15(d) Vortex contours of flows over a ridge of semicircular cross section in a channel of finite depth with a shear velocity profile at far upstream ($K \approx 1.5$)

(Figure5.15(b)), we know that the variation of velocity is smaller in the region over the critical layer. The development of vorticity contours (Figure5.15(d)) shows that the strong vortex is generated in the region under the critical layer, especially in the area near critical layer.

This phenomenon will be explained by suitable vortex generation in the layer, which is investigated in detail using Model D.

For comparison, Figure 5.16 gives some results in Model B, in which there is no critical layer in all flow field ($R_i = \infty$). From the streamline (Fig.16(a)) and perturbation streamline (Fig.16(b)), we know that the inner waves induced by the obstacle propagate upward till upper solid boundary. Fig.5.16(c) gives the contours of density gradient $\partial\rho/\partial x$. Fig.5.16(d) gives the contours of vorticity. The area with a symbol (−) represents that in this area the value of $\partial\rho/\partial x$ is negative, and The area with a symbol (+) represents that in this area the value of $\partial\rho/\partial x$ is positive. According to Eq.3.17, the vorticity will be increase or decrease by $-\frac{g}{\rho_0}\frac{\partial\rho}{\partial x}$. From Fig.5.16(c) and Fig.5.16(d), we know that the generated vorticity (represented by $-\frac{g}{\rho_0}\frac{\partial\rho}{\partial x}$) often have same symbol with the vorticity advected, so that the internal waves propagate in all region.

Figure 5.17~Figure 5.32 gives the results in Model D, in which the existence of a critical layer is ensured by employing a hyperbolic tangent profile of horizontal velocity. From these results, we know that the critical layer has a great influence on the characteristic of the flow.

Figure 5.17~Figure 5.22 is the results when Richardson number Ri=5.0. Figure 5.17 shows the development of streamlines. For displaying the strong shear area clearly, the interval of streamline in the area near critical layer is 1/20 of that in other area. The development of density contours is displayed in Fig.5.18. From Fig.5.17 and Fig.5.18, we know that the adverse flow only occurs in the area

near critical layer, and it is always limited under the critical layer with the increase of calculation time. In the adverse flow area, the fluid with heavy density will run over the fluid with light density, so the flow in this area is unstable. The development of perturbation streamlines (Fig.5.19) and the contours of vertical velocity (Fig.5.20) confirms that when Ri>0.25 the perturbation induced by obstacle cannot overcome critical layer to propagate upward. After long calculation time, the perturbation will be propagated downward under critical layer with a series cell structure. From the contours of density gradient $\partial\rho/\partial x$ (Fig.5.21) and the contours of voriticity (Fig.5.22), we know that the vorticity advected by flow is canceled out by the vorticity generated by $-\frac{g}{\rho_0}\frac{\partial\rho}{\partial x}$, and all vortices are collapsed in the area near the critical layer.

Figure 5.23～Figure 5.28 is the results when Richardson number Ri=0.1. The development of streamlines and contours of density is displayed in Fig.5.23 and Fig.5.24, respectively. For displaying the strong shear area clearly, the interval of streamline in the area near critical layer is 1/10 of that in other area. The flow pattern of Kelvin cat's-eye configuration, which is the analytical result of a strong shear stratified flow [16], is also reproduced. With the increase of calculation time, the amplitude of internal waves becomes very large, and no steady result can be gotten. From the development of perturbation streamlines (Fig.5.25) and the contours of vertical velocity (Fig.5.26), we know that the perturbation induced by obstacle will propagate left-upward and right-downward due to the influence of critical layer. From the contours of density gradient $\partial\rho/\partial x$ (Fig.5.29) and the contours of voriticity (Fig.5.30), we know that in all flow field the vorticity advected by the flow is always strengthened by the vorticity generated by $-\frac{g}{\rho_0}\frac{\partial\rho}{\partial x}$.

To investigate the influence of the critical layer on the over-reflection of

internal wave, the equation of perturbation energy Eq.5.5 must be considered.

$$\frac{1}{2}\frac{\partial}{\partial t}\{\overline{u'u'}+\overline{w'w'}\}=-\frac{dU}{dz}\overline{u'w'}-\frac{\partial}{\partial z}\overline{p'w'} \qquad (5.5)$$

where u' and w' are perturbation velocity components in x,z direction, respectively, p' is perturbation pressure, the line upper parameters means the time average, $\frac{1}{2}(\overline{u'u'}+\overline{w'w'})$ is perturbation kinetic energy, $\overline{u'w'}$ is Reynolds stress and $\overline{p'w'}$ is the vertical flux of perturbation kinetic energy, they are calculated by Eq.5.6 and Eq.5.7

$$\frac{1}{2}(\overline{u'u'}+\overline{w'w'})=\frac{\sum(u'u')+\sum(w'w')}{STEP} \qquad (5.6)$$

$$\overline{u'w'}=\frac{\sum(u'w')}{STEP}, \qquad \overline{p'w'}=\frac{\sum(p'w')}{STEP} \qquad (5.7)$$

where STEP is the average time, in our calculation $STEP=100$.

Reynolds stress represents the momentum exchange between the background flow and perturbation. In calculation Model D,

$$\frac{dU(z)}{dz}=-\frac{U_0}{b}\sec h^2(\frac{z_c-z}{b})<0 \qquad (5.8)$$

Therefore, if $\overline{u'w'}>0$, the energy will be withdrawal from the background flow, and perturbation energy will increase. If $\overline{p'w'}<0$, the energy will be transported downward, which means the occurrence of over-reflection of internal wave [17].

Figure 5.29 and Fig.30 shows the results of $\overline{u'w'}$, $\overline{p'w'}$, $\frac{1}{2}(\overline{u'u'}+\overline{w'w'})$ when t=50 at the section x=180 and x=200. In our calculation, $z_c = 40$, which means the position of critical layer. In case of Ri=5.0, there is not an exchange of the energy between the basic flow and perturbation in the area up the critical layer (z>40), in the area under the critical layer (z<40) the perturbation energy propagates upward ($\overline{p'w'}$>0) and supplies basic flow with the energy. However, the perturbation energy decreases according to the increase of the distance from the obstacle. In case of Ri=0.1, in the area up the critical layer (z>40) the perturbation energy propagates upward ($\overline{p'w'}$>0), and in the area under the critical layer (z<40) the perturbation energy propagates downward ($\overline{p'w'}$<0). The inner wave is conveyed up beyond the critical layer ($\overline{p'w'}$>0 in the area z>40) simultaneously with the over-reflection ($\overline{p'w'}$<0 when z<40). In this case, the energy flows from the basic flow to the inner wave ($\overline{u'w'} > 0$). Due to the influence of over-reflection, the perturbation energy $\frac{1}{2}(\overline{u'u'}+\overline{w'w'})$ in the area under the critical layer (z<40) increases substantially.

Figure 5.31 gives the results of vorticity and $\frac{\partial \rho}{\partial x}$ when Ri=5.0 (t=35) at different horizontal levels indicated in Fig.5.17(a), where a is at $z = z_c + 10$level, b is at $z = z_c + 5$level, c is at $z = z_c$ level and d is at $z = z_c - 5$level, respectively. From Fig.5.31, we know that the phase of vorticity advected by flow and the phase of baroclinic term $-\frac{g}{\rho_0}\frac{\partial \rho}{\partial x}$ is nearly opposite. The vorticity transported right-upward will be canceled out at some degree due to the vorticity generated by baroclinic term at that place, so that the vorticity is declined in a density stratified fluid with a shear velocity profile (Fig.5.22). The counteraction of the vorticity in the shear region is the main reason that the perturbation

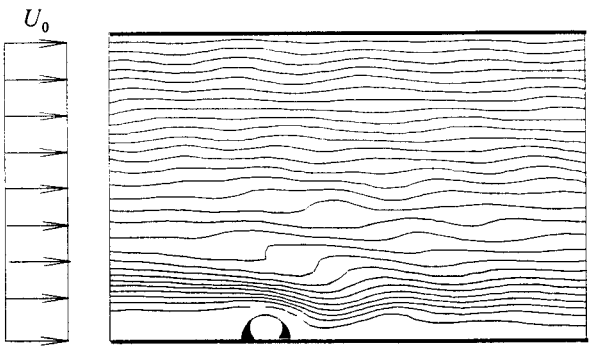

(a) Streamlines

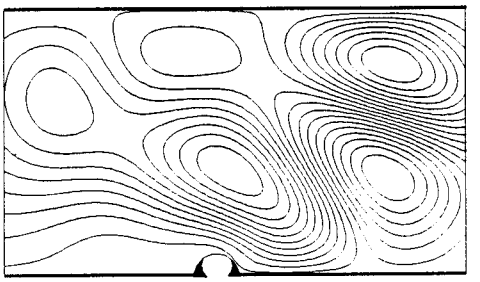

(b) Perturbation streamlines

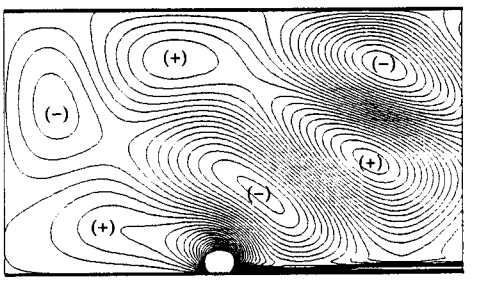

(c) Contours of $\partial p/\partial x$

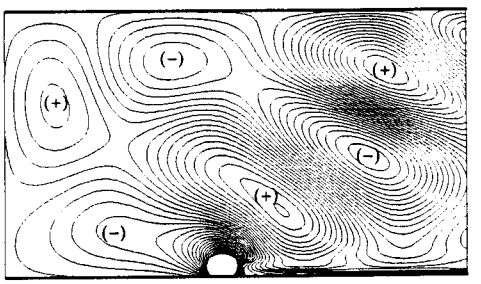

(d) Contours of vorticity

Fig.5.16 Flow over a ridge of semicircular cross section in a channel of finite depth with an uniform velocity profile at far upstream for $K = 4\,(R_i = \infty)$

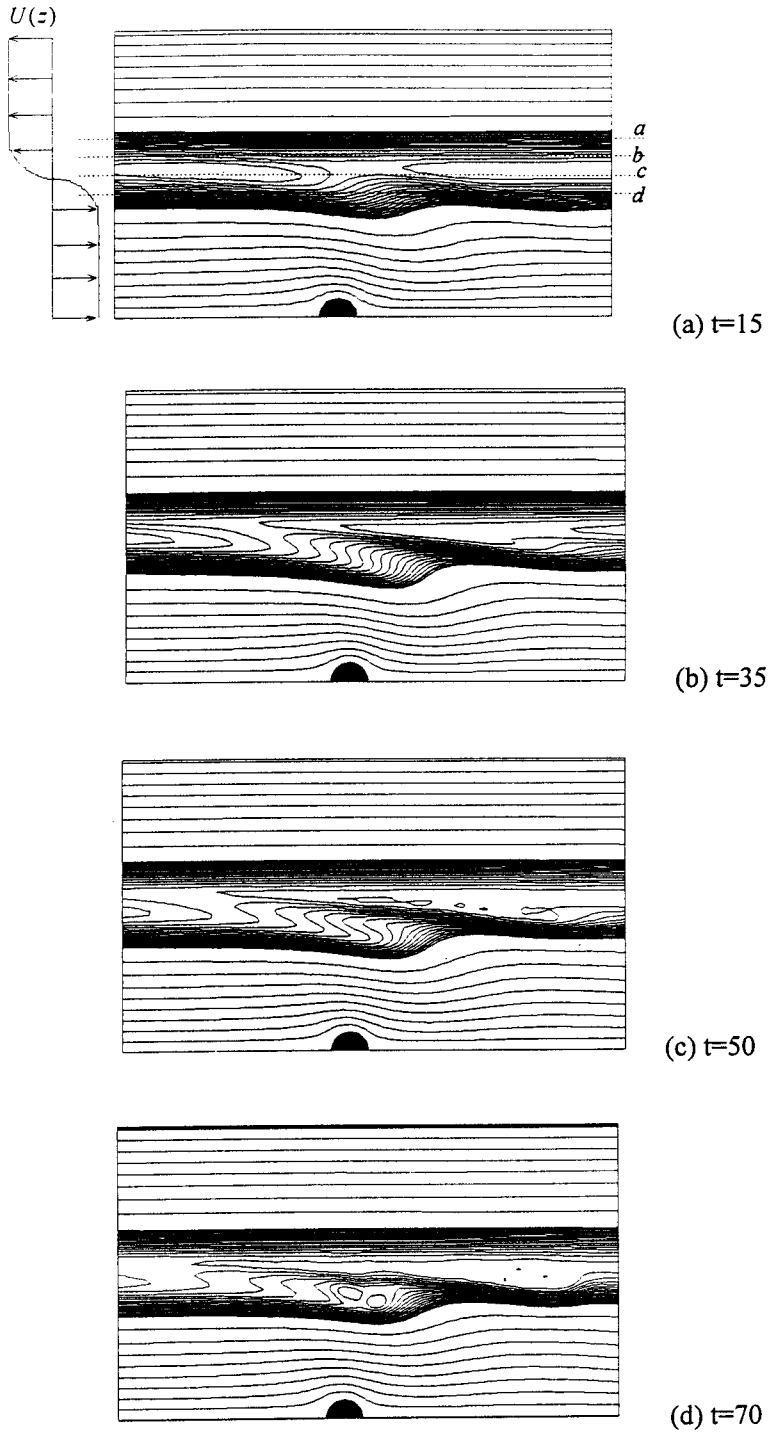

Fig. 5.17 Streamlines at different times when Ri=5.0

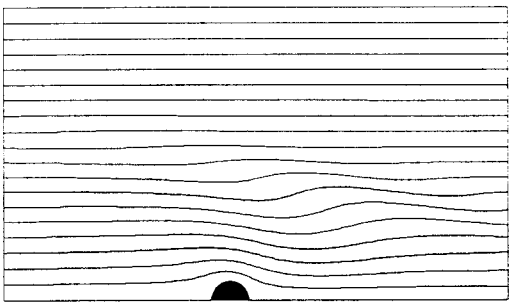

(a) t=15

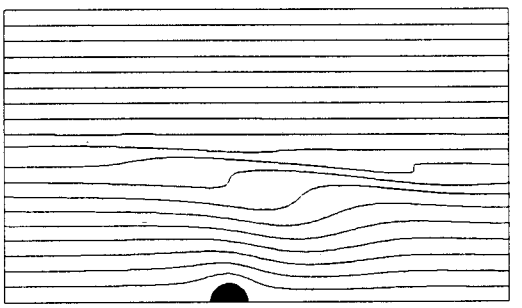

(b) t=35

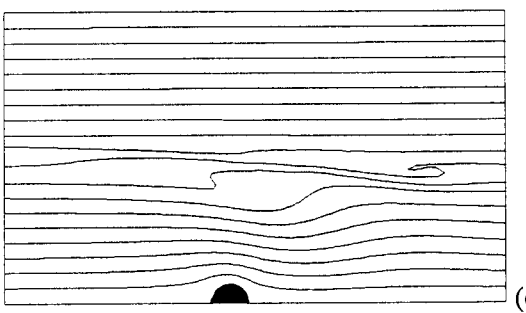

(c) t=50

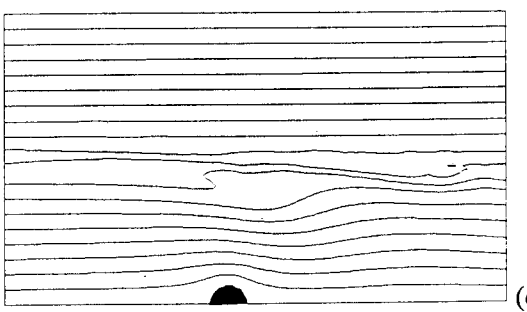

(d) t=70

Fig.5.18 Contours of density at different times when Ri=5.0

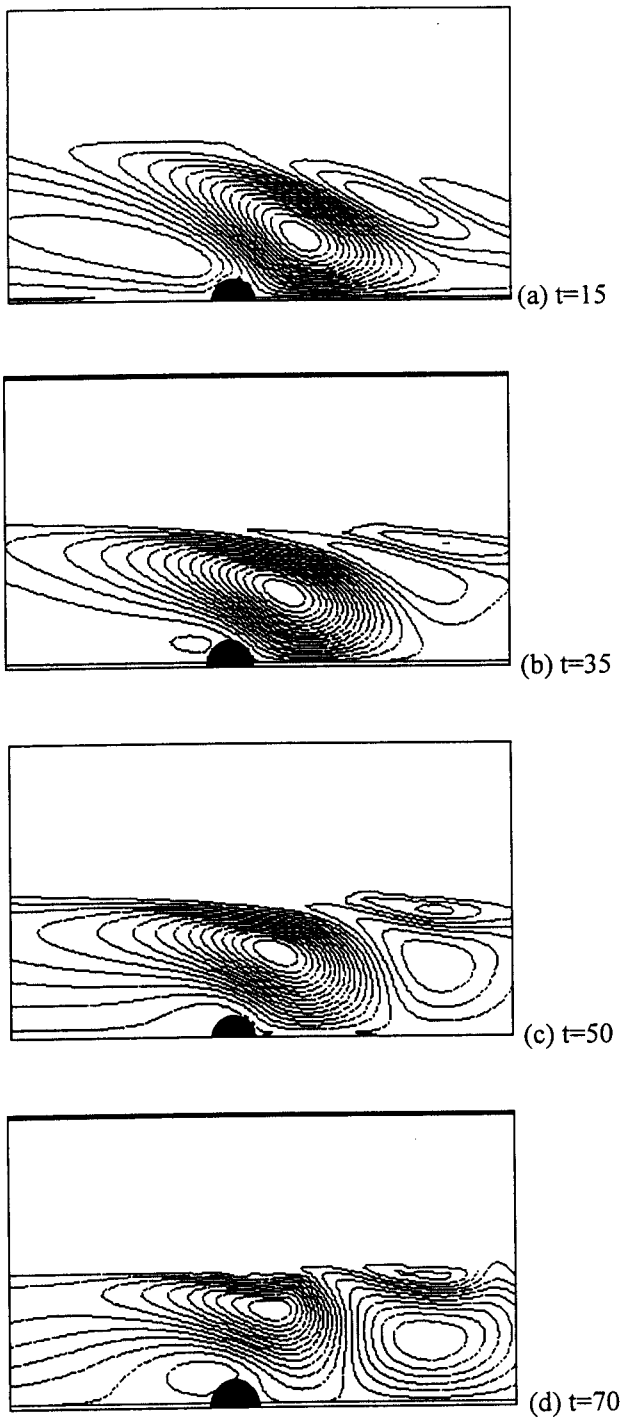

Fig.5.19 Perturbation streamlines at different times when Ri=5.0

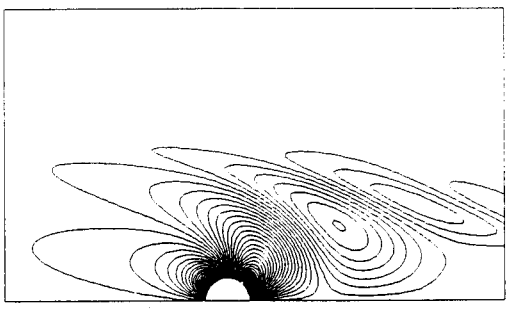

(a) t=15

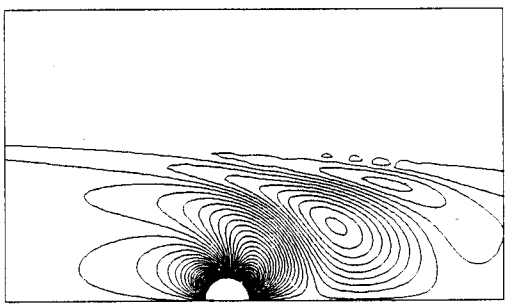

(b) t=35

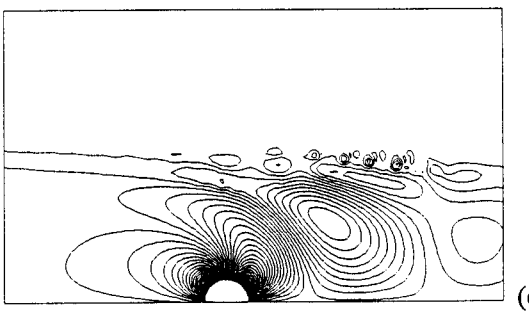

(c) t=50

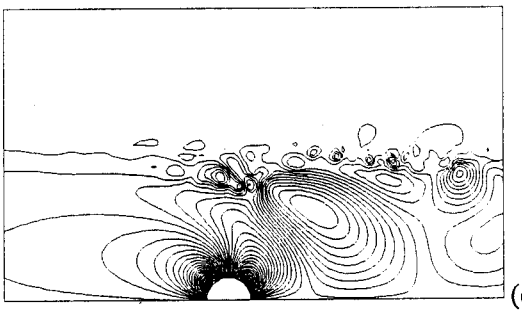

(d) t=70

Fig.5.20 Contours of vertical velocity at different times when Ri=5.0

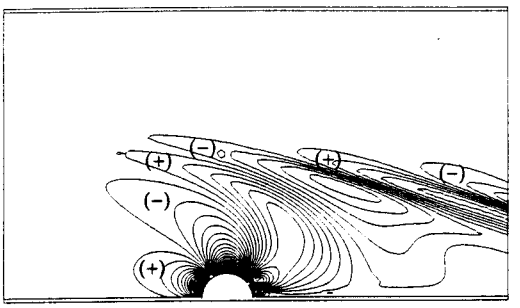

(a) t=15

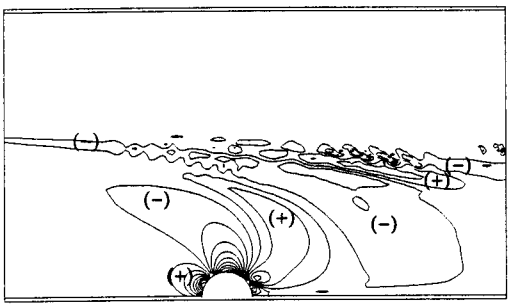

(b) t=35

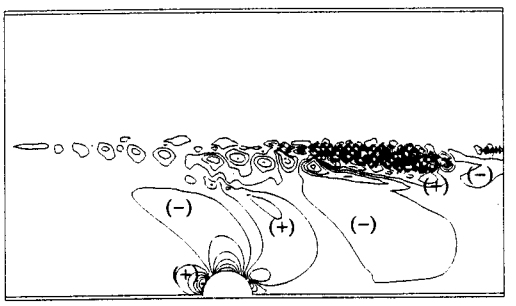

(c) t=50

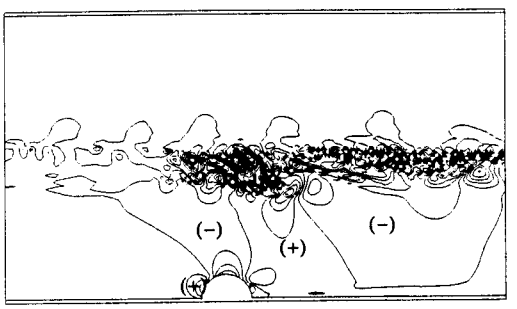

(d) t=70

Fig.5.21 Contours of $\partial\rho/\partial x$ at different times when Ri=5.0

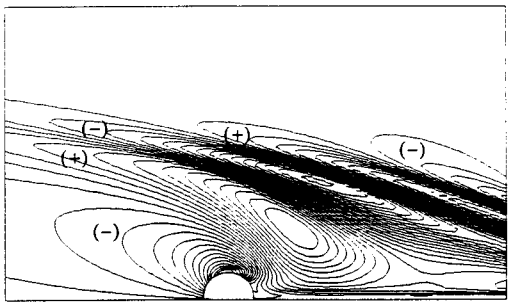

(a) t=15

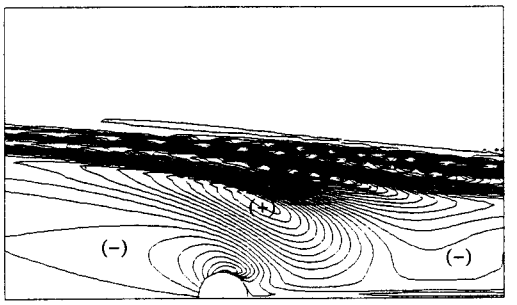

(b) t=35

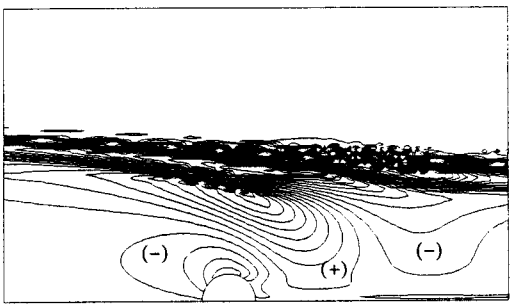

(c) t=50

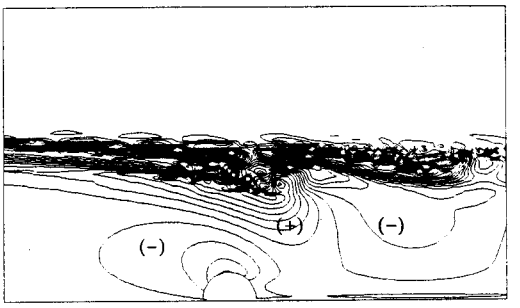

(d) t=70

Fig.5.22 Contours of vorticity at different times when Ri=5.0

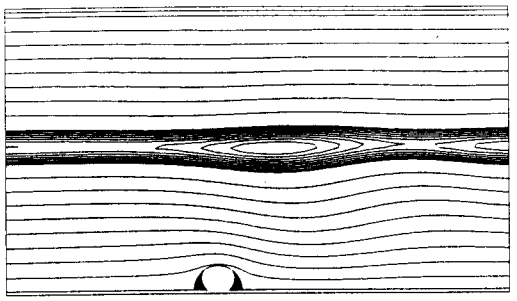

(a) t=15

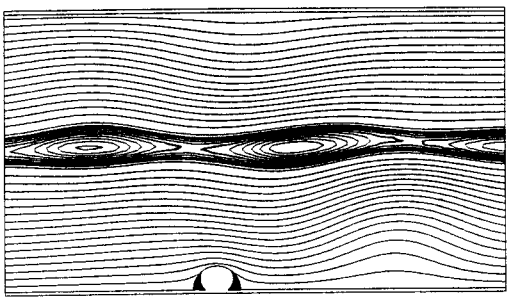

(c) t=50

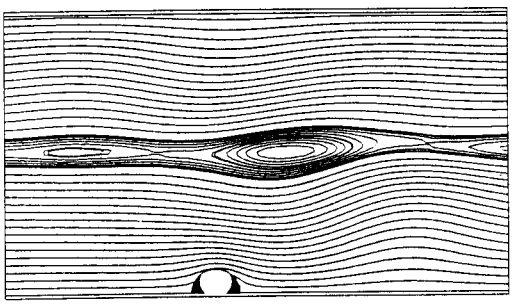

(b) t=35

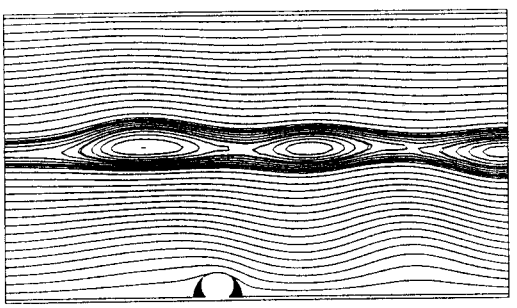

(d) t=70

Fig.5.23 Streamlines at different times when Ri=0.1

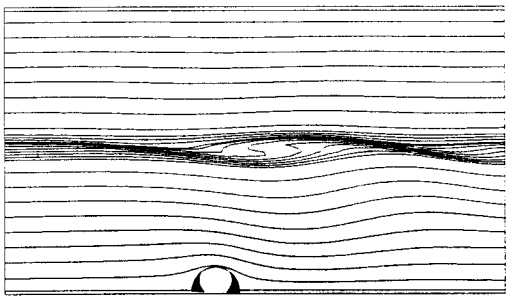

(a) t=15

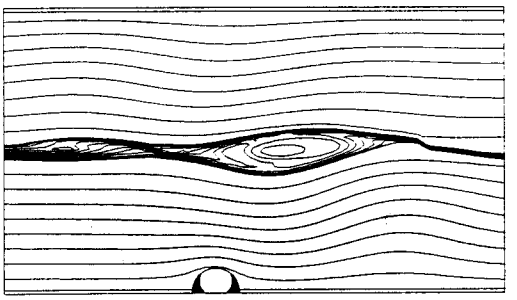

(b) t=35

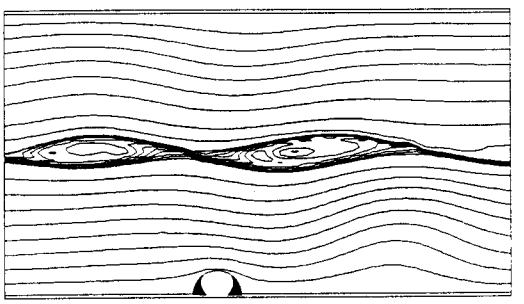

(c) t=50

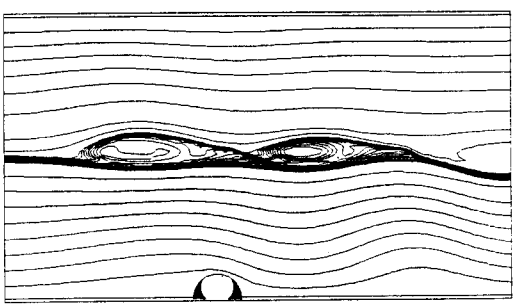

(d) t=70

Fig.5.24 Contours of density at different times when Ri=0.1

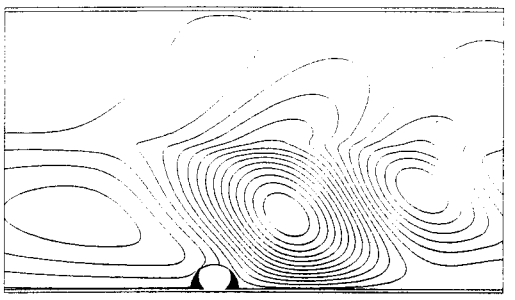

(a) t=15

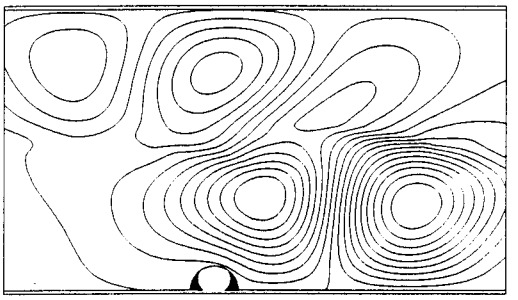

(b) t=35

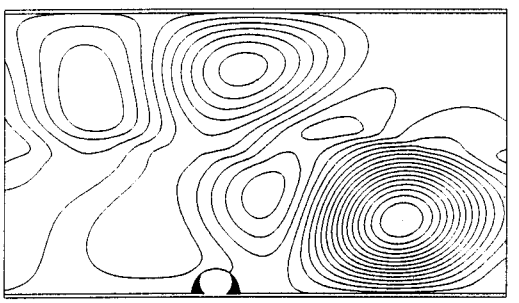

(c) t=50

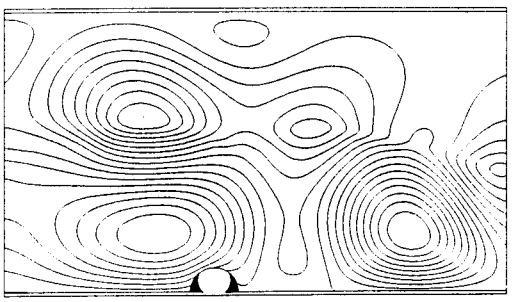

(d) t=70

Fig.5.25 Perturbation streamlines at different times when Ri=0.1

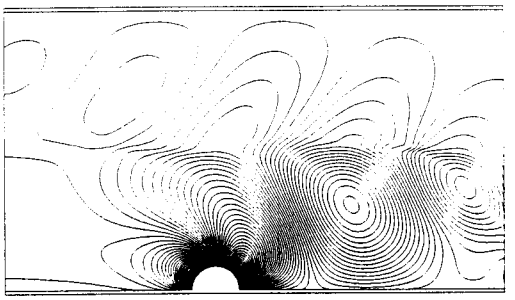

(a) t=15

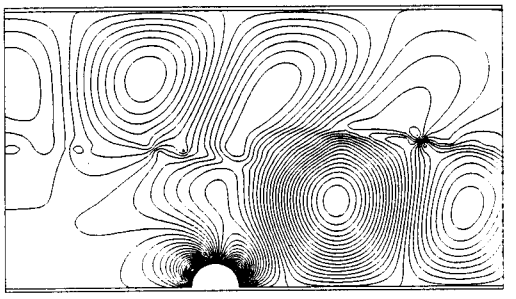

(b) t=35

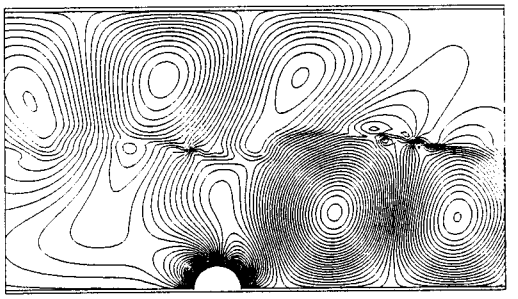

(c) t=50

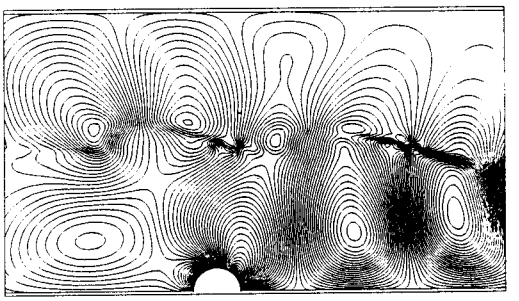

(d) t=70

Fig.5.26 Contours of vertical velocity at different times when Ri=0.1

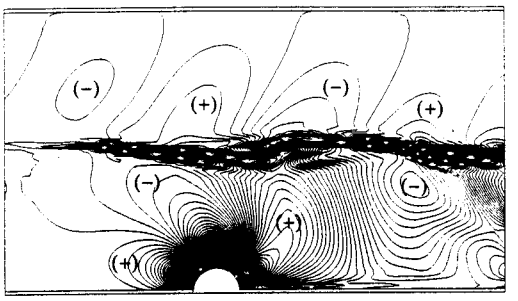

(a) t=15

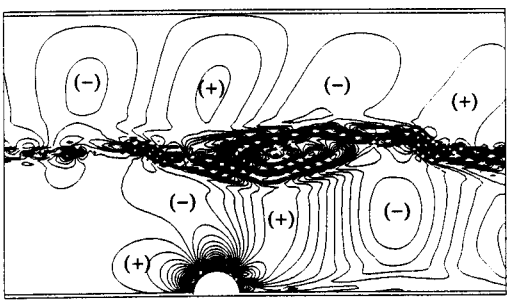

(b) t=35

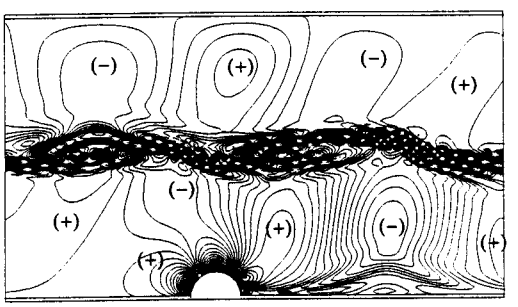

(c) t=50

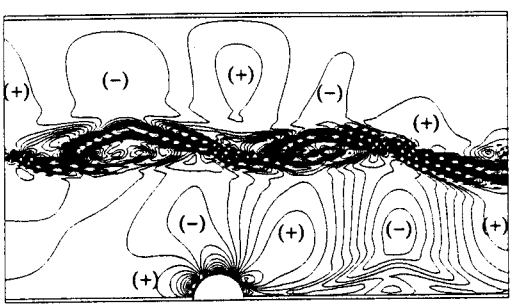

(d) t=70

Fig.5.27 Contours of $\frac{\partial \rho}{\partial x}$ at different times when Ri=0.1

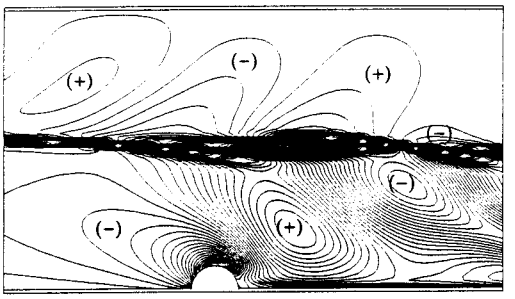

(a) t=15

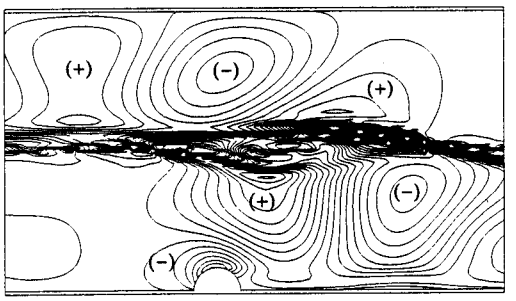

(b) t=35

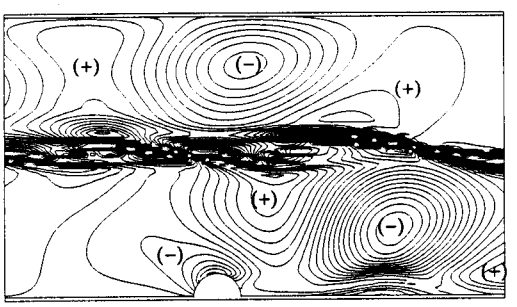

(c) t=50

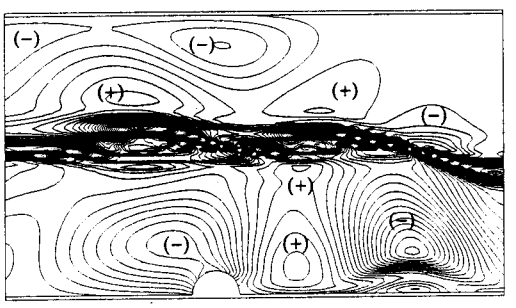

(d) t=70

Fig.5.28 Contours of vorticity at different times when Ri=0.1

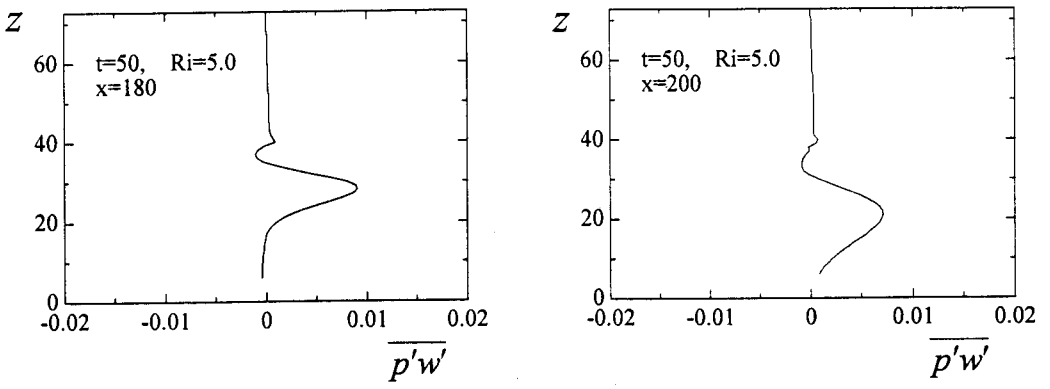

(A) Distribution of $\overline{p'w'}$ at different vertical sections x=180 and x=200

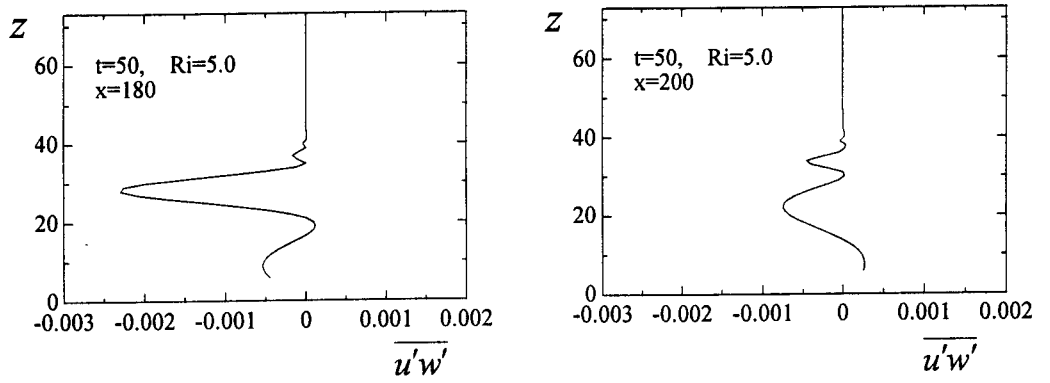

(B) Distribution of $\overline{u'w'}$ at different vertical sections x=180 and x=200

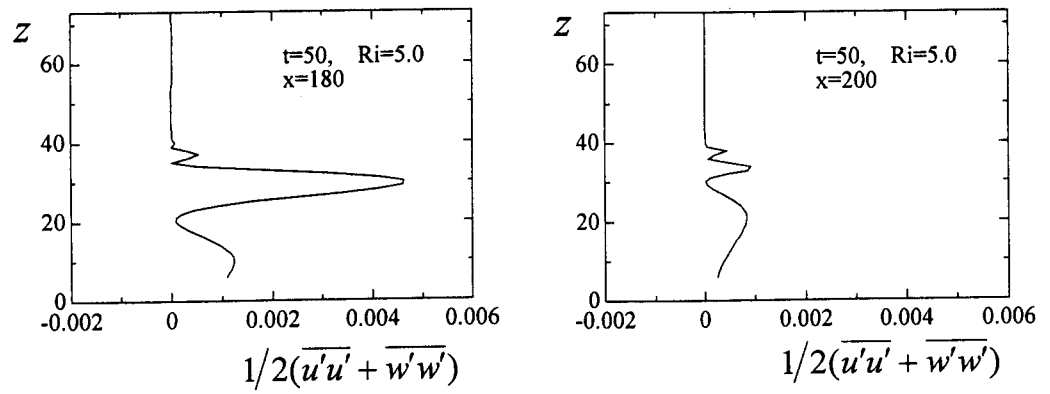

(C) Distribution of $1/2(\overline{u'u'}+\overline{w'w'})$ at different vertical sections x=180 and x=200

Fig.5.29 Distributions of vertical perturbation energy flux $\overline{p'w'}$, Reynolds stress $\overline{u'w'}$ and perturbation kinetic energy $1/2(\overline{u'u'}+\overline{w'w'})$ at different vertical section x when Ri=5.0 (t=50)

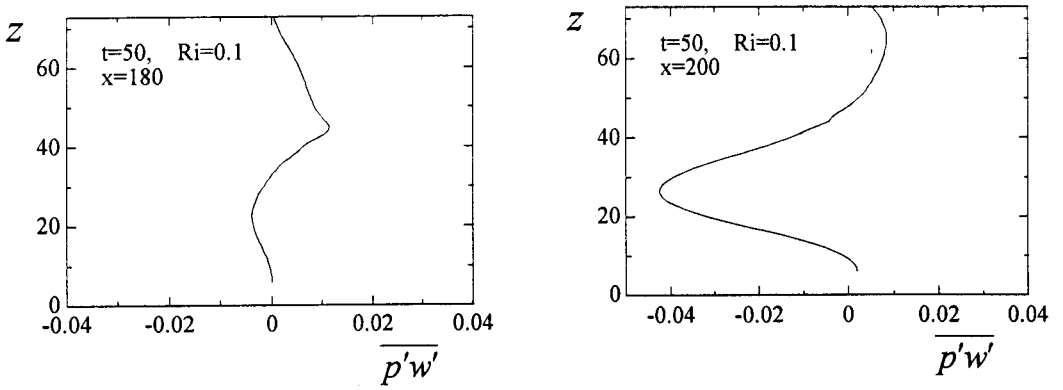

(A) Distribution of $\overline{p'w'}$ at different vertical sections x=180 and x=200

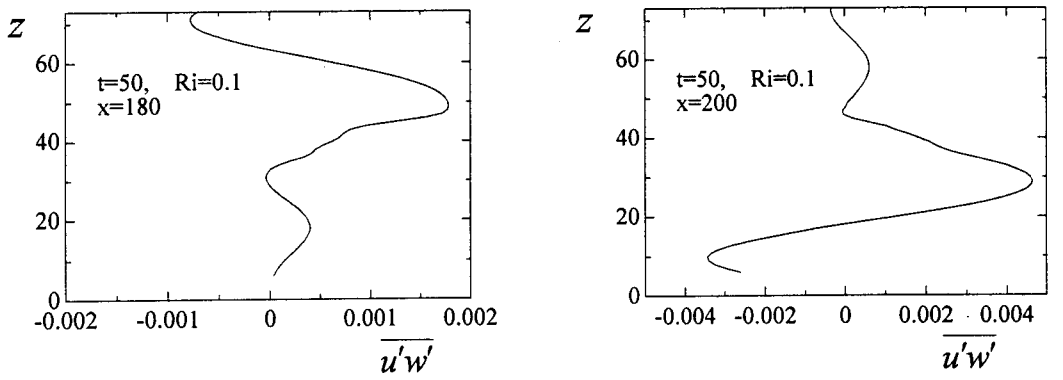

(B) Distribution of $\overline{u'w'}$ at different vertical sections x=180 and x=200

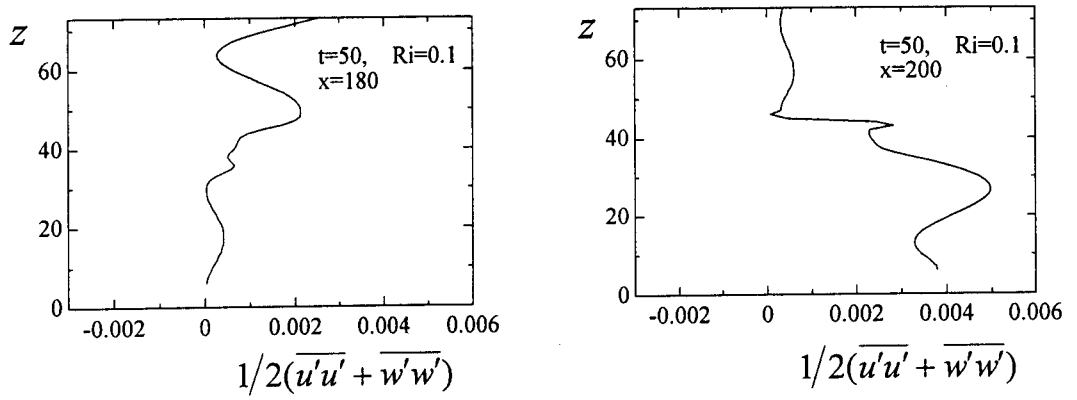

(C) Distribution of $1/2(\overline{u'u'}+\overline{w'w'})$ at different vertical sections x=180 and x=200

Fig.5.30 Distributions of vertical perturbation energy flux $\overline{p'w'}$, Reynolds stress $\overline{u'w'}$ and perturbation kinetic energy $1/2(\overline{u'u'}+\overline{w'w'})$ at different vertical section x when Ri=0.1 (t=50)

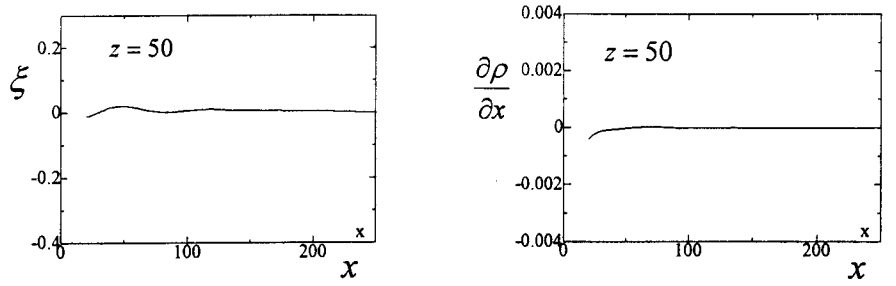

(a) Distribution of ξ and $\partial\rho/\partial x$ at horizontal level *a* (z=50)

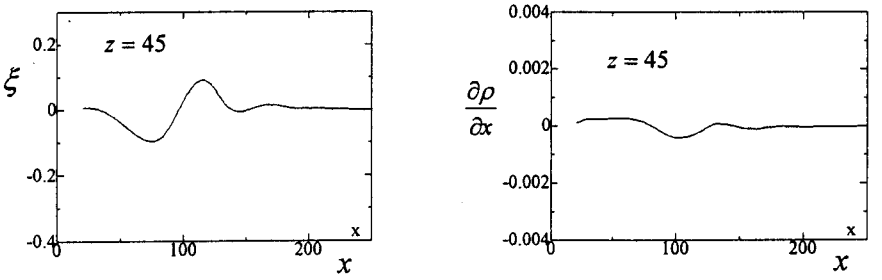

(b) Distribution of ξ and $\partial\rho/\partial x$ at horizontal level *b* (z=45)

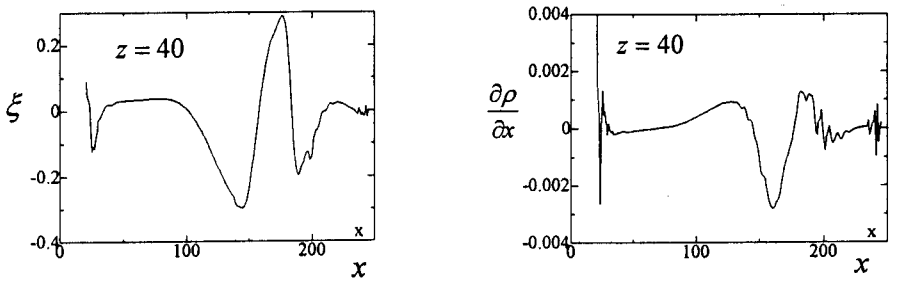

(c) Distribution of ξ and $\partial\rho/\partial x$ at horizontal level *c* (z=40)

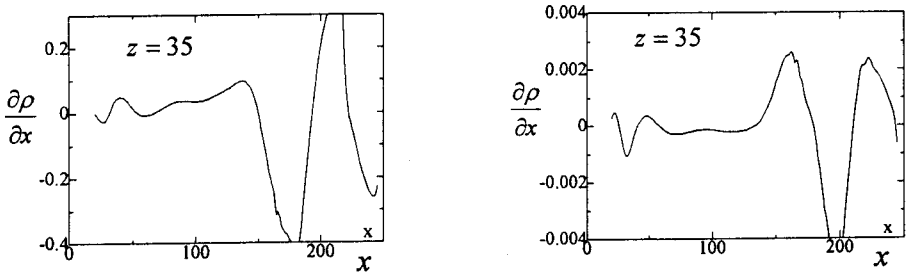

(d) Distribution of ξ and $\partial\rho/\partial x$ at horizontal level *d* (z=35)

Fig.5.31 Distribution of vorticity ξ and density gradient $\partial\rho/\partial x$ at different horizontal levels in strong shear region (Ri=5.0, t=35)

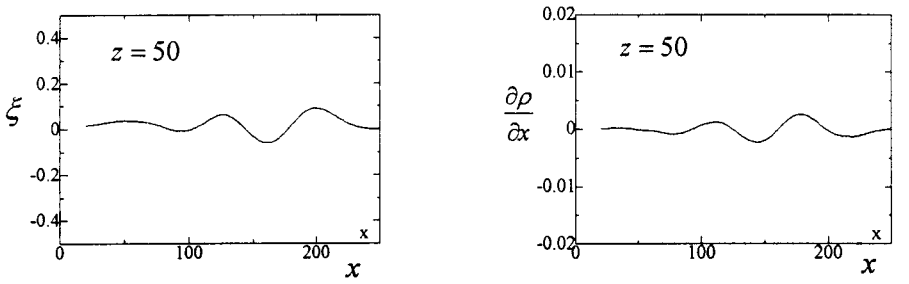

(a) Distribution of ξ and $\partial\rho/\partial x$ at horizontal level a (z=50)

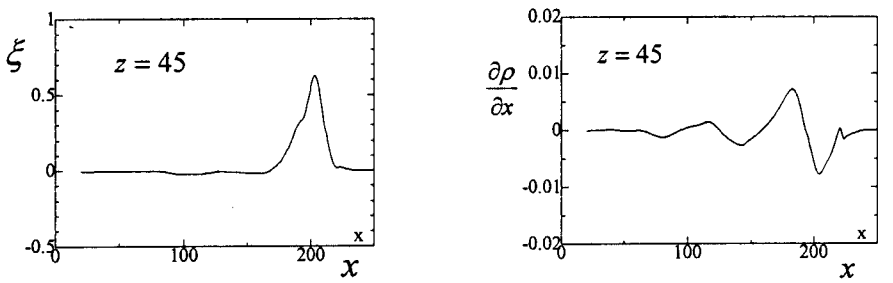

(b) Distribution of ξ and $\partial\rho/\partial x$ at horizontal level b (z=45)

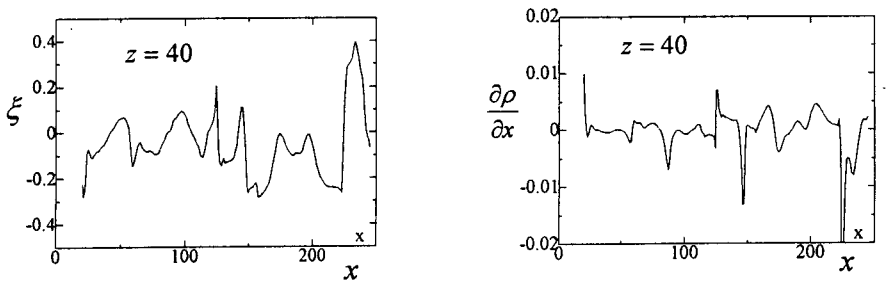

(c) Distribution of ξ and $\partial\rho/\partial x$ at horizontal level c (z=40)

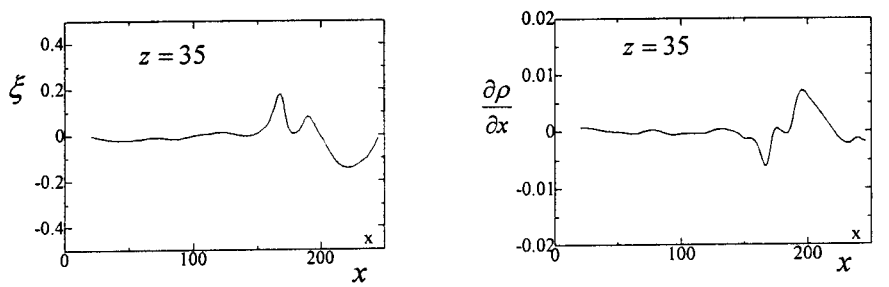

(d) Distribution of ξ and $\partial\rho/\partial x$ at horizontal level d (z=35)

Fig.5.32 Distribution of vorticity ξ and density gradient $\partial\rho/\partial x$ at different horizontal levels in strong shear region (Ri=0.1, t=35)

induced by obstacle can not overcome the shear layers to transport upward when $R_i > 0.25$.

Figure 5.32 gives the results of vorticity and $\frac{\partial \rho}{\partial x}$ when Ri=0.1 (t=35) at different horizontal levels indicated in Fig.5.17(a), where a is at $z = z_c + 10$ level, b is at $z = z_c + 5$ level, c is at $z = z_c$ level and d is at $z = z_c - 5$ level, respectively. From Fig.5.32, we know that the phase of vorticity advected by flow and the phase of baroclinic term $-\frac{g}{\rho_0}\frac{\partial \rho}{\partial x}$ is nearly same. Nearly in all field the vorticity transported by flow is strengthened at some degree due to the vorticity generated by baroclinic term at that place, especially in the area near the critical layers the baroclinic term $-\frac{g}{\rho_0}\frac{\partial \rho}{\partial x}$ acts as an amplifier. The strength of the vorticity in the shear region due to the effects of critical layers is the main reason that the over-reflection of internal wave occurs when $R_i < 0.25$. The perturbation induced by obstacle will propagate left-up upstream and right-down due to the effects of critical layers. With the increase of calculation time, the amplitude of internal wave will become larger.

5.4 Concluding remarks

The density stratified fluid flows with critical layers are simulated by the lattice vortex method. From the generation mechanism of vorticity and its motion, it is explained that a gravity wave incident upon a critical layer exhibits different properties depending on Richardson number. When Richardson number $R_i > 0.25$, the transported vorticity and generated vorticity near the critical

layers are canceled out, the critical layers act as a absorber: the perturbation induced by an obstacle can not pass through critical layers to propagate upward. For Richardson number $R_i < 0.25$, the over reflection, predicted from the linear theory, is observed. From considering the streamline, the perturbation streamline, the contours of vorticity and density gradient $\partial\rho/\partial x$, the interaction between critical layer and lee wave is discussed. The reason why the perturbation induced by obstacle can not pass through the critical layers when $R_i > 0.25$ and the "over-reflection" of internal waves when $R_i < 0.25$ is explained by the effects between vorticity transported by the flow and that created by the baroclinic term.

Chapter 6

Numerical Simulation of 3D Stratified Flows by Lattice Vortex Method

6.1 Introductory remarks

As a branch of numerical method in the computational fluid dynamics, vortex method is widely used in the simulation of many practical phenomena. Many incompressible flows at high Reynolds numbers are characterized by regions of concentrated vorticity imbedded in irrotational fluid. By the theorems of Helmholtz and Kelvin, we know that the inviscid motion of the vorticity in these regions is given by the local fluid velocity which in turn is determined kinematically from the vorticity field. Thus, it is mathematically correct and often very convenient to consider inviscid fluid dynamics in terms of parcels of vorticity which induce motion on each other as an alternative to pressure-velocity considerations. For two-dimensional fluid flow, many techniques are proposed to treat vortex in the flow, and most all show a great advantage in the improvement of calculation speed and accuracy. It is can be said that the vortex method for

two-dimensional flow has been established perfectly. However, the vortex method for three-dimensional flow is also in the way of investigation. In three-dimensional vortex method, vortex stretching must be considered. The difficulty of considering the effect of vortex stretching is great barrier extending vortex method from two-dimension to three-dimension. As explanation in chapter 2, we proposed a simple method to consider the effect of vortex stretch in three-dimensional flow.

In this chapter, we will use the lattice vortex method to simulate a three-dimensional density stratified flow.

6.2 Calculation model and boundary conditions

We consider a channel with three solid boundaries which is full of a density stratified fluid, and on one of its solid wall there is a wave source. The wave source will induce inner waves in the density stratified fluid. We will simulate the propagation of the inner wave by lattice vortex method.

The calculation model is displayed in Fig.6.1.

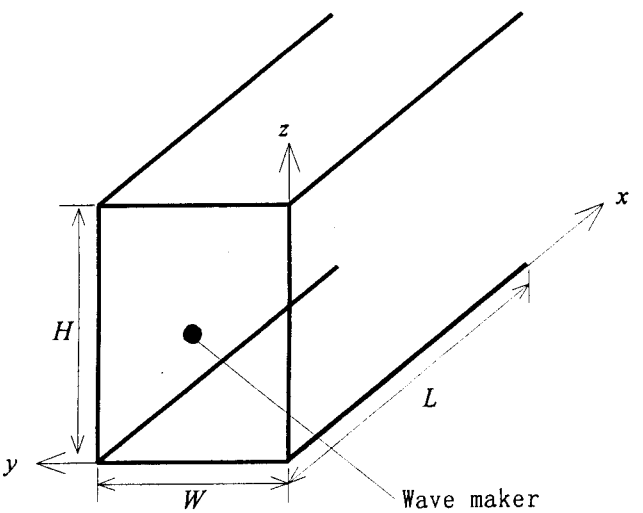

Fig.6.1 The calculation model

In our calculation, the solid wall is treated by panel method. The position of control points is displayed in Fig.6.2.

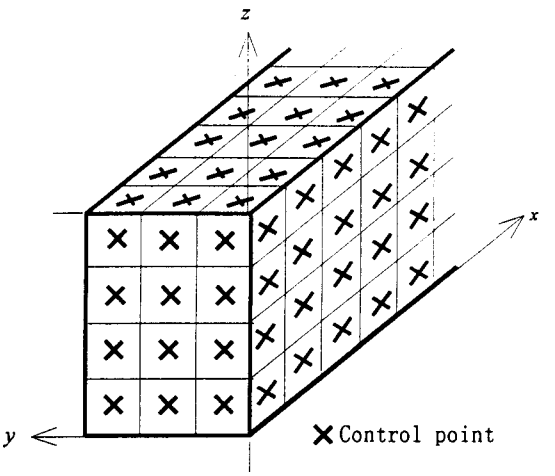

Fig.6.2 Definition of control point

The solid wall is replaced by boundary circulations, which situated on the solid walls' mesh cell. The control point locates on the center of each solid walls' mesh cell.

The definition of the parameters is as follows:

H: Channel depth

W: Channel width

L: Calculation range

U_0: Reference velocity

ρ_0: Reference density

N: *Brunt – Väisälä* frequency $N^2 = -\frac{g}{\rho_0}\frac{d\overline{\rho}}{dz}$

K: Density stratification degree $K = \frac{NH}{\pi U_0}$

F_r: *Froude* number $Fr = \frac{U_0}{Nh} = \frac{H/h}{\pi K}$

t^* : Dimensionless time $t^* = Nt$

The boundary conditions are as follows:

$\frac{\partial \rho}{\partial x} = 0, \quad \frac{\partial \Gamma}{\partial x} = 0$ at far downstream

$\rho = \rho_1, \ u_n = 0, \ \Gamma = 0$ on the upper wall

$\rho = \rho_0, \ u_n = 0, \ \Gamma = 0$ on the lower wall

$\frac{\partial \rho}{\partial x} = 0, \ u_n = 0, \ \Gamma = 0$ on the side wall in yz plane

$\frac{\partial \rho}{\partial y} = 0, \ u_n = 0, \ \Gamma = 0$ on the side wall in xz plane

where the subscript n denotes the normal direction to the boundary and u_n is the velocity component in the n direction, Γ is circulation, ρ is density, ρ_0 and ρ_1 is a constant.

The wave source locates at the center of the side wall in yz plane. The coordinate of wave source is $(X_{source}, Y_{source}, Z_{source})$.

$$X_{source} = 0, \ Y_{source} = H/2, \ Z_{source} = W/2 \qquad (6.1)$$

and we assume that the wave source velocity $(u_{source}, v_{source}, w_{source})$ is

$$u_{sourcee} = U_{\max} \sin \frac{2\pi}{T_{source}} t, \quad v_{source} = 0, \quad w_{source} = 0 \qquad (6.2)$$

where T_{source} is the period of the wave source.

We assume that in initial the fluid inside the channel is rest and its density distribution (Fig.6.3) described by Eq.6.3

$$\rho = \frac{\rho_0 + \rho_1}{2} - \left(\frac{\rho_0 - \rho_1}{2} \right) \tanh\left(\frac{z - z_c}{b} \right) \qquad (6.3)$$

where b is the range in which density varies greatly.

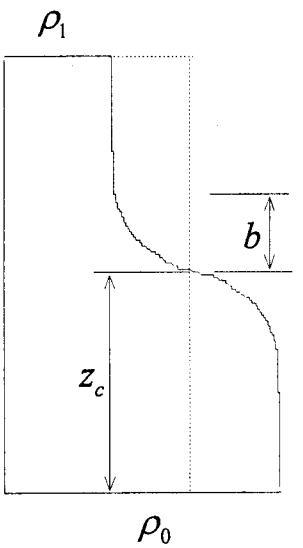

Fig.6.3 Density distribution

According to density distribution Eq.6.3, the *Brunt – Väisälä* frequency N is calculated by Eq.6.4

$$N^2 = -\frac{g}{\rho_0} \frac{\rho_1 - \rho_0}{b} \qquad (6.4)$$

In our calculation, we choose $z_c = H/2$ to ensure the wave source locates in the area , in which density varies greatly.

The boundary condition is displayed in Fig.6.4.

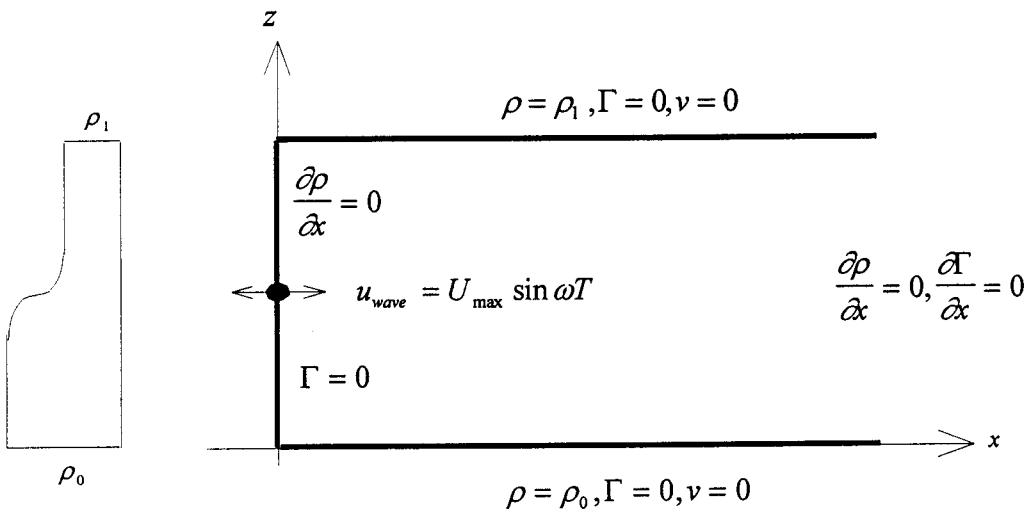

Fig.6.4 Boundary condition

6.3 Numerical results and discussions

We calculated the model: $L = 40, W = 10, H = 20$, there are two wave source on the side wall in yz plane, which position is $(0,4.5,9.5),(0,4.5,10.5)$, the period of wave source is $T_{source} = 10$, $U_{\max} = 0.0001$, $\rho_0 = 1.5$, $\rho_1 = 1.0$, $b = 1$.

Figur 6.5, Figure 6.6 and Figure 6.7 gives the development of the contours of density , vertical velocity and the component of vorticity in y direction on the middle horizontal surface (z=H/2) with calculation time, respectively.

They all show that the inner wave induced by wave source advances towards the x direction with the time development. Because the width of the channel is too narrow ($W = 10$), the solid wall in xz plane will have great influence on the

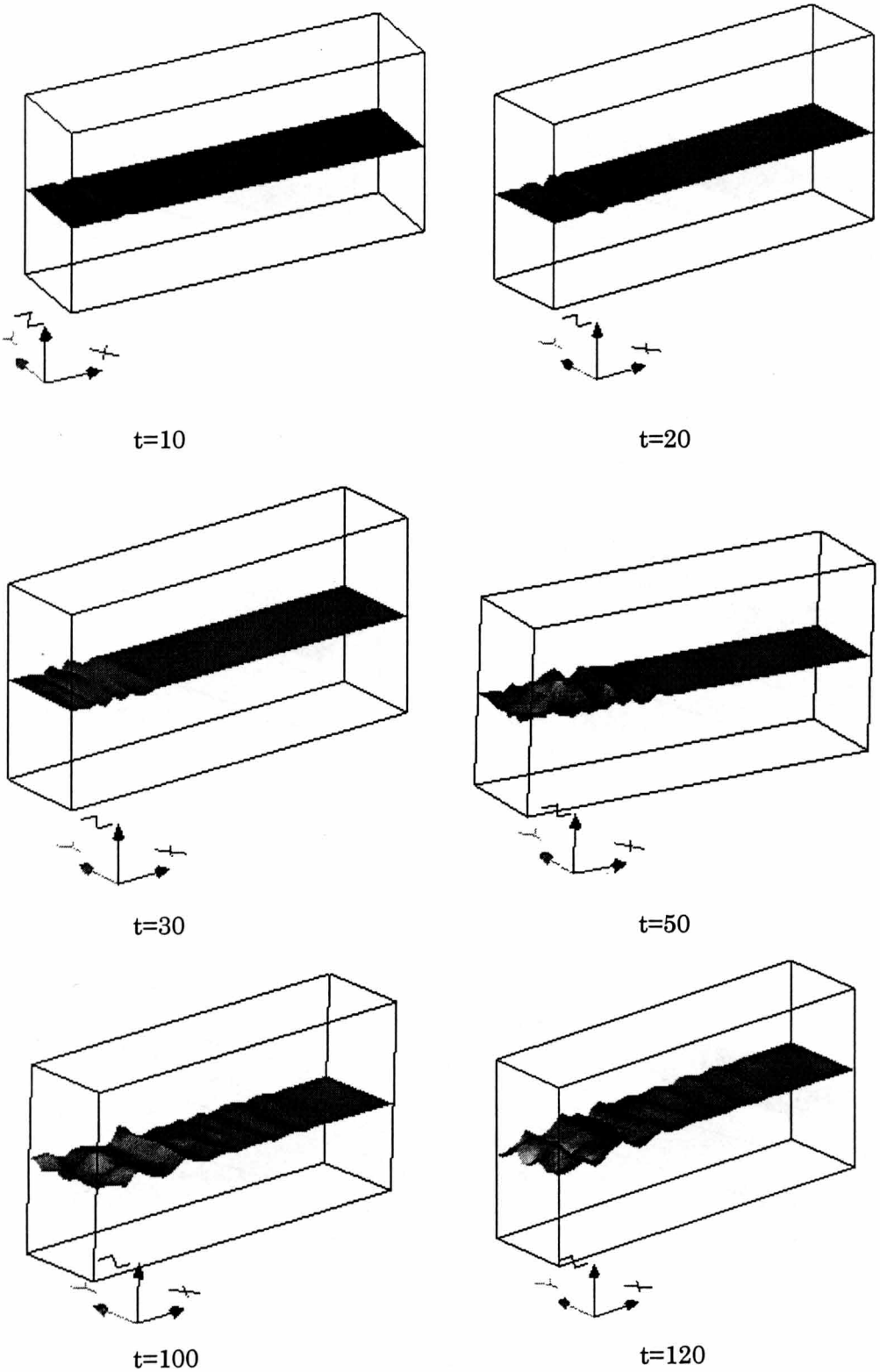

Fig.6.5 Contours of density on the middle horizontal surface (Z=H/2) at different times

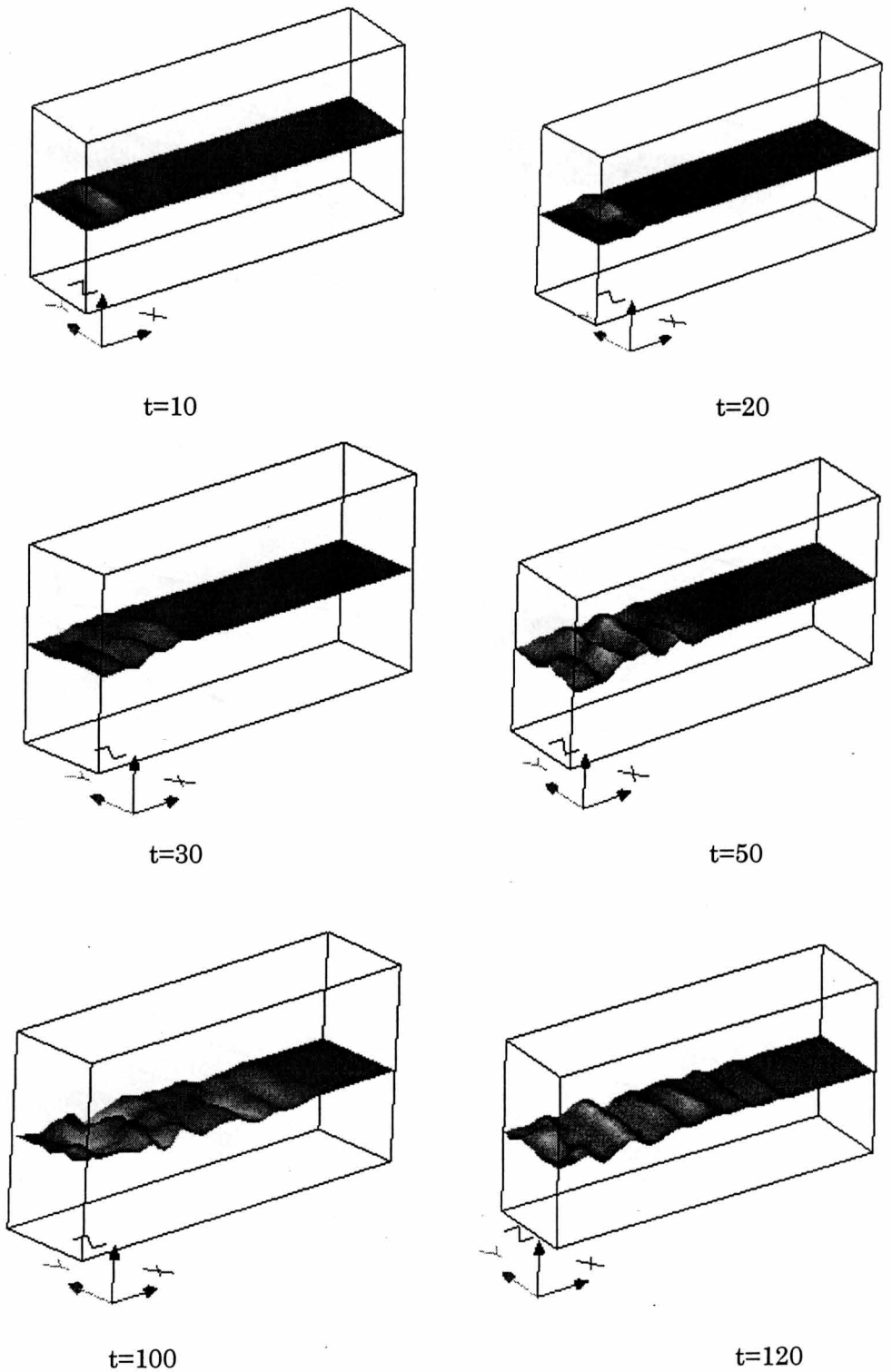

Fig.6.6 Contours of Vz on the middle horizontal surface (Z=H/2) at different times

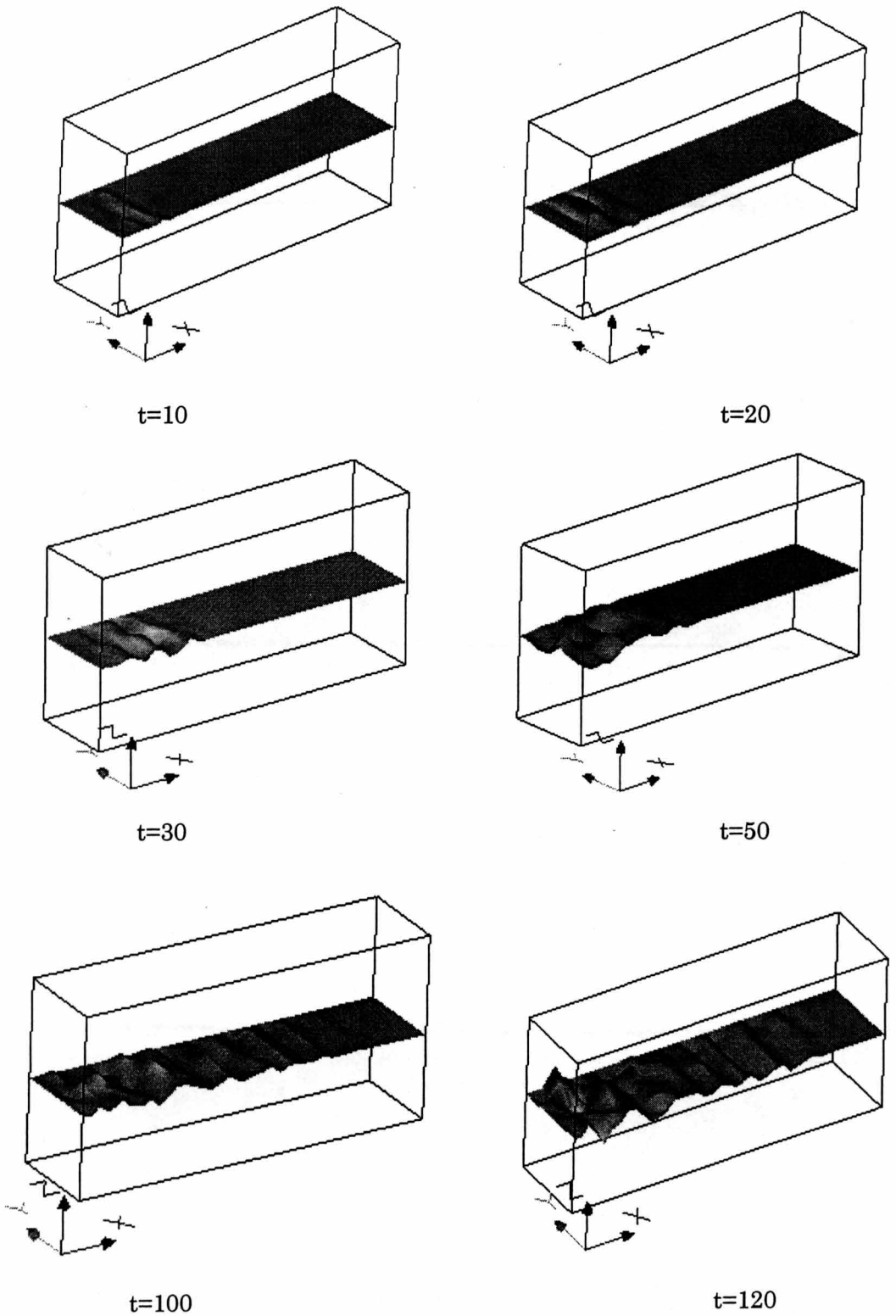

Fig.6.7 Contours of the component of vorticity in y direction on the middle horizontal surface (Z=H/2) at different times

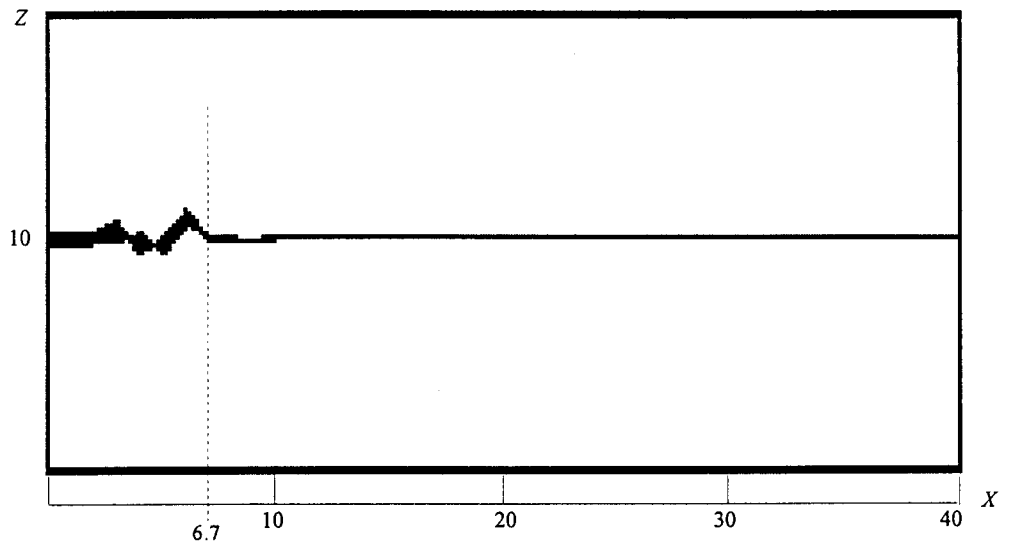

t=25

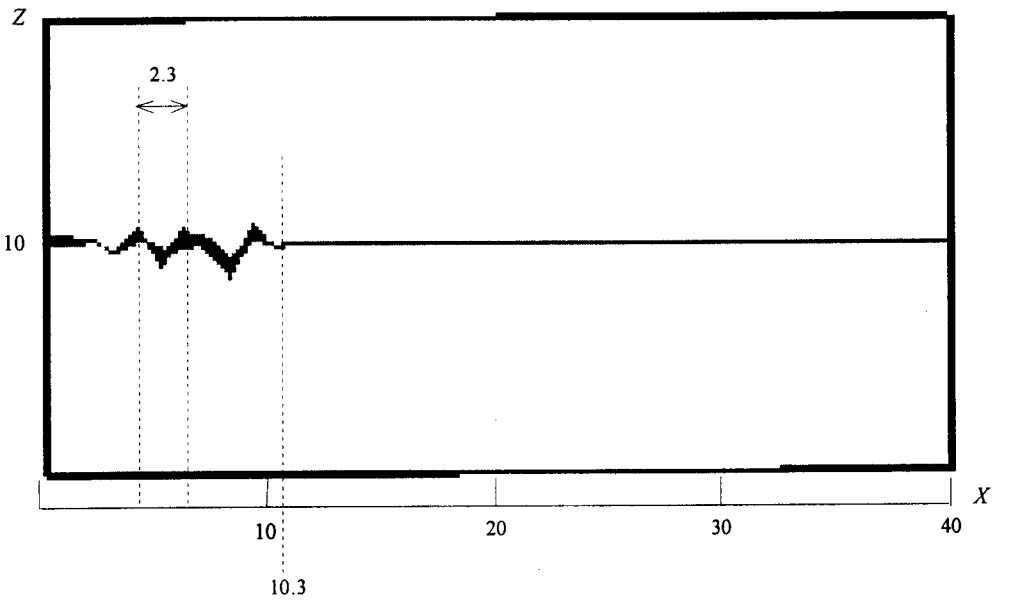

t=30

Fig.6.8 Propagation of internal waves on the middle horizontal surface (Z=H/2)

propagation of the internal wave. Due to their effect, the computation becomes unstable. In our calculation, a very smaller value of U_{max} is used to reduce this influence.

In theory, the propagation speed of internal wave in the two-layer density fluid with finite depth is calculated by Eq.6.5 [18]

$$c = \sqrt{\frac{k}{g}\frac{\rho_1 - \rho_2}{\rho_1 \coth kh_1 + \rho_2 \coth kh_2}} \qquad (6.5)$$

where c is the propagation speed of internal wave, ρ_1 is the density of lower layer, h_1 is the depth of lower layer, ρ_2 is the density of upper layer, h_2 is the depth of upper layer, k is wave number and

$$k = \frac{2\pi}{\lambda} \qquad (6.6)$$

in which λ is the wavelength.

Figure 6.8 gives the position of the front of the internal wave at time t=25 and t=30. The wavelength is also given, λ=2.3.

In numerical simulation, the propagation speed of internal wave is calculated by Eq.6.7

$$c = \frac{\Delta l}{\Delta t} \qquad (6.7)$$

where Δl is the distance the internal wave propagated in time interval Δt.

Therefore, in our calculation, the propagation speed of internal wave is

$$c = \frac{\Delta l}{\Delta t} = \frac{10.3 - 6.7}{30 - 25} \approx 0.72 \qquad (6.8)$$

According to Eq.6.5, the propagation speed of internal wave is

$$c = \sqrt{\frac{k}{g}\frac{\rho_1 - \rho_2}{\rho_1 \coth kh_1 + \rho_2 \coth kh_2}} = \sqrt{\frac{2\pi}{g\lambda}\frac{\rho_1 - \rho_2}{\rho_1 \coth\frac{2\pi}{\lambda}h_1 + \rho_2 \coth\frac{2\pi}{\lambda}h_2}}$$

$$= \sqrt{\frac{2\pi}{2.3g}\frac{1.5_1 - 1.0}{\rho_1 \coth\frac{2\pi}{2.3}10 + \rho_2 \coth\frac{2\pi}{2.3}10}} \qquad (6.9)$$

$$\approx 0.847$$

For the propagation speed of internal wave, there is a good agreement between numerical result and analytical one. In some degree, it certificates that the lattice vortex method is valid for the simulation of a three-dimensional density stratified flow.

6.4 Concluding remarks

The lattice vortex method is used to simulate the propagation of the internal wave induced by a wave maker in a three-dimensional density stratified fluid flow. The numerical result shows the propagation of internal wave quantitatively. The propagation speed of internal wave predicted by our numerical result is in a good agreement with analytical one quantitatively. In some degree, it certificates that the lattice vortex method is valid for the simulation of a three-dimensional density stratified flow.

Chapter 7

Conclusions

In this research, we simplified the vortex in cell (VIC) method, and proposed a new version Lattice vortex method. The lattice vortex method has combined some of the best features of both the Lagrangian and Eulerian approaches. There is no limitation of the CFL condition, which is a severe restriction condition in most explicit method. In lattice vortex method, the vortex distribution scheme is used to limit the number of vorticity in the flow field, which improved the computational efficiency dramatically. We extended the application of vortex method to nonhomogeneous flow.

Density stratified flows are simulated by lattice vortex method. The special phenomena (selective withdrawal, blocking and lee wave) in density stratified flows are investigated by LVM method. Its results have a good agreement with theoretical ones, which indicates that the vortex method is suitable for a stratified flow. With the vortex method, the mechanism of these phenomena in a stratified flow is explained.

In Chapter 2, the principle of lattice vortex method is explained in detail.

In Chapter 3, the basic theory of density stratified flows is given, and the

numerical procedure of lattice vortex method is suitable for the simulation of density stratified flows is explained in detail

In Chapter 4, the line sink flows in a channel of finite depth are calculated. Its results show that the blocking area is formed by the development of several eddy regions of cell structures in the stagnant region, which are propagated upstream.

In Chapter 5, the flows past an obstacle (a plate and a semicircular ridge) in a channel of finite depth are calculated. The lee wave is formed by the columnar disturbances, which arise from an isolated source (an obstacle), and propagated upstream and downstream due to the movement of generated vortices in a stratified flow. The effect of critical layer in a stratified flow is also investigated in this chapter. From the generation of vorticity and the motion of vortex in the stratified flow with critical layer, the dependence on Richardson number of a stratified flow with critical layer is explained. a gravity wave incident upon a critical layer exhibits different properties depending on the Richardson number. When Richardson number $R_i > 0.25$, the transported vorticity and generated vorticity near the critical layers are canceled out, the critical layers act as a absorber: the perturbation induced by an obstacle can not pass through critical layers to propagate upward. For Richardson number $R_i < 0.25$, the over reflection, predicted from the linear theory, is observed, but because the system is dynamically unstable no over-reflecting steady state is ever reached.

In Chapter 6, we extended lattice vortex method to a three-dimensional flow. A propagation of internal waves induced by a wave maker in a three-dimensional density stratified flow is simulated. The numerical result shows the propagation of internal wave quantitatively. The propagation speed of internal wave predicted by our numerical result is in a good agreement with analytical one quantitatively. In some degree, it certificates that the lattice vortex method is valid for the simulation of a three-dimensional density stratified flow.

Bibliography

[1] L. Rosenhead, "The Formation of Vortices from a Surface of Discontinuity", Proc. Roy. Soc. Lond., A, 134, pp.170~192, 1931.

[2] J. C. Wu and J. F. Thompson, "Numerical Solutions of Time-Dependent Incompressible Navier-Stokes Equations using an Intego-Differntial Formulation", Computer & Fluids, 1, pp.197~215, 1973.

[3] A. Leonard, "Vortex Methods for Flow Simulation", Journal of Computational Physics, 37, pp.289~335, 1980.

[4] Turgut Sarpkaya, "Computational Methods with Vortices---the 1988 Freeman Scholar Lecture", Journal of Fluids Engineering, 111, pp.5~46, 1989.

[5] Chia-shun Yih, "Stratified Flows", Academic Press, 1980.

[6] Peter G. Baines, "Topographic Effects in Stratified Flows", Cambridge University Press, 1995.

[7] John W. Miles, "On the Stability of Heterogeneous Shear Flows", Journal of Fluid Mechanics, 10, pp.496~508, 1960.

[8] Louis N. Howard, "Note on a Paper of John W. Miles", Journal of Fluid Mechanics, 10, pp.509~512, 1960.

[9] C.-S. Yih, "On the Flow of a Stratified Fluid", Proc. 3rd U. S. Nat. Cong. Appl. Mech., pp.857~861, 1958.

[10] W. E. Debler, "Stratified Flow into a Line Sink", Journal of Eng. Mech. Div., Proc. A. S. C. E., 85, pp.51~65, 1959.

[11] Hsien-ping Pao and Timothy W. Kao, "Dynamics of Establishment of Selective Withdrawal of a Stratified Fluid from a Line Sink. Part 1. Theory", Journal of Fluid Mechanics, 65, pp.657~688, 1974.

[12] Michihisa Tsutahara, Akio Tomiyama and Kazuhiro Mari, "Two Dimensional Selective Withdrawal in Stratified Fluids in Reservoirs", Journal of Japan Society of Fluid Mechanics, 13, pp.380~388, 1994.

[13] K. Yaetsu, "Study of Selective Withdrawal from a Point Sink", Master Thesis of Kobe University, 1996.

[14] Hideshi Hanazaki, "Upstream Advancing Columnar Disturbances in Two Dimensional Stratified Flow of Finite Depth", Physics of Fluids A, 1, pp.1976~1987, 1989.

[15] John W. Miles and Herbert E. Huppert, "Lee Waves in a Stratified Flow Part 2.Semi-circularf Obstacle", Journal of Fluid Mechanics, 33, pp.803~814, 1968.

[16] S. A. Maslowe, "Critical Layers in Shear Flows", Annual Reviews of Fluid Mechanics, 18, pp.405~432, 1986.

[17] R. S. Lindzen and K. K. Tung, "Wave Overreflection and Shear Instability", Journal of the Atmospheric Sciences, 35, pp.1626~1632, 1978.

[18] James Lighthill, "Waves in Fluids", Cambridge University Press, 1978.

[19] Alex D. D. Craik, "Wave Interactions and Fluid Flows", Cambridge University Press, 1985.

[20] P. G. Saffman, "Vortex Dynamics", Cambridge University Press, 1992.

[21] J. S. Turner, "Buoyancy Effects in Fluid", Cambridge University Press, 1973.

[22] G. K. Batchelor, "an Introduction to Fluid Dynamics", Cambridge University Press, 1967.

[23] M. G. Wurtele, R. D. Sharman, and A. Datta, "Atmospheric Lee Waves", Annual Reviews of Fluid Mechanics, 28, pp.429~476, 1996.

[24] Jorg Imberger and Chris Fandry, "Withdrawal of a Stratified Fluid from a Vertical Two-dimensional Duct", Journal of Fluid Mechanics, 70, pp.321~332, 1975.

[25] Timothy W. Kao, "Selective Withdrawal Criteria of Stratified Fluids", Journal of the Hydraulics Division, Proceedings of the American Society of Civil Engineers, June 1976, pp.717~729.

[26] Jorg Imberger, "Two-dimensional Sink Flow of a Stratified Fluid Contained in a Duct", Journal of Fluid Mechanics, 53, pp.329~349, 1972.

[27] Chia-shun Yih, "Exact Solutions for Steady Two-dimensional Flow of a Stratified Fluid", Journal of Fluid Mechanics, 9, pp.161~174, 1960.

[28] Norman H. Brooks, F. ASCE and Robert C. Y. Koh, "Selective Withdrawal from Density-stratified Reservoirs", Journal of the Hydraulics Division, Proceedings of the American Society of Civil Engineers, July 1969, pp.1369~1400.

[29] Hideshi Hanazaki, "A Numerical Study of Three-dimensional Stratified Flow past a Sphere", Journal of Fluid Mechanics, 192, pp.393~419, 1988.

[30] Hideshi Hanazaki, "Drag Coefficient and Upstream Influence in Three Dimensional Stratified Flow of Finite Depth", Fluid Dynamics Research, 4, pp.317~332, 1989.

[31] Hideshi Hanazaki, "On the Three-dimensional Internal Waves Excited by Topography in the Flow of a Stratified fluid", Journal of Fluid Mechanics, 263, pp.293~318, 1994.

[32] Hideshi Hanazaki, "Numerical Study of Nonlinear Waves in a Transcritical Flow of Stratified Fluid past an Obstacle", Physics of Fluids A, 4, pp.2230~2243, 1992.

[33] John W. Miles, "Lee Waves in a Stratified Flow Part 1. Thin Barrier", Journal of Fluid Mechanics, 32, pp.549~567, 1967.

[34] Herbert E. Huppert and John W. Miles, "Lee Waves in a Stratified Flow Part 3.Semi-elliptical Obstacle", Journal of Fluid Mechanics, 35, pp.481~496, 1969.

[35] Richard S. Lindzen, "Instability and Wave Over-reflection in Stably Stratified Shear Flow", Journal of Fluid Mechanics, 151, pp.189~217, 1985.

[36] Dale R. Durran and Joseph B. Klemp, "Another Look at Downslope Winds. Part II: Nonlinear Amplification beneath Wave-Overturning Layers", Journal of the Atmospheric Sciences, 44, pp.3402~3412, 1987.

[37] Steve Arendt, "Vorticity in Stratified Fluids. I: General Formulation", Geophys. Astrophys. Fluid Dynamics, 68, pp.59~83, 1992.

[38] Steve Arendt, "Vorticity in Stratified Fluids. II: Finite Cross-section Tubes and Rings", Geophys. Astrophys. Fluid Dynamics, 70, pp.161~193, 1992.

[39] T. L. Clark and W. R. Peltier, "Critical Level Reflection and the Resonant Growth of Nonlinear Mountain Waves", Journal of the Atmospheric Sciences, 41, pp.3122~3134, 1984.

[40] J. F. Scinocca and W. R. Peltier, "On the Richardson Number Dependence of Nonlinear Critical-layer Flow over Localized Topography", Journal of the Atmospheric Sciences, 48, pp.1560~1572, 1991.

[41] J. T. Bacmeister and R. T. Pierrehumbert, "On High-Drag States of Nonlinear Stratified Flow over an Obstacle", Journal of the Atmospheric Sciences, 45, pp.63~80, 1988.

[42] James W. Rottman, Dave Broutman and Roger Grimshaw, "Numerical Simulations of uniformly Stratified Fluid Flow over Topography", Journal of Fluid Mechanics, 306, pp.1~30, 1996.

[43] KevinG.Lamb, "Numerical Simulations of Stratified Inviscid Flow over a Smooth Obstacle", Journal of Fluid Mechanics, 260, pp.1~22, 1994.

[44] W. D. Smyth and W. R. Peltier, "The Transition between Kelvin-Helmholtz and Holmboe Instability: An Investigation of the Overreflection Hypothesis", Journal of the Atmospheric Sciences, 46, pp.3698~3721, 1989.

[45] I. A. Eltayeb and J. F. Mckenzie, "Critical-level Behaviour and Wave Amplification of a Gravity Wave Incident upon a Shear Layer", Journal of Fluid Mechanics, 72, pp.661~671, 1975.

[46] John W. Miles and Herbert E. Huppert, "Lee Waves in a Stratified Flow Part 4. Perturbation Approximations", Journal of Fluid Mechanics, 35, pp.497~525, 1968.

[47] R. J. Breeding, "A Non-linear Investigation of Critical Levels for Internal Atmospheric Gravity Waves", Journal of Fluid Mechanics, 50, pp.545~563, 1971.

[48] John R. Booker and Francis P. Bretherton, "The Critical Layer for Internal Gravity Waves in a Shear Flow", Journal of Fluid Mechanics, 27, pp.513~539, 1967.

[49] Julio T. Bacmeister and Mark R. Schoeberl, "Breakdown of Vertically Propagating Two-dimensional Gravity Waves Forced by Orography", Journal of the Atmospheric Sciences, 46, pp.2109~2134, 1989.

[50] David G. Schowalter, Charles W. Van Atta and Juan C. Lasheras, "A Study of Streamwise Vortex Structure in a Stratified Shear Layer", Journal of Fluid Mechanics, 281, pp.247~291, 1994.

[51] Chantal Staquet, "Two-dimensional Secondary Instabilities in a Strongly Stratified Shear Layer", Journal of Fluid Mechanics, 296, pp.73~126, 1995.

[52] R. H. J. Grimshaw and N. Smyth, "Resonant Flow of a Stratified Fluid over Topography", Journal of Fluid Mechanics, 169, pp.429~464, 1986.

[53] Young-Joon Kim and Akio Arakawa, "Improvement of Orographic Gravity Wave Parameterization Using a Mesoscale Gravity Wave Model", Journal of the Atmospheric Sciences, 52, pp.1875~1902, 1995.

[54] P. G. Drazin and D. W. Moore, "Steady Two-dimensional Flow of Fluid of Variable Density over an Obstacle", Journal of Fluid Mechanics, 28, pp.353~370, 1967.

[55] Poitr K. Smolarkiewicz and Richard Rotunno, "Low Froude Number Flow past Three-dimensional Obstacles. Part I: Baroclinically Generated Lee Vortices", Journal of the Atmospheric Sciences, 46, pp.1154~1164, 1989.

[56] Steve Arendt, "Two-dimensional Vortex Dynamics in a Stratified Barotropic Fluid", Journal of Fluid Mechanics, 314, pp.139~161, 1995.

[57] Piotr K. Smolarkiewicz and Janusz A. Pudykiewicz, "A Class of Semi-Lagrangian Approximations for Fluids", Journal of the Atmospheric Sciences, 49, pp.2082~2098, 1992.

[58] S. I. Chernyshenko and Ian P. Castro, "High-Reynolds-number Weakly Stratified Flow past an Obstacle", Journal of Fluid Mechanics, 317, pp.155~178, 1996.

[59] P. C. Patnaik, F. S. Sherman and G. M. Corcos, "A Numerical Simulation of Kelvin-Helmholtz Waves of finite amplitude", Journal of Fluid Mechanics, 73, pp.215~240, 1976.

[60] G. M. Corcos and F. S. Sherman, "Vorticity Concentration and the Dynamics of Unstable Free Shear Layers", Journal of Fluid Mechanics, 73, pp.241~264, 1976.

[61] Y. T. Fung and Simon W. Chang, "Surface and Internal Signatures of Organized Vortex Motion in Stratified Fluids", Physical Fluids, 8, pp.3023~3056, 1996.

[62] S. T. Thoroddsen and C. W. Van Atta, "Baroclinic Generation of Vorticity by an Axisymmetric Vortex in a Linearly Stratified Fluid; in the Passive Limit", Phys. Fluids, 8, pp.2274~2276, 1996.

[63] Bruno Voisin, "Internal Wave Generation in Uniformly Stratified Fluids. Part 1: Green's Function and Point Sources", Journal of Fluid Mechanics, 231, pp.439~480, 1991.